

©2010

Dinali Nelun Fernando

ALL RIGHTS RESERVED

PREDICTING AND MONITORING DROUGHT IN THE HUMID TROPICS:

A CASE STUDY ON SRI LANKA

by

DINALI NELUN FERNANDO

A Dissertation submitted to the

Graduate School-New Brunswick

Rutgers, The State University of New Jersey

in partial fulfillment of the requirements

for the degree of

Doctor of Philosophy

Graduate Program in Geography

written under the direction of

Prof. David A. Robinson

and approved by

---

---

---

---

New Brunswick, New Jersey

October, 2010

ABSTRACT OF THE DISSERTATION

**PREDICTING AND MONITORING DROUGHT IN THE HUMID TROPICS:**

**A CASE STUDY ON SRI LANKA**

By DINALI NELUN FERNANDO

Dissertation Director:  
Prof. David A. Robinson

This dissertation develops an operational tool for predicting and monitoring drought applicable to the humid tropics. Using Sri Lanka as a case example, it examines whether droughts in the humid tropics are predictable on an operational basis, and investigates how moisture stress may be monitored as a season unfurls.

Droughts in Sri Lanka occur when rainfall during the main cultivation season – the *Maha* (October-March) – fails. Such droughts profoundly impact rice production. From 1951-2008, there were 4 extreme [Standardized Precipitation Index (SPI)  $< -2.0$ ], 1 severe ( $-1.9 < \text{SPI} < -1.5$ ), 5 moderate ( $-1.49 < \text{SPI} < -1.0$ ) and 4 mild ( $-0.99 < \text{SPI} < -0.5$ ) droughts.

*Maha* droughts can be operationally predicted by forecasting the failure of the two rainfall regimes during the season. The contemporaneous westerly zonal wind at 850hPa (U850), over 60°E-105°E and 5°S-15°N, controls the strength of the October-November convective rains – with rain failure associated with anomalously strong U850. The contemporaneous northerly vertical shear of the mean meridional wind ( $V_s$ ), over 80°E-90°E and 0°N-20°N, controls the strength of the December-February northeast monsoon

rains – with rain failure associated with an anomalously weak  $V_s$ . Drought forecast skill was assessed for 1981-2002 using predicted fields of U850 issued in September, and  $V_s$ , issued in November, from the NCEP Climate Forecast System and the ECHAM4.5 forced with two scenarios of prescribed sea surface temperature (SST) anomalies. October-November rain failure can be predicted with good skill over the rice cultivation areas in the central and southeastern regions using forecast U850 from the two versions of the ECHAM4.5. December-February rain failure can be predicted with good skill in the rice cultivation areas in the eastern, central and north central regions with forecast  $V_s$  from the ECHAM4.5 forced with constructed analogues of SST anomalies.

The utility of the Vegetation Temperature Condition Index (VTCI) – calculated with Terra-MODIS Land Surface Temperature and Normalized Difference Vegetation Index products – as an indicator of abnormally wet or dry conditions was tested for the *Maha* season. Results show that the VTCI is a suitable metric for the near-real time monitoring of *Maha* drought because it captures the onset and progression of moisture stress as the season unfurls and complements the seasonal rainfall forecast.

### **Acknowledgement and Dedication**

I am profoundly grateful to my advisor Prof. David A. Robinson for guiding my dissertation research and for his unstinting support, advice and guidance since I joined the Graduate Program in Geography at Rutgers University in the fall of 2006. He was always accessible whenever I needed to get his advice. Discussions with him always opened my eyes to directions of research I should consider exploring or delve at greater depth. I do not remember ever having left his office without the thought: “Oh, now that is an aspect I had not considered before” crossing my mind.

I am very grateful to Dr. Neil Ward for his advice and support on tackling the seasonal climate prediction section of the dissertation and for guiding me on how to access relevant climate model output datasets. I am very grateful to Dr. Laura Schneider who advised me on the remote sensing section of this dissertation. It was by working with her as a Teaching Assistant and as a Research Assistant that I learned and mastered remote sensing analysis techniques while at Rutgers. I thank her for her patient mentoring and advice. I thank Dr. Ming Xu for useful discussions during the formative stages of the dissertation – particularly related to the influence of the Asian winter monsoon over Sri Lanka and statistical analysis techniques.

My graduate studies and dissertation research at Rutgers were supported in the first two years through Teaching Assistantships awarded by the Department of Geography, and in the third and fourth years through the William H. Greenberg Dissertation Fellowship awarded by the Rutgers Climate and Environmental Change Initiative. A pre-dissertation travel award from the Graduate School-New Brunswick and

discretionary funding from the Chair, Department of Geography, Rutgers facilitated field work in Sri Lanka and helped offset costs of data purchased for the dissertation.

I am very thankful to Mr. K.H.M.S. Premalal and Dr. B.R.S.B. Basnayake, at the Sri Lanka Department of Meteorology, who were extremely helpful in providing me access to essential meteorological datasets for Sri Lanka. Mr. Premalal has, over the last 3 years, also provided helpful feedback and suggestions on my dissertation research. I thank Mr. D.H.P. Dharmwardena (former Director-General, Sri Lanka Department of Meteorology), Ms. Janaki Meegastenna (Sri Lanka Department of Irrigation), Prof. R.B. Mapa (Department of Soil Science, University of Peradeniya, Sri Lanka), Dr. B.V.R. Punyawardena (Agro-climatology Unit, National Resource Management Center, Department of Agriculture, University of Peradeniya, Sri Lanka), and Dr. P. Thenkabail (International Water Management Institute) for useful and leading discussions during the pre-dissertation stage that helped identify gaps in knowledge related to droughts in Sri Lanka.

I thank Ousmane Ndiaye for helping me understand the archival structure of GCM retrospective hindcasts. I thank Zach Christman for advice on extracting and interpreting MODIS QC images.

I thank Robin Rašín, Ramya Kumar and John Mioduszewski who provided comments and proof read drafts of various chapters of the dissertation.

My heartfelt gratitude to Deniz Kustu, Ramya Kumar, Robin Rašín, Imtiaz Rangwala and Kritee, Rosana Grafals-Soto, Patricia Alvarez, Gwangyong Choi, Asher Siebert, Monalisa Chatterjee, John Mioduszewski, Debjani Ghatak, Lisa Ojanen, Kalpana Venkatasubramanian, Hasula Rajapakse, Kanthi Vitarana, Nimanthi Rajasingham, Kari

Burnett, Michelle Martel, Kusala Wettasinghe, Arthur and Janet Askew, Shamala Kumar and Savitri Kumar for their friendship and moral support during my graduate career and particularly during the final “dissertating phase”.

I am very grateful to Betty Ann Abbatemarco, Theresa Kirby, Michelle Martel and Mike Siegel at the Rutgers Department of Geography for administrative, cartographic and essential computing assistance. I also thank Melissa Arnesen, Rutgers Center for Environmental Prediction, who handled administrative and financial matters related to disbursement of the Greenberg fellowship.

I am deeply indebted to my father, my stepmother and my sister and her family for their love and unstinting support throughout the years I have spent in graduate school. My little daughter Kahthi brightened my days particularly during the last few months of intensive dissertating! She was a constant reminder, yet consoling presence, of my other little children far away back home in Sri Lanka.

This dissertation is dedicated to the memory of my mother whose enthusiasm for observing and reading about natural phenomena – be it weather events, geomorphological features, comets or eclipses – greatly influenced my interest in the fascinating field of physical geography.

## Table of Contents

<i>Section</i>	<i>page</i>
Abstract	ii
Acknowledgements and dedication	iv
List of figures	x
List of tables	xvi
<b>Chapter 1: Introduction</b>	<b>1</b>
1.1: Drought in the humid tropics	1
1.2: Drought in Sri Lanka	4
1.3: Knowledge gaps regarding drought in Sri Lanka	12
1.4: Research goal and objectives	14
 <b>Chapter 2: <i>Maha</i> seasonal drought</b>	 <b>16</b>
2.1: Introduction	16
2.2: Methodology and datasets used	16
2.2.1: Drought analysis based on the Standardized Precipitation Index (SPI)	16
2.2.2: Drought return periods	19
2.2.3: Spatial dimension of drought	21
2.2.4: Influence of drought on the <i>Maha</i> season	21
2.2.4.1: Influence of drought on rice production during the <i>Maha</i>	21
2.2.4.2: Influence of the October-November and December-February rains on <i>Maha</i> drought	22
2.2.5: Dominant modes of drought variability and change in such modes over time (Wavelet Transform Analysis), and spatial trends in drought occurrence	23
2.3: Results	29
2.3.1: Drought occurrence	29
2.3.2: Drought return periods	30
2.3.3: Spatial dimension of drought	31
2.3.4: Effect of <i>Maha</i> droughts on rice production and influence of October-November and December-February rainfall on <i>Maha</i> drought	35
2.3.4.1: Effect of <i>Maha</i> droughts on rice production	35
2.3.4.2: Influence of October-November and December-February rainfall on <i>Maha</i> drought:	36
2.3.5: Dominant modes of drought variability and change in such modes over time (Wavelet Transform Analysis), and spatial trends in drought occurrence	39
2.4: Conclusion	48



<b>Chapter 3: Predictability of the October-November season</b>	51
3.1: Introduction	51
3.2: Methodology and datasets used	55
3.2.1: Analysis of atmospheric factors influencing October-November rain failure	55
3.2.1.1: Datasets used	55
3.2.1.2: Analysis method	55
3.2.2: Assessment of the predictability of October-November rain failure	60
3.2.2.1: Datasets used	60
3.2.2.2: Analysis method	62
3.3: Results	63
3.3.1: Atmospheric dynamics driving failure of the October-November rains	63
3.3.2: Predictability of the October-November season	66
3.4: Conclusion	71
<b>Chapter 4: Predictability of the December-February season</b>	73
4.1: Introduction	73
4.2: Methodology and datasets used	76
4.2.1: Analysis of atmospheric factors influencing December-February rain failure	76
4.2.1.1: Datasets used	76
4.2.1.2: Analysis method	77
4.2.2: Assessment of the predictability of December-February rain failure	78
4.2.2.1: Datasets used	78
4.2.2.2: Analysis method	78
4.3: Results	78
4.3.1: Atmospheric dynamics driving the failure of December-February rainfall	78
4.3.2: Predictability of the December-February season	82
4.4: Conclusion	88
<b>Chapter 5: Monitoring moisture conditions on the ground in near-real time</b>	90
5.1: Introduction	90
5.2: Methodology and datasets	95
5.2.1: Generating the Vegetation Temperature Condition Index (VTCI) for the two seasons	95

5.2.2: Datasets used	97
5.3: Results	100
5.3.1: VTCI analysis for October-November	100
5.3.2: VTCI analysis for the entire Maha season	107
5.4: Conclusion	114
<b>Chapter 6: Conclusion</b>	116
<b>Annexures</b>	
1. Modifications made to original Matlab Code for Wavelet Transform Analysis	125
2. Sri Lanka rice production statistics 1952-2009	130
3. List of identification numbers of original MODIS imagery analyzed in Chapter 5	132
<b>References</b>	137
<b>Curriculum Vitae</b>	146

## List of Figures

### Chapter 1: Introduction

<b>Figure 1.1:</b> Location of Sri Lanka	4
<b>Figure 1.2:</b> Cultivation seasons in Sri Lanka and associated rainfall regime. The yellow box highlights the main cultivation season known as the <i>Maha</i> .	6
<b>Figure 1.3:</b> Distribution of rice fields and the “Dry Zone” and “Wet Zone” delineated by the 2000mm isohyet (thick blue line). The isohyets were obtained by interpolating annual average rainfall from 1971-2000 at a 132 rain gauges (red dot) used in the study.	7
<b>Figure 1.4:</b> Elevation map generated using the ASTER 30m resolution digital elevation model (DEM) product.	8
<b>Figure 1.5(a):</b> Spatial distribution of rainfall during the first inter-monsoon from March-April (i), during the southwest monsoon (May to September) and the first month of the second inter-monsoon (October) (ii) (Adapted from Wickramagamage, 2009, Figure 3(a) and 3(b), pp 6)	9
<b>Figure 1.5(b):</b> Spatial distribution of rainfall during the second month of the second inter-monsoon (November) (i) and during the northeast monsoon (December-February) (ii) (Adapted from Wickramagamage, 2009, Figure 3(c) and 3(d), pp 7)	10

### Chapter 2: *Maha* seasonal drought

<b>Figure 2.1:</b> District boundaries (data source: <a href="http://www.iwmidsp.org">http://www.iwmidsp.org</a> )	20
<b>Figure 2.2:</b> Location of stations with long precipitation records used to generate wavelet transforms of <i>Maha</i> drought time series.	28
<b>Figure 2.3:</b> Mean drought occurrence during the period 1951-2008 derived by calculating the 6-monthly Standardized Precipitation Index (SPI) on district-wise interpolated rainfall data.	30
<b>Figure 2.4:</b> Drought severity category at district level for the extreme drought events of (clockwise from top left) 1976, 2000, 2001 and 2002. Colour coding is by severity level with dark orange indicating “extreme” drought, light orange indicating “mild” drought and white indicating “non-drought”.	32
<b>Figure 2.5:</b> Drought severity categories at district level for the 2003 “severe” drought event	33

<b>Figure 2.6:</b> Districts affected by moderate droughts in (clockwise from left) 1956, 1980, 1983 and 2005	34
<b>Figure 2.7:</b> Detrended total Maha production and yield per hectare versus 6-monthly SPI (October)	36
<b>Figure 2.8:</b> ON standardized anomalies (solid bright blue line) and DJF standardized anomalies (broken light blue line) plotted against 6-month SPI (solid orange bars) for October for the period 1961-2005.	35
<b>Figure 2.9:</b> Standardized anomalies of ON (a) and DJF (b) rainfall in 2002. Blue circles indicate negative anomalies and red circles indicate positive anomalies	35
<b>Figure 2.10 (a):</b> Wavelet Transform for Trincomalee where the predominant frequency is 2-8 years. The top panel is the original SPI time series. The second panel is the Wavelet Power Spectrum (WSP) with frequencies significant at the 95% confidence level contoured in bold. The thin curved line running from left to right in the WSP is the Cone of Influence (COI) indicating the region below which edge effects distort results. The right box is the Global Wavelet Spectrum where the broken line indicates the 95% confidence level. Frequencies below the dashed line are the significant spectral peaks in the time series. The bottom panel shows the scale-average wavelet power (expressed as SPI variance) – where the scale is selected based on significant frequency bands identified from the WSP.	38
<b>Figure 2.10 (b):</b> Same as in 2.10(a) but for Hambantota	39
<b>Figure 2.10 (c):</b> Same as in 2.10(a) but for Jaffna	40
<b>Figure 2.10 (d):</b> Same as in 2.10(a) but for Kandy	41
<b>Figure 2.11 (a):</b> Same as in Figure 2.10 but for Galle where the predominant frequency band is 16-32 years	42
<b>Figure 2.11(b):</b> Same as in Figure 2.11(a) but for Colombo	43
<b>Figure 2.11 (c):</b> Same as in Figure 2.11(a) but for Negombo	44
<b>Figure 2.11 (d):</b> Same as in Figure 2.11(a) but for Mannar	45
<b>Figure 2.12:</b> Dominant wavelet frequencies at stations used in wavelet transform analysis	46

**Figure 2.13:** Interpolated map of trend in 6-month SPI for October at the 132 rain gauges. Orange depicts an increase in drought and blue depicts a decrease in drought. Trend values show changes in units of SPI per year. 47

### Chapter 3: Predictability of the October-November season

**Figure 3.1:** Mean 850hPa wind field over Sri Lanka for October, November, December, January and February from NCEP-NCAR reanalysis data for 1951-2005 54

**Figure 3.2:** Correlation between zonal winds at 850hPa and mean ON rainfall over Sri Lanka. Broken lines show regions negatively correlated, and solid lines show regions positively correlated, with ON rainfall. Blue (negative correlation) and orange (positive correlation) shading depict correlation significant at the 95% confidence level. The contour interval is 0.2 correlation units. 59

**Figure 3.3:** Temporal composites of the October-November U850 field (left) and associated negative anomalies in mean ON rainfall over Sri Lanka in years when ON rainfall failed (right) 63

**Figure 3.4:** Temporal composites of October-November anomalies of the vertical shear of the zonal wind (a), vertical velocity at 500hPa (b) and relative vorticity at 850hPa (c) in years when ON rainfall failed 64

**Figure 3.5:** Mean October-November U850 for the domain 5°S-15°N and 60°E-105°E (yellow bars); mean SOI for September-November (red line); the Indian Ocean Dipole mode index (dashed green line) calculated as the standardized difference between the spatial mean SST over the western (50°E-70°E and 10°S-10°N) and eastern (90°E-110°E and 10°S-0°S) Indian Ocean (Vinayachandran et al., 2002); and years when ON rainfall anomalies were negative (black circles above yellow bars) 65

**Figure 3.6:** Leading canonical modes and associated temporal scores of the spatial loadings for the ECHAM4.5\_PSST (a); the ECHAM4.5\_CA (b); and the CFS (c). Red in the spatial loadings of U850 spatial loadings and ON rainfall anomalies indicates positive anomalies and blue indicates negative anomalies. The red line in the temporal scores depicts the predictor and the green line depicts the predictand. 67

**Figure 3.7:** Pearson's correlation skill maps for the ECHAM4.5\_PSST (a); the ECHAM4.5\_CA (b); and the CFS (c). Contour interval is 0.1 correlation units. Correlation values significant at the 95% confidence level are depicted as solid black lines and correlation values significant at the 99% confidence level are depicted as solid red lines. 68

**Figure 3.8:** Examples of predicted (from ECHAM4.5\_PSST) versus observed rainfall at rain gauge stations with an average Hit Skill Score (a) and at a station with a Hit Skill Score in the 90<sup>th</sup> percentile (b). Filled orange circles in the map of rain gauge stations (right) show the location of the stations selected randomly. 69

**Figure 3.9:** Tercile probability forecasts of ON rainfall in 2001 generated from the CFS depicting the above-normal (a), near-normal (b) and below-normal (c) categories. Blues indicates lower probabilities and reds indicate higher probabilities. 71

## Chapter 4: Predictability of the December-February season

**Figure 4.1:** Plot of standardized anomalies of mean DJF rainfall (blue bar) at a 132 rain gauges versus August-September (ASO) mean value of the Southern Oscillation Index (SOI) (red line) for the period 1961-2005. Values on the y-axis are units of standardized anomalies. 75

**Figure 4.2:** Temporal composites of the December-February  $V_s$  field (left) and associated negative anomalies in mean DJF rainfall over Sri Lanka in the drought years 1976, 1980, 1984, 1986, 1996, 2001 and 2003 when DJF rainfall was below normal. Blues indicate negative  $V_s$  anomalies and reds indicate positive anomalies. 79

**Figure 4.3:** Mean December-February wind vector at 850hPa in drought years (a) and mean DJF wind vector (1961-2004) (b). Red square in (a) denotes region where the wind stream weakens in drought years. 80

**Figure 4.4:** Same as in 4.2 but for the domain 40<sup>0</sup>E-270<sup>0</sup>E and 30<sup>0</sup>S-65<sup>0</sup>N. Blues indicate negative  $V_s$  anomalies and red indicate positive anomalies. The black box encloses the broad region of reduced  $V_s$ . 80

**Figure 4.5:** Leading canonical modes and associated temporal scores of the spatial loadings for the ECHAM4.5\_CA (a); the ECHAM4.5\_PSST (b); and the CFS (c). Red in the spatial loadings of  $V_s$  and DJF rainfall anomalies indicates positive anomalies and blue indicates negative anomalies. The red line in the temporal scores depicts the predictor and the green line depicts the predictand. 84

**Figure 4.6:** Pearson's correlation skill maps for the ECHAM4.5\_CA. Contour interval is 0.05 correlation units. Correlation values significant at the 95% confidence level are depicted as solid black lines and correlation values significant at the 99% confidence level are depicted as solid red lines. Broken blue lines depict values of negative correlation. Thin grey lines depict positive correlation values that are not statistically significant. 85

**Figure 4.7:** Examples of predicted (from ECHAM4.5\_CA) versus observed rainfall at rain gauge stations with an average Hit Skill Score (a) and at a station with a Hit Skill Score in the 90<sup>th</sup> percentile (b). Filled orange circles in the map of rain gauge stations (right) show the location of the stations selected randomly. 86

**Figure 4.8:** Tercile probability forecasts of DJF rainfall in 2001 generated from the ECHAM4.5\_CA depicting the above-normal (a), near-normal (b) and below-normal (c) categories. Blues indicates lower probabilities and reds indicate higher probabilities. 87

## Chapter 5: Monitoring moisture conditions on the ground in near-real time

**Figure 5.1:** Schematic of the LST-NDVI scatterplot depicting the physical interpretation of the VTCI (Adapted from Wan et al., 2004, Figure 1, pp 65) 93

**Figure 5.2:** Two tiles of the MODIS MOD11A2 day time LST product for the period 7 September to 14 October 2000 97

**Figure 5.3:** Two tiles of the MODIS MOD13A2 day time NDVI product for the period 29 September to 14 October 2000 98

**Figure 5.4:** Observed (a) and predicted (b) standardized anomalies of October-November rainfall in 2000. VTCI images for early-October 2000 (c), late-October 2000 (d), early-November 2000 (e) and late-November 2000 (f). 102

**Figure 5.5:** Observed (a) and predicted (b) standardized anomalies of October-November rainfall in 2001. VTCI images for early-October 2001 (c), late-October 2001 (d), early-November 2001 (e) and late-November 2001 (f). 103

**Figure 5.6:** Observed (a) and predicted (b) standardized anomalies of October-November rainfall in 2002. VTCI images for early-October 2002 (c), late-October 2001 (d), early-November 2002 (e) and late-November 2002 (f). 104

**Figure 5.7:** Observed (a) and predicted (b) standardized anomalies of October-November rainfall in 2004. VTCI images for early to mid-October 2004 (c) and late-November 2004 (d). 105

**Figure 5.8:** Observed (a) and predicted (b) standardized anomalies of October-November rainfall in 2005. VTCI images for early-October 2005 (c), late-October 2005 (d) and late-November 2005 (e). 106

**Figure 5.9:** Observed (a) and predicted (b) standardized anomalies of October-November rainfall in 2003. VTCI images for early-October 2003 (c), late-October 2003 (d), and mid-November 2003 (e). 108

**Figure 5.10:** Observed (a) and predicted (b) standardized anomalies of December-February rainfall in 2003. VTCI images for early-December 2003 (c), late-December 2003 (d), early-January 2003 (e), late-January 2003 (f), early-February 2003 (g), and late-February 2003 (h). 110

**Figure 5.11:** Examples of VTCI images and relevant MODIS Quality Control (QC) images for late-October 2003 (left panel) and early-December (right panel). Left panel: VTCI image for late-October (a); LST QC (b); NDVI QC (c) and Combined QC mask (d) prepared by intersecting raster masks of ‘Good Quality’ pixels extracted from the LST QC and NDVI QC images. Right panel: same as for left panel but for early-December. 111

**Figure 5.12:** Time series of VTCI presented for three locations in the four districts affected by extreme drought (dark orange) in 2003 (a). Top right (b) is an image created by stacking the nine images used to study the entire Maha season in 2003 and extracting the cells falling within the districts affected by extreme drought. The display shows three of the nine images. The yellow squares are the areas-of-interest (AOIs) selected to plot VTCI values at each time step. Reds indicate higher VTCI (wetter) values and blues and greens indicate lower VTCI (drier) values in the three images used in the display. The lower plot (c) shows mean VTCI values within each AOI from early-October to late-February. The numerals 1-9 along the x-axis indicate each VTCI image stacked in chronological order from early-October (1) through late-February (9). 113



## **List of Tables**

### **Chapter 2: *Maha* seasonal drought**

**Table 2.1:** Names and location for stations used in Wavelet Transform analysis 28

**Table 2.2:** Drought return periods calculated using non-exceedance probability 30

**Table 2.4:** Rainfall anomalies associated with each drought event 37

### **Chapter 3: Predictability of the October-November season**

**Table 3.1:** Summary of tercile probability forecasts of ON rainfall from the two versions of the ECHAM4.5 and the CFS. BN refers to below-normal and AN refers to above-normal. 70

### **Chapter 4: Predictability of the December-February season**

**Table 4.1:** Summary of tercile probability forecast of DJF rainfall from the ECHAM4.5\_CA. BN refers to below-normal. 87

### **Chapter 5: Monitoring moisture conditions on the ground in near-real time**

**Table 5.1:** VTCI images produced and LST and NDVI composites used for each VTCI image 96

## Chapter 1: Introduction

### 1.1: Drought in the humid tropics

Droughts like floods are natural extremes of the hydrological cycle. Droughts are “creeping” phenomena with no clearly distinguishable onset or end. Their impacts are spread over a much larger area than other natural hazards (Wilhite, 1996). With the likely increase in extreme events due to climate change (Parry et al., 2007), there is a greater need for the explicit understanding of how droughts currently affect different parts of the globe. Such understanding is essential not only to design drought adaptation measures appropriate to a given location under future scenarios of drought but also to design and implement adaptive measures to cope with drought in the present day, as drought is a recurrent phenomenon.

Drought is a condition of insufficient moisture caused by a deficit in precipitation over time (McKee, et al., 1993). It is distinct from aridity or seasonal aridity as found in locations with a distinct dry season (WMO, 2006). A universal definition of drought does not exist and any study on drought requires a functional definition of drought accounting for drought duration, magnitude, intensity and frequency<sup>1</sup> – all aspects intrinsically linked to timescale (McKee et al., 1993).

This dissertation focuses on droughts that occur in the humid tropics. The humid tropics are regions of the Earth under the rising limb of the Hadley Cell stretching on average from 30<sup>0</sup>S to 30<sup>0</sup>N. Convection associated with the north-south migration of the Inter-tropical Convergence Zone (ITCZ) and monsoonal troughs provide rainfall to the

---

<sup>1</sup> **Drought duration** is the time period in which precipitation or any other form of usable water source (e.g. soil moisture, groundwater, snow pack, streamflow or reservoir storage (McKee, et al., 1993)) remains below average; **drought magnitude** is: “the deviation from a threshold value” (Sheffield and Wood, 2007); **drought intensity** is: “the mean magnitude over the duration” (Sheffield and Wood, 2007); and **drought frequency** is the number of drought events within a given timescale.

humid tropics. The high inter-annual variability in the strength and location of the ITCZ and the monsoon troughs results in the humid tropics experiencing a high inter-annual variability in rainfall (Stahl and Hisdal, 2006) and hence soil moisture. High inter-annual variability in soil moisture results in higher drought intensities in the humid tropics compared to other regions of the globe (Sheffield and Wood, 2007). A majority of the world's population resides in countries located within the humid tropics where rice is the staple food crop cultivated. Rice is a crop with a high water demand. Water stress during the growing and maturing phases of a cropping season can have a devastating impact on rice production. Droughts, therefore, affect food security in countries in the humid tropics. Droughts also have dramatic impacts on the livelihoods of people in locations such as the densely populated tropical regions of South Asia where agriculture is the main livelihood (Stahl and Hisdal, 2006).

Drought, unlike other hydro-meteorological hazards such as flooding, often has a gradual onset. Thus, there is sufficient lead time in most cases to initiate drought adaptation measures. Drought adaptation is contingent on the existence of a drought prediction and early-warning system. Identifying factors causing drought provides the basis for the design of such a drought prediction and early-warning system.

Droughts occur due to a combination of reasons including: the failure of seasonal rainfall; local factors such as land cover change that exacerbate an initial deficiency in water availability on the ground; and significant shifts in mean climatic conditions.

The failure of seasonal rainfall is the key driver of recurrent drought in the humid tropics. Therefore, this dissertation focuses primarily on understanding factors controlling the failure of seasonal rainfall with the aim of proposing a drought forecasting

methodology applicable to locations in the humid tropics. It recognizes the critical importance of the two other factors in determining the overall magnitude of drought at a given location. Delving into the finer details of either land change or global change-induced shifts in mean climatic conditions is beyond the scope of the dissertation and will be addressed in detail in future studies.

Seasonal rainfall failure may be attributed to factors driving seasonal climate variability. The overall strength of the seasonal cycle is a result of the interaction of processes active at intraseasonal (30-90 days), interannual to multi-decadal timescales. Foremost among factors influencing seasonal climate variability are boundary conditions such as sea surface temperatures (SSTs) and land surface characteristics. The surface boundary layer has a relatively longer time scale of variability and thus allows for predictability that extends to the seasonal time scale – i.e. a few months. Such an extended range of predictability is believed to exist due to atmospheric-oceanic-land coupling (Palmer, 1993). Anomalous boundary conditions can produce statistically significant anomalies in the seasonal mean atmospheric circulation. Such anomalous boundary conditions are more influential in the tropics than in the midlatitudes (Shukla and Kinter, 2006). If such boundary conditions and associated climate impacts are predictable, skillful seasonal climate forecasts may be generated (Goddard et al., 2001).

The primary mode of seasonal predictability in the tropics is the El Niño Southern Oscillation (ENSO) (Hastenrath, 1995). Many studies have attempted to characterize the influence of ENSO on droughts over the Indian subcontinent (Kumar et al., 2006; Rajeevan and Pai, 2007). All such studies have focused on droughts associated with the failure of the Indian summer monsoon. There is a noticeable dearth of studies looking at

droughts caused by the failure of the winter monsoon over South Asia and the failure of convective rainfall regimes in equatorial regions.

## 1.2: Drought in Sri Lanka

*“The occurrence of dry spells and droughts would not normally be expected to be a feature of the weather of a tropical island. However, prolonged periods of dry, or at least relatively dry, weather are not uncommon in Sri Lanka.....” (Jayamaha, 1975).*

Drought, as the above quote reflects, is not an uncommon phenomenon in Sri Lanka located southeast of the Indian subcontinent between 5°55'-9°50'N and 79°42'-81°53' (Fig. 1.1).. It is a frequent occurrence that has been documented since ancient times (Maddumabandara, 1982; and Basnayake, 1990).

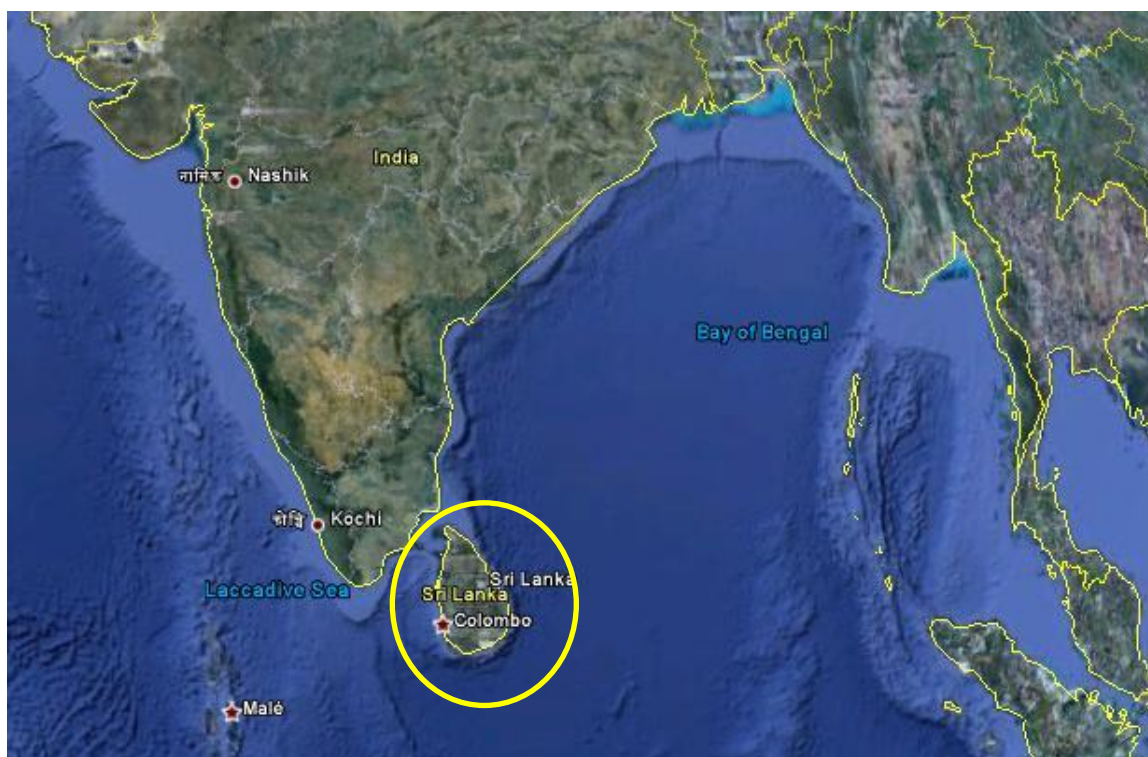


**Figure 1.1:** Location of Sri Lanka

Droughts in Sri Lanka occur when the precipitation regime associated with the *Maha* cultivation season fails. The *Maha* is the main rice cultivation season in the country that lasts from October to March in a given year. These droughts have durations of 6 to 9 months (Lyon et al., 2009) and are, thus, typical of droughts in the humid tropics where drought duration is normally 6 months (Sheffield and Wood, 2007). Multi-year droughts are rare but have taken place (Basnayake, 1990).

The dissertation uses Sri Lanka as a case study as it is a representative example of a location in the humid tropics that is frequently subject to droughts. It also has a dense network of over 300 rain gauges with quality-controlled rainfall data. Some of these rainfall records extend as far back as 1870. Furthermore, certain aspects of the geography of Sri Lanka – including marked topographical variations, proximity to the equator, and location in the central Indian Ocean – add interesting dimensions to the study of drought there.

Proximity to the equator results in there being four distinct rainfall seasons over the country: the first inter-monsoon (March-April); the southwest monsoon (May to September); the second inter-monsoon [October-November (ON)] and the northeast monsoon [December to February (DJF)]. The second inter-monsoon and the northeast monsoon are the two rainfall regimes that provide critical moisture during the *Maha* (Fig. 1.2).

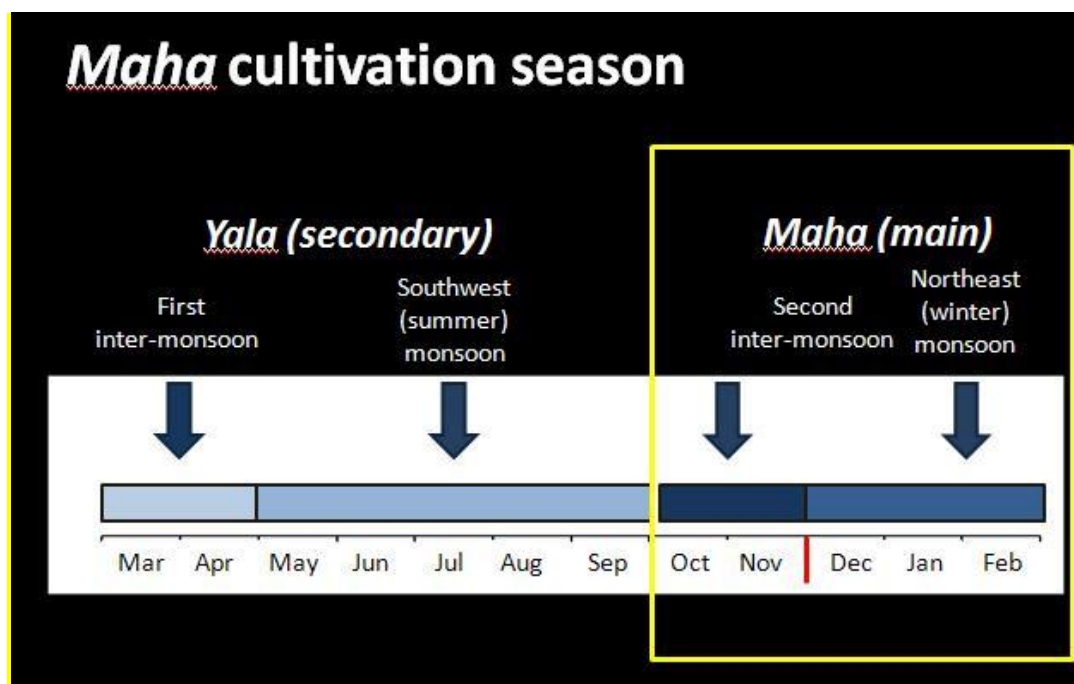


**Figure 1.2:** Cultivation seasons in Sri Lanka and associated rainfall regime. The yellow box highlights the main cultivation season known as the *Maha*.

Mean *Maha* rainfall is 1160mm (with a standard deviation of 260mm), with a mean ON rainfall of 590mm (standard deviation - 140mm) and mean DJF rainfall of 480mm (standard deviation - 190). The failure of either or both of these regimes leads to drought, particularly over the northern, north-central, and southeastern portions of the island. These areas fall within the “Dry Zone” – often delimited by the 2000mm isohyet – of the country (Domrös, 1974; Yoshino and Suppiah, 1984) that covers approximately 65% of the land mass. Rice is the main crop cultivated, and approximately 75% of the country’s rice fields are located, in the “Dry Zone” (Fig. 1.3). This zone experiences a dry season during the months of May to September when the southwest monsoon (Indian summer monsoon) is in swing due to the rain shadow effect of the central highlands of Sri Lanka. The central highlands extend up to 2800m (Fig. 1.4) and have a significant impact on the spatial distribution of rainfall across the island [Fig. 1.5(a) and (b)]. The

dry season is an annual occurrence. It does not result from the failure of seasonal rainfall and, therefore, cannot be considered as seasonal drought.

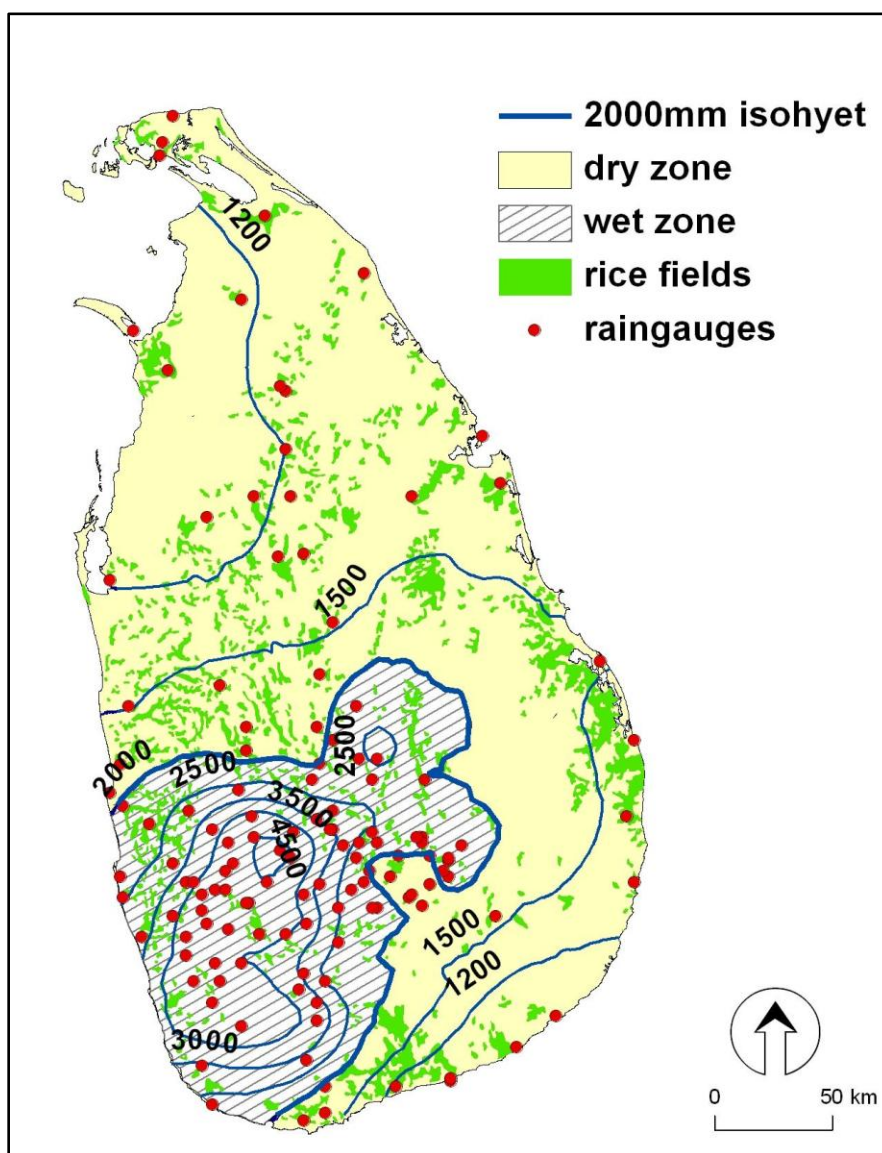


**Figure 1.3:** Distribution of rice fields and the “Dry Zone” and “Wet Zone” delineated by the 2000mm isohyet (thick blue line). The isohyets were obtained by interpolating annual average rainfall from 1971-2000 at a 132 rain gauges (red dot) used in the study.



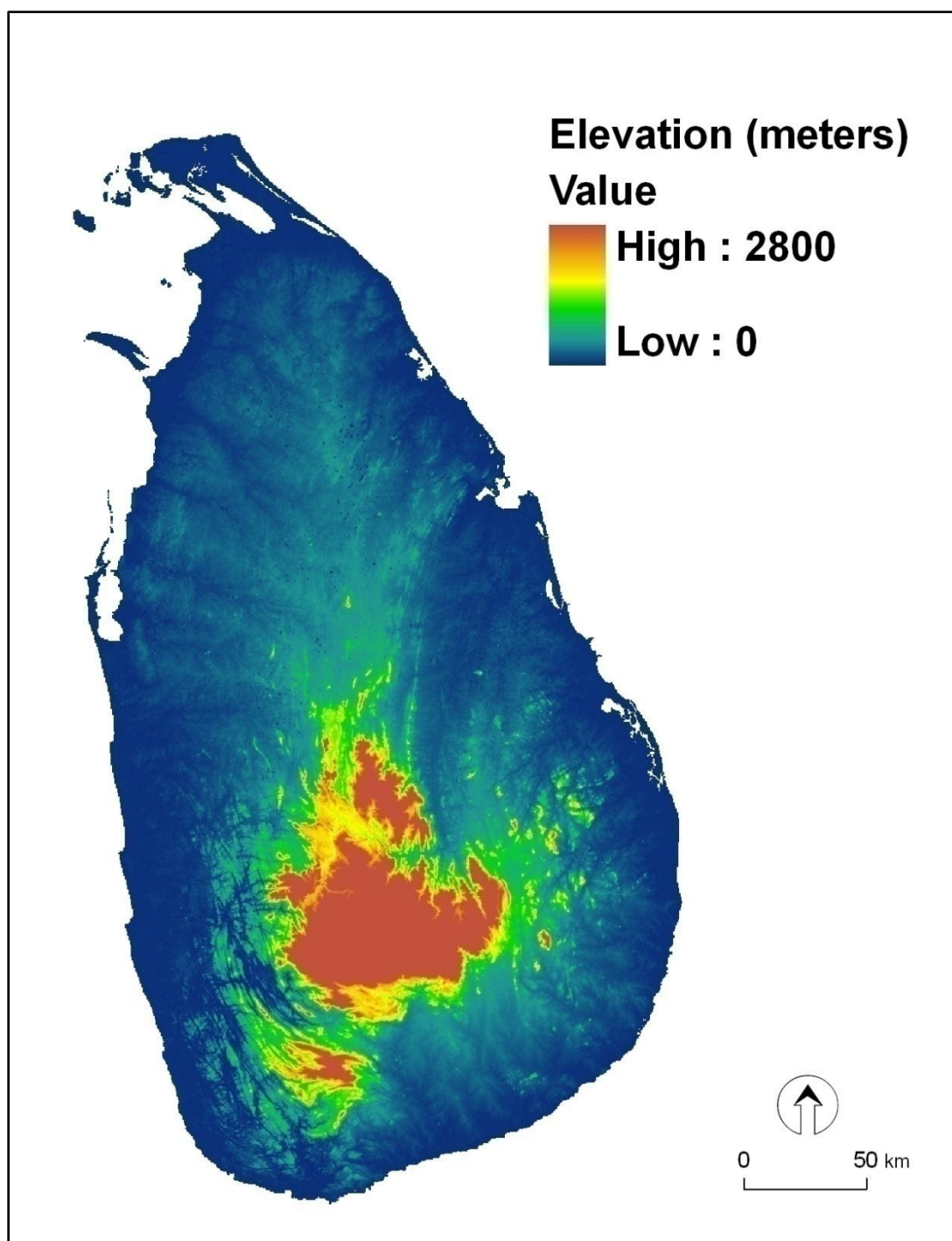


**Figure 1.4:** Elevation map generated using the ASTER 30m resolution digital elevation model (DEM) product.

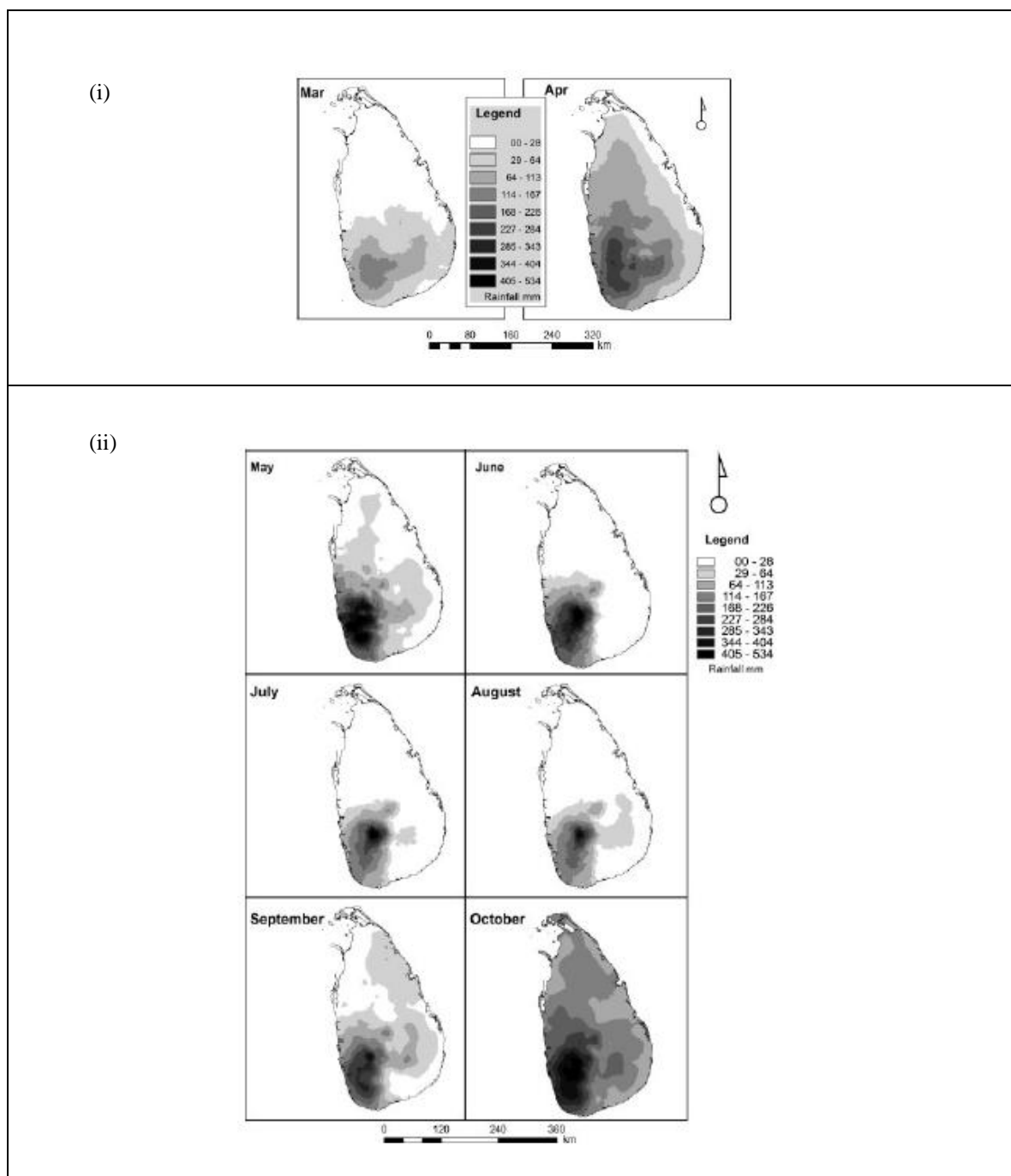


**Figure 1.5(a):** Spatial distribution of rainfall during the first inter-monsoon from March-April (i), during the southwest monsoon (May to September) and the first month of the second inter-monsoon (October) (ii) (Adapted from Wickramagamage, 2009, Figure 3(a) and 3(b), pp 6)

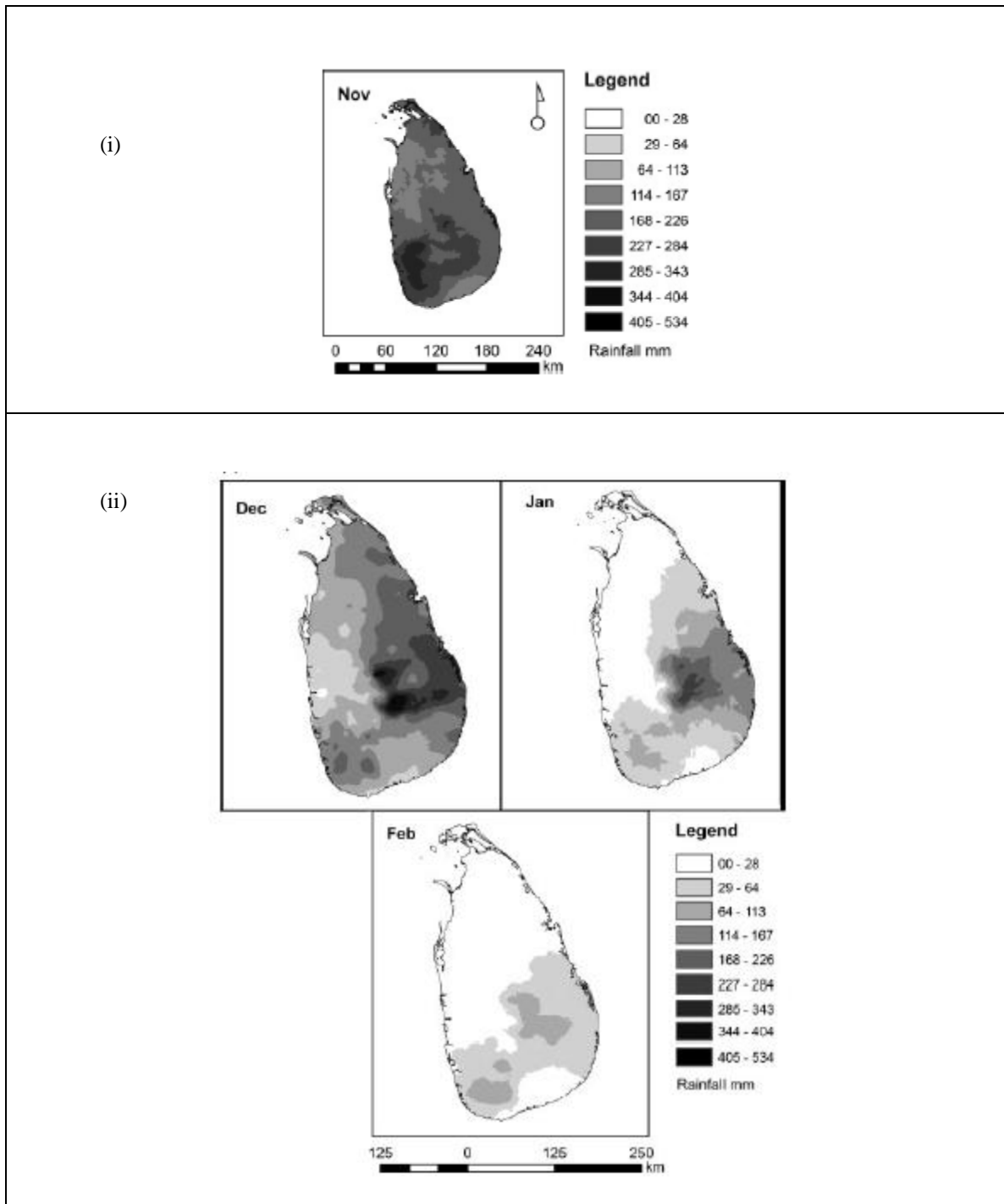


**Figure 1.5(b):** Spatial distribution of rainfall during the second month of the second inter-monsoon (November) (i) and during the northeast monsoon (December-February) (ii) (Adapted from Wickramagamage, 2009, Figure 3(c) and 3(d), pp 7)

Sri Lanka's location in the central Indian Ocean makes it a good test bed to contribute to ongoing research efforts in the region because the central Indian Ocean is a “happening” ocean basin – both in terms of the observed increased warming in ocean temperatures over the last three decades, and in terms of increased efforts underway in the climate and oceanography communities to better understand coupled ocean-atmospheric processes at work there.

Although regular, drought occurrence over Sri Lanka exhibits no clear periodicity. It thus poses a challenge to seasonal crop planning, irrigation scheduling and hydropower generation. Knowing in advance the likelihood of whether a forthcoming season could be affected by drought is essential for planning adaptive measures – particularly for drought-sensitive crops like rice. Such knowledge needs to be generated through a characterization of past drought occurrence – including frequency, intensity and return periods – and an assessment of factors that induce drought. Seasonal forecasts of precipitation expected during a forthcoming *Maha* season could be utilized for drought prediction in Sri Lanka. Key decisions on what to plant during the *Maha* season are made at a seasonal conference convened in September each year by the Sri Lanka Department of Agriculture. If seasonal forecasts of rainfall expected during a forthcoming *Maha* season could be made in time for the September seasonal conference, they could aid decisions in drought preparedness and adaptation, particularly in the agriculture sector.

### **1.3: Knowledge gaps regarding drought in Sri Lanka**

Several recent studies have characterized the influence of ENSO on rainfall over Sri Lanka (Rasmusson and Carpenter, 1983; Suppiah, 1996; Zubair et al., 2007). Others have addressed the influence of Indian Ocean sea surface temperatures (SSTs) and the Indian Ocean Dipole (IOD) Mode (Li et al., 2003; Saji and Yamagata, 2003) on rainfall over Sri Lanka (Malmgren et al., 2007; Zubair et al., 2003). These studies have not specifically delved into the predictability of drought or other climate extremes. Their focus has consistently been to explain the influence of various teleconnection mechanisms on the inter-annual variability of precipitation over Sri Lanka. Studies on the seasonal predictability of rainfall over Sri Lanka are limited and have focused primarily on ENSO-driven predictability (e.g. Suppiah, 1989; Zubair et al., 2007). These investigations provide invaluable insight into some of the atmospheric processes influencing seasonal rainfall. However, they are not directly applicable to operational planning due to two reasons. First, the predictor fields – most often SSTs in the Nino3.4 region, the Southern Oscillation Index (SOI)<sup>2</sup> or the IOD mode index – do not account for all the variance in seasonal rainfall and their associated empirical relationships are not constant through time. Second, past studies on the predictability of seasonal rainfall over Sri Lanka have considered the months October to December (OND) as comprising a single season – often referring to it as the northeast monsoon season (Zubair and Ropelewski, 2006; Zubair et al., 2007). Critical information on processes influencing a particular rainfall season is lost if different seasons are clustered together.

This dissertation differs from prior studies by identifying critical factors that control the strength of the October-November and December-February rainfall seasons

---

<sup>2</sup> The SOI is the difference in mean sea level pressure between Tahiti and Darwin (Walker and Bliss, 1932)

with the explicit aim of assessing the predictability of rain failure and, hence, drought over Sri Lanka. Such an investigation has not been undertaken before.

While seasonal precipitation forecasts provide an indication of whether an oncoming season in its entirety is likely to be susceptible to drought, they cannot provide information on how moisture stress might evolve on the ground as the season progresses. Farmers, agricultural extension officers and other decision-makers in the agriculture and irrigation sectors in Sri Lanka need information on where moisture stress, and hence drought, may be setting in, to launch protective measures such as mulching or increasing releases of irrigation water. Therefore, drought prediction must be complemented with a spatially explicit real or near-real time monitoring of moisture stress at the ground. Remote sensing techniques could be utilized to monitor the onset, progression and spatial variability of moisture stress. This dissertation tests the applicability of the Vegetation Temperature Condition Index (VTCI) (Wang et al., 2001; Wan et al., 2004a) that combines vegetation indices (derived from remotely sensed data in the optical wavelengths) with land surface temperature (derived from remotely sensed data in the thermal infrared wavelengths) to monitor moisture stress on the ground in Sri Lanka. The technique has not previously been applied to monitor moisture stress in Sri Lanka.

#### **1.4: Research goal and objectives**

The study demonstrates a methodology that combines seasonal climate forecasting with remote sensing so that the spatial characteristics of drought onset and progression are identified at a scale useful for the implementation of drought adaptation measures. The study will contribute to understanding atmospheric circulation patterns that drive drought over Southeastern India and Sri Lanka. It contributes to enhancing current capacity to predict rainfall during the inter-monsoonal and northeast (winter) monsoonal seasons, and to improving drought early warning capacity in Sri Lanka. In the long-term it will inform drought preparedness and drought adaptation measures in the country. The specific research objectives of the study are to:

- Characterize drought occurrence in Sri Lanka over the last 6 decades
- Develop a methodology for predicting drought in Sri Lanka based on seasonal climate forecasts
- Develop a methodology to monitor seasonal moisture stress in near-real time during the *Maha* cultivation season.

The dissertation has three major research thrusts based on the above research objectives. The first thrust, covered in Chapter 2, characterizes *Maha* seasonal drought occurrence by addressing the following specific research questions: 1) How frequently has drought affected the *Maha* cultivation season during the period 1951-2008? 2) What are the return periods of different categories of drought? 3) What regions of Sri Lanka are particularly vulnerable to drought? 4) How does *Maha* drought affect rice cultivation and how do the October-November rains and the northeast monsoon (December-February) over Sri Lanka influence *Maha* drought? 5) What are the dominant modes of drought

variability, how do such modes vary over time, and is there any spatial trend in drought occurrence?

The second research thrust, covered in Chapters 3 and 4, proposes a methodology for predicting drought in Sri Lanka by addressing the following specific research questions: 1) What atmospheric factors drive the failure of the October-November (Chapter 3) and December-February (Chapter 4) rains? 2) Can seasonal forecasts from Global Climate Model (GCM) ensembles be used to predict the failure of October-November and December-February rainfall?

The third research thrust, covered in Chapter 5, proposes a methodology to monitor moisture stress in near-real time during the Maha season by addressing the following specific research questions: 1) Does the Vegetation Temperature Condition Index (VTCI) capture drought progression during the early-Maha (October-November) season for the period? and 2) Can the VTCI be applied to monitor drought progression through the entire Maha season?

The datasets and methodologies used to address the research questions listed above are explained in the chapters covering each research thrust. Key results are presented at the end of each chapter. A summary of all the results, their wider implications and future research directions are presented in Chapter 6.



## Chapter 2: Maha seasonal drought

### 2.1: Introduction

The objectives of this chapter are: to characterize past *Maha* seasonal droughts; and to characterize the influence of the ON and DJF rains on such droughts.

The specific research questions addressed by this chapter are: 1) How frequently has drought affected the *Maha* season? 2) What are the return periods of the different drought categories? 3) What regions of Sri Lanka are particularly vulnerable to drought? 4) How does *Maha* drought affect rice cultivation and how do the October-November rains and the northeast monsoon (December-February) over Sri Lanka influence *Maha* drought?, and, 5) What are the dominant modes of drought variability, how do such modes vary over time, and is there a spatial trend in drought occurrence?

### 2.2: Methodology and datasets used

#### 2.2.1: Drought analysis

##### *Analysis method:*

The Standardized Precipitation Index (SPI)<sup>3</sup> (McKee et al., 1993) is the metric used to identify drought incidence in this study. The SPI can be calculated for a variety of timescales ranging from 1-, 3-, 6-, 12- to 24-months (McKee et al., 1993, Guttman, 1999, Quiring, 2009). The 6-monthly timescale was selected for this study as droughts in the humid tropics, and in Sri Lanka, have a typical duration of 6 months (Section 1.2, Chapter 1). Calculation of the SPI requires the selection of a probability density function (PDF) that fits historical precipitation observations (Guttman, 1999). The selected PDF

---

<sup>3</sup> The Standardized Precipitation Index (SPI) has been recommended as the index that national meteorological and hydrological services across the world should use to characterize meteorological drought (Castillo, 2009).

is used to normalize precipitation at a given location. The normalized value of precipitation is the SPI value for the given location.

The gamma ( $\Gamma$ ) distribution is flexible at representing a variety of precipitation distributions and is thus commonly used to calculate SPI (Husak et al., 2007). It is defined by the following probability density function:

$$f(x) = \frac{x/\beta^{\alpha-1} \exp(-x/\beta)}{\beta\Gamma(\alpha)}, \quad x, \alpha, \beta > 0 \quad (\text{Eq. 2.1})$$

Where,

$$\Gamma(k) = \int_0^{\infty} t^{\alpha-1} e^{-t} dt \quad (\text{Eq. 2.2})$$

and  $\alpha$  = shape parameter;  $\beta$  = scale parameter and  $x$  = precipitation

The parameters of shape and scale needed to estimate the gamma function are obtained from the historical precipitation record using a Maximum Likelihood Estimator (Husak et al., 2007). The shape estimator is expressed as:

$$\alpha = \frac{1 + \sqrt{4 + D/3}}{4D} \quad (\text{Eq. 2.3})$$

Where,

$$D = \ln(\bar{x}) - \frac{1}{n} \sum_{i=1}^n \ln(x_i) \quad (\text{Eq. 2.4})$$

Where,  $\bar{x}$  = sample mean;  $n$  = number of observations

The scale estimator is derived such that:

$$\beta = \frac{\bar{x}}{\alpha} \quad (\text{Eq. 2.5})$$

The gamma function needs to be evaluated numerically (Wilks, 2006, pp 78). Therefore, the SPI program available through the National Drought Mitigation Center, University of Lincoln-Nebraska (<http://drought.unl.edu/monitor/spi.htm>) was used to calculate SPI. The program permits the specification of timescale for which the SPI should be calculated. As droughts in Sri Lanka are typically of 6-month duration, 6-month SPI values were calculated for each data point. SPI values for the month of October were then extracted for further analysis.

For the purposes of this study, drought is defined as instances when the SPI over a 6-month period is greater than one standard deviation below the mean. The thresholds for categories of drought are: extreme drought ( $SPI < -2.0$ ), severe drought ( $-1.9 < SPI < -1.5$ ) and moderate drought ( $-1.49 < SPI < -1.0$ ). The category of mild drought ( $-0.99 < SPI < -0.5$ ) is also considered for the purposes of characterizing all drought events that have taken place during the period of analysis.

#### ***Data used for SPI calculation:***

A district<sup>4</sup>-wise (Fig. 2.1) interpolated monthly precipitation dataset from 1951-2008 was used for SPI calculation. The dataset is a new product generated by the Sri Lanka Department of Meteorology<sup>5</sup> using all available quality controlled stations across the country with the Thiessen Polygon interpolation method.

---

<sup>4</sup> A district is the second level of regional administration in Sri Lanka. There are 25 districts in the country.

<sup>5</sup> The Sri Lanka Department of Meteorology is the national meteorological service of the country.

### 2.2.2: Return periods

A mean SPI value for each year was obtained by averaging the district-wise SPI data from 1951-2008. Return periods of the different drought categories were calculated using non-exceedence probability (Tallaksen et al., 2004; pp 204-206). Non-exceedence probability is the average time interval between events and is expressed as:

$$T = \frac{1}{p} \quad (\text{Eq. 2.6})$$

Where,

$T$  = Average time between the occurrence of an event  $X \leq x_p$

$p$  = Cumulative probability with the following Cumulative Distribution Function (CDF):

$$FP_x(x) = Pr\{X \leq x\} \quad (\text{Eq. 2.7})$$

Where,  $X$  = a random variable;  $x$  = a real number

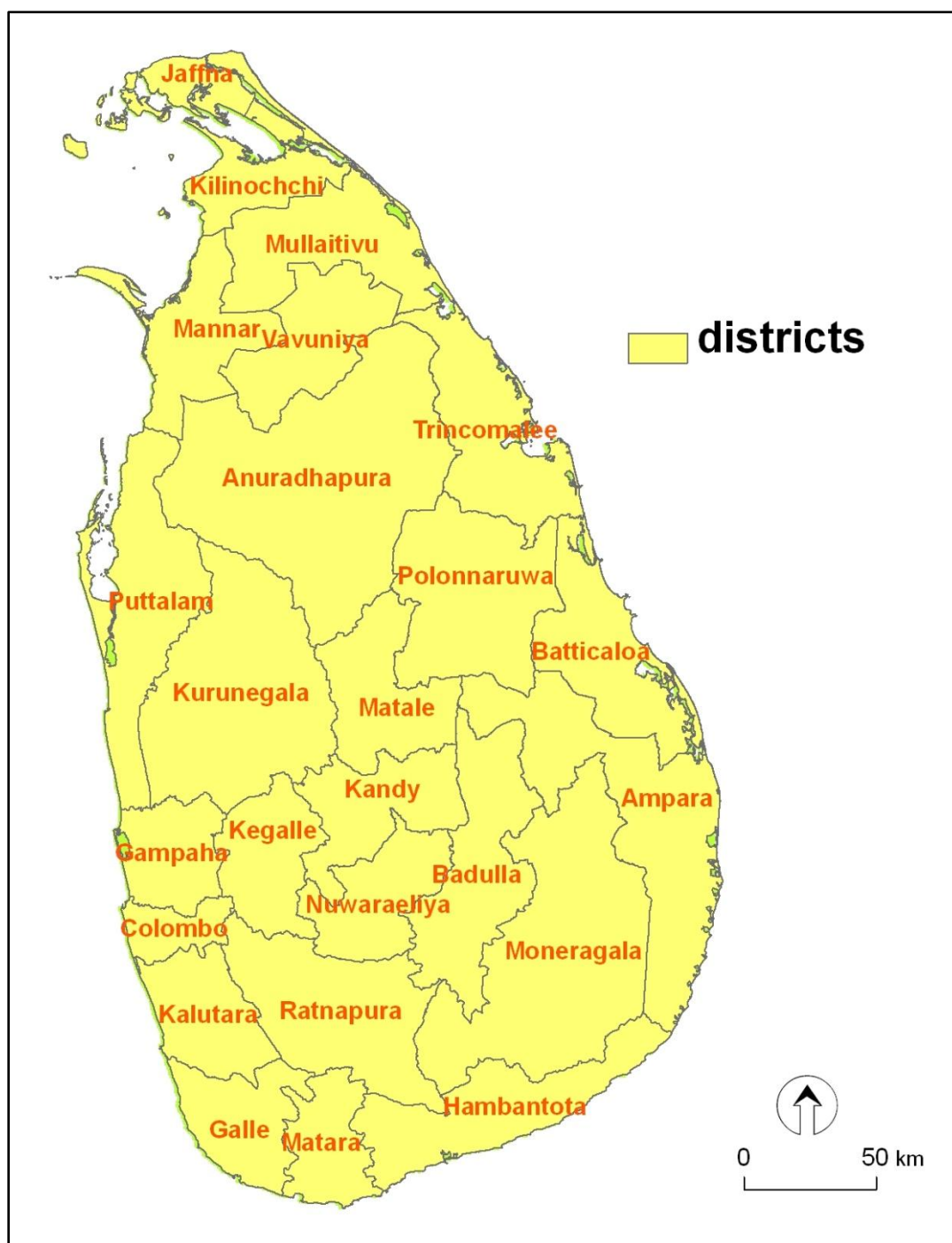


**Figure 2.1:** District boundaries (data source: <http://www.iwmidsp.org>)

### 2.2.3: Spatial dimension of drought occurrence

The spatial distribution of the severity of each drought event was analyzed by calculating the SPI using the district-wise interpolated precipitation dataset. The results were then visualized using attribute table manipulation in ArcGIS.

### 2.2.4: Influence of drought on the Maha season

#### 2.2.4.1: *Influence of drought on rice production during the Maha*

As the *Maha* season is the main rice cultivation season, the first step was to establish whether or not there is a significant difference in rice production between drought and non-drought years (identified in section 2.2). A two-tailed t-test for differences in mean under independence (Wilks, 2006; pp 140) was undertaken to establish whether or not the difference in total rice production and yield<sup>6</sup> in years of drought versus years of non-drought is significant. The test statistic is expressed as:

$$z = \frac{\bar{x}_1 - \bar{x}_2}{\left[ \frac{S_1^2}{n_1} + \frac{S_2^2}{n_2} \right]} \quad (\text{Eq. 2.8})$$

Where,  $\bar{x}_1, \bar{x}_2$  = means of the two samples;  $S_1, S_2$  = variances of the two samples and  $n_1, n_2$  = number of elements in each sample (i.e. drought and non-drought years). The t-distribution is used to test the test statistic when the sample size is small ( $n < 30$ ) (Wilks, 2006; pp 141). The null hypothesis is that the means are equal. If the test statistic exceeds the critical value of 2.02 (at the 95% confidence level), the null hypothesis is rejected.

---

<sup>6</sup> Total production is a gross figure of rice harvested in a given season. Yield is a measure of the productivity of rice cultivation and is expressed as yield per hectare.

The period of analysis used in the t-test was 1961-2005<sup>7</sup>. Rice production and yield data were obtained from the Sri Lanka Department of Agriculture.

#### ***2.2.4.2: Influence of the ON and DJF rains on Maha drought***

Next, the influence of the two rainfall regimes on Maha drought was analyzed using partial correlation analysis where :

$$P_{r_1} = \frac{r_{y_1} - r_{y_2}r_{12}}{\sqrt{(1 - r_{12}^2)(1 - r_{y_2})}} \text{ (Eq. 2.9)}$$

Where,

$r_{y_1}$  - simple correlation of the dependant variable  $y_1$  and the causative variable  $X_1$

$r_{y_2}$  - simple correlation between  $y_1$  and  $X_2$

$r_{12}$  - correlation between  $X_1$  and  $X_2$

$P_{r_1}$  - correlation between  $y$  and  $X_1$  from which  $X_2$  has been partialled

The significance of  $r_{12}$  is assessed using a t-test where t is expressed as:

$$t = r_{12} \sqrt{\frac{n - 2 - k}{1 - r_{12}^2}} \text{ (Eq. 2.10)}$$

Where, k = number predictor variables

6-monthly SPI for October was the predictand and standardized anomalies of ON and DJF rainfall were the predictors. Standardized anomalies of ON and DJF rainfall were calculated using a second precipitation dataset with daily rainfall data from 1961-

---

<sup>7</sup> The period of analysis was limited to 1961-2005 as analysis beyond this point required use of the station-based dataset that had data from 1961-2005.

2005 at 132 rain gauges (Fig. 1.3) maintained by the Sri Lanka Department of Meteorology. The data at these stations have been subjected to quality control procedures by the Department of Meteorology. The stations were selected based on longevity of record and spatial distribution<sup>8</sup>. The daily rainfall values at the stations were aggregated to monthly values prior to calculating the SPI. The anomalies of seasonal rainfall associated with each drought event are also presented in tabular form.

### **2.2.5: Dominant modes of variability, change in such modes over time, and spatial trends in drought occurrence**

Dominant modes of variability in drought occurrence, and change in such modes over time, were analyzed using Wavelet Transform (WT). A climate signal is the culmination of processes operating at the local and global scale. The WT is invaluable to climate data analysis as it is able to simultaneously represent both the local and global signals and can be used to study non-stationary processes occurring over a finite spatial and temporal domain (Lau and Weng, 1995). It has been used to study numerous geophysical phenomena (Torrence and Compo, 1998 and references therein; Lau and Weng, 1995 and references therein). WT differs from spectral analysis – which is often used to isolate dominant frequencies in a given time series (Wilks 2006; pp 383) – as it is able to capture how such frequencies change with time.

WT uses local base functions known as “wavelets” that are windows with flexibility in the time and frequency domain. Wavelets are described as: “....small packets of waves with a specific frequency that approach zero at both ends” (Trauth, 2007). Wavelets are able to map changes in the time-frequency domain precisely

---

<sup>8</sup> An attempt was made to ensure as wide a spatial coverage as possible.



because they can be stretched and translated with a flexible resolution in both domains (Trauth, 2007). There are many different wavelets that could be applied to a time series – for example, Morlet wavelet, Paul wavelet, Haar wavelet and Daubechies wavelet (Torrence and Compo, 1998; Trauth, 2007). The Morlet wavelet is the most popular wavelet in the geosciences (Trauth, 2007).

A WT decomposes a signal  $y(t)$  into elementary functions  $\psi_{a,b}(t)$  - also called “wavelets” – derived from a mother wavelet  $\psi(t)$  by dilation and translation. The elementary functions are expressed as:

$$\psi_{a,b} = \frac{1}{(s)^{1/2}} \psi\left(\frac{t-n}{s}\right) \quad (\text{Eq. 2.11})$$

Where,  $n$  = position or length (translation) of a wavelet;  $s(> 0)$  = scale (dilation) of a wavelet

The WT of the signal  $y(t)$  about the mother wavelet  $\psi(t)$  is defined as the convolution integral:

$$W(n,s) = \frac{1}{(s)^{\frac{1}{2}}} \int \psi^*\left(\frac{t-n}{s}\right) y(t) dt \quad (\text{Eq. 2.12})$$

Where,  $\psi^*$  =complex conjugate of  $\psi$

The commonly used Morlet wavelet is defined by:

$$\psi_0(\eta) = \pi^{-1/4} e^{i\omega_0 \eta} e^{-\eta^2/2} \quad (\text{Eq. 2.13})$$

Where,  $\eta$  =non-dimensional time;  $\omega_0$  = wavenumber representing the number of oscillations with the wave (=6 for the Morlet wavelet)

A set of scales  $s$  to use in the WT needs to be chosen after selecting a wavelet function, (Torrence and Compo, 1998).

$$s_j = s_0 2^{j\delta j}, \quad j = 0, 1, \dots, J \quad (\text{Eq. 2.14})$$

$$J = \delta j^{-1} \log_2(N\delta t/s_0) \quad (\text{Eq. 2.15})$$

Where,  $s_0$  =smallest resolvable scale;  $\delta j$  = sampling interval

For a Morlet wavelet,  $\delta j = 0.5$  is the largest value that could be used to ensure adequate sampling in scale. Smaller values of  $\delta j$  provide for finer resolution in the analysis (Torrence and Compo, 1998).

The absolute value squared of the wavelet transform produces the wavelet power spectrum that provides a measure of the variance of a time series at each scale (Torrence and Webster, 1999).

It is common to pad the ends of a finite time series with zeroes prior to performing a wavelet transform so that errors that could occur at the beginning and end of a time series could be reduced. A cone of influence (COI) is plotted to indicate the area in the wavelet spectrum where edge effects become important. It is defined as the e-folding time  $\tau_s$  for the autocorrelation of wavelet power at each scale. For the Morlet wavelet,  $\tau_s = \sqrt{2}s$ . The true power spectrum of a time series can be obtained using global wavelet spectra (Torrence and Compo, 1998). The global wavelet spectrum is calculated by time-averaging a wavelet spectrum over all local wavelet spectra using:

$$\bar{W}^2(n, s) = \frac{1}{N} \sum_{n=0}^{N-1} |W(n, s)|^2 \quad (\text{Eq. 2.16})$$

Where,  $N$  =number of points in a time series

A background Fourier red noise spectrum is assumed for each scale. The red noise spectrum can be modeled by fitting a lag-1 autoregressive model (AR1) (Wilks, 2006; pp 352; Von Storch and Zwiers 1999, pp 255) to the time series using:

$$\alpha = \text{corr}_{xx}(k) = \frac{\text{cov}_{xx}(k)}{\sigma_x^2} \quad (\text{Eq. 2.17})$$

Where,

$\alpha$  = lag-1 autocorrelation;  $\sigma_x^2$  = variance of time series  $x(t)$

And,

$$\text{cov}_{xx}(k) = \text{autocovariance} = \frac{1}{N-k-1} \sum_{t=1}^{N-k} (x_t - \bar{x})(x_{t+k} - \bar{x}) \quad (\text{Eq. 2.18})$$

Where,

$k = 1$ (first time lag);  $N$  =data points sample at constant time intervals  $\Delta t$

Once the lag-1 autocorrelation is calculated, the normalized Fourier red noise spectrum is generated using

$$P_k = \frac{1 - \alpha^2}{1 + \alpha^2 - 2\alpha \cos\left(\frac{2\pi k}{N}\right)} \quad (\text{Eq. 2.19})$$

Where,  $k = 0 \dots \frac{N}{2}$  is the Fourier frequency index

Once the Fourier red noise spectrum is calculated for each scale, the chi-square distribution is used to find frequency contours significant at the 95% confidence level (Torrence and Compo, 1998).

Fluctuations in power over selected scales  $s_1$  to  $s_2$  scales can be defined using the scale-averaged wavelet power using:

$$\bar{W}^2(n, s) = \frac{\delta j \delta t}{C_\delta} \sum_{j=j_1}^{j_2} \frac{|W_n(s_j)|^2}{s_j} \quad (\text{Eq. 2.20})$$

Where,

$C_\delta$  = a constant for each wavelet function (0.776 for the Morlet wavelet)

Precipitation data from 15 rain gauges, for the period 1870-2005<sup>9</sup>, were obtained from the Global Historical Climatology Network (Vose et al., 1992). These gauges are well-distributed across the island (Fig. 2.2). Wavelet transforms were generated on 6-monthly SPI values for October for each rain gauge. The following values were selected for the different variables in the WT:

$dt = 1$  (representing the annual sampling resolution of the dataset)

$\delta_j = 0.125$

$s_0 = 1 * dt$  (the smallest resolvable scale is 1 year)

The lag-1 autocorrelation parameter was estimated for each station prior to generating the red noise Fourier spectrum for each station. Time scales with significant power at each station were identified from the Wavelet Spectrum prior to averaging the wavelet power for those particular time bands.

---

<sup>9</sup> A few stations had records commencing in 1881 while one had records commencing in 1901.

Wavelet software was provided by C. Torrence and G. Compo and is available at URL: <http://paos.colorado.edu/research/wavelets/>. Annex No. 1 provides an example of modifications made to the original Matlab code prior to running the WT analysis.

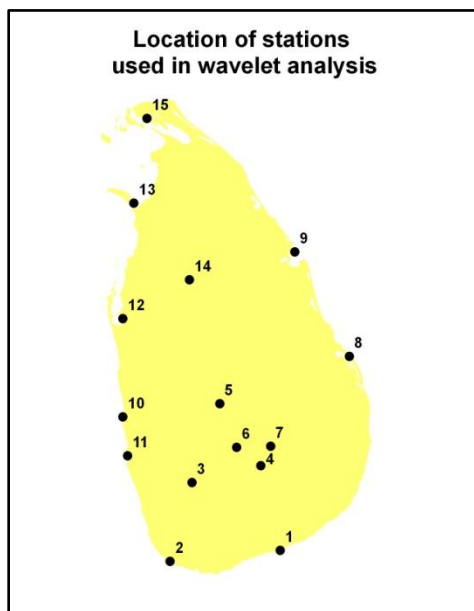


**Figure 2.2:** Location of stations with long precipitation records used to generate wavelet transforms of Maha drought time series. Station names are given in Table 2.1.

<i>Station No.</i>	<i>Station name and location</i>
1	Hambantota (southeast)
2	Galle (southwest)
3	Ratnapura (southwestern slopes, wet zone)
4	Bandarawela (central hills, wet zone)
5	Kandy (central hills, wet zone)
6	Nuwara Eliya (central hills, wet zone)
7	Badulla (southeastern slopes, dry zone)
8	Batticaloa (east)
9	Trincomalee (east)
10	Negombo (west)
11	Colombo (west)
12	Puttalam (northwest)
13	Mannar (northwest)
14	Anuradhapura (central plains)
15	Jaffna (north)

**Table 2.1:** Names and location for stations used in Wavelet Transform analysis

Spatial trends in drought incidence was studied for the period 1961-2005 using rain fall data at a 132 quality controlled rain gauges obtained from the Sri Lanka Department of Meteorology (Fig. 1.3). 6-monthly SPI for October was first calculated at each station. Next, trend values at each station were obtained by fitting a least squares fit to the SPI time series. A continuous surface of SPI trend values for Sri Lanka was generated by interpolating the SPI trend (slope) values at each station using Ordinary Kriging.

## **2.3: Results**

### **2.3.1: Drought occurrence:**

There were 14 drought years and 31 non-drought years during the period 1951-2008 (Fig. 2.3). Of the 14 drought years, 4 were “extreme” droughts, 1 was a “severe” drought, 5 were “moderate” droughts and 4 were “mild” droughts. An outstanding feature of drought occurrence during the period of study is the increased occurrence of droughts of all categories in the post-1975 period. Not a single severe or extreme event is recorded from 1951-1975. Another feature of note is the consecutive occurrence of droughts in the severe to extreme category from 2000-2005.

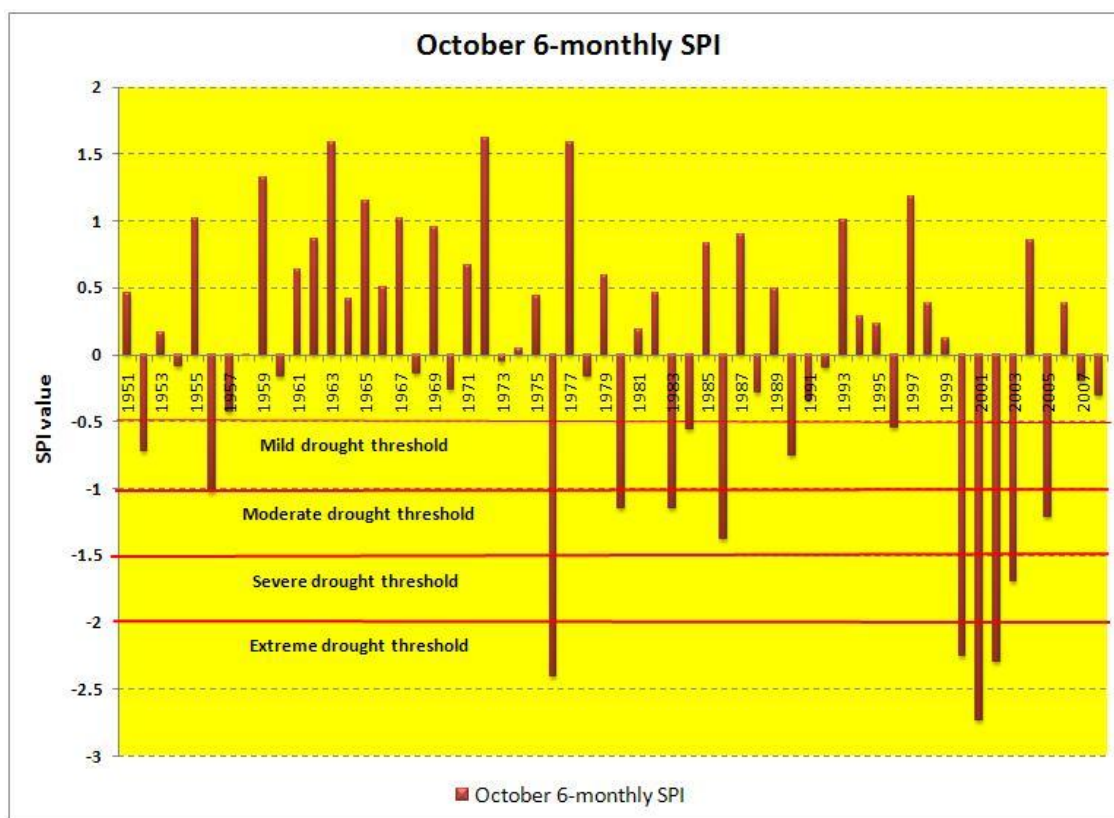


**Figure 2.3:** Mean drought occurrence during the period 1951-2008 derived by calculating the 6-monthly Standardized Precipitation Index (SPI) on district-wise interpolated rainfall data.

### 2.3.2: Drought return periods

The average time between the occurrences of droughts of a particular category are listed in Table 2.2

Drought category	SPI range	Frequency	Years	Probability	Cumulative probability %	Non-exceedance (average time between occurrence of a drought event)
Extreme	$SPI < -2$	4	1976, 2000, 2001, 2002	0.07	0.07	14.5
Severe	$-1.99 < SPI < -1.5$	1	2003	0.02	0.09	11.6
Moderate	$-1.49 < SPI < -1$	5	1956, 1980, 1983, 1986, 2005	0.09	0.17	5.8
Mild	$-0.99 < SPI < -0.5$	4	1952, 1984, 1990, 1996	0.07	0.24	4.1

**Table 2.2:** Drought return periods calculated using non-exceedance probability

The return periods need to be interpreted with caution – particularly in the case of extreme droughts. Although, the average time between the occurrence of extreme drought events is 14.5 years, that return period does not hold for the extreme droughts of 2000, 2001 and 2002.

### **2.3.3: Spatial dimension**

The spatial extent and severity differs with each drought event. Comparison of the district-wise distribution of drought severity for each extreme drought event clearly highlights such differences (see Figure 2.4). In terms of the number of districts affected by drought, those of 1976 and 2000 are the worst as all 25 districts are under some category of drought. Similarly, although the 2003 drought falls within the “severe” category, there were a number of districts that fell under the “extreme” category that year (see Figure. 2.5). It is clear, therefore, that some drought events are characterized by the localized occurrences of “extreme” or “severe” categories.



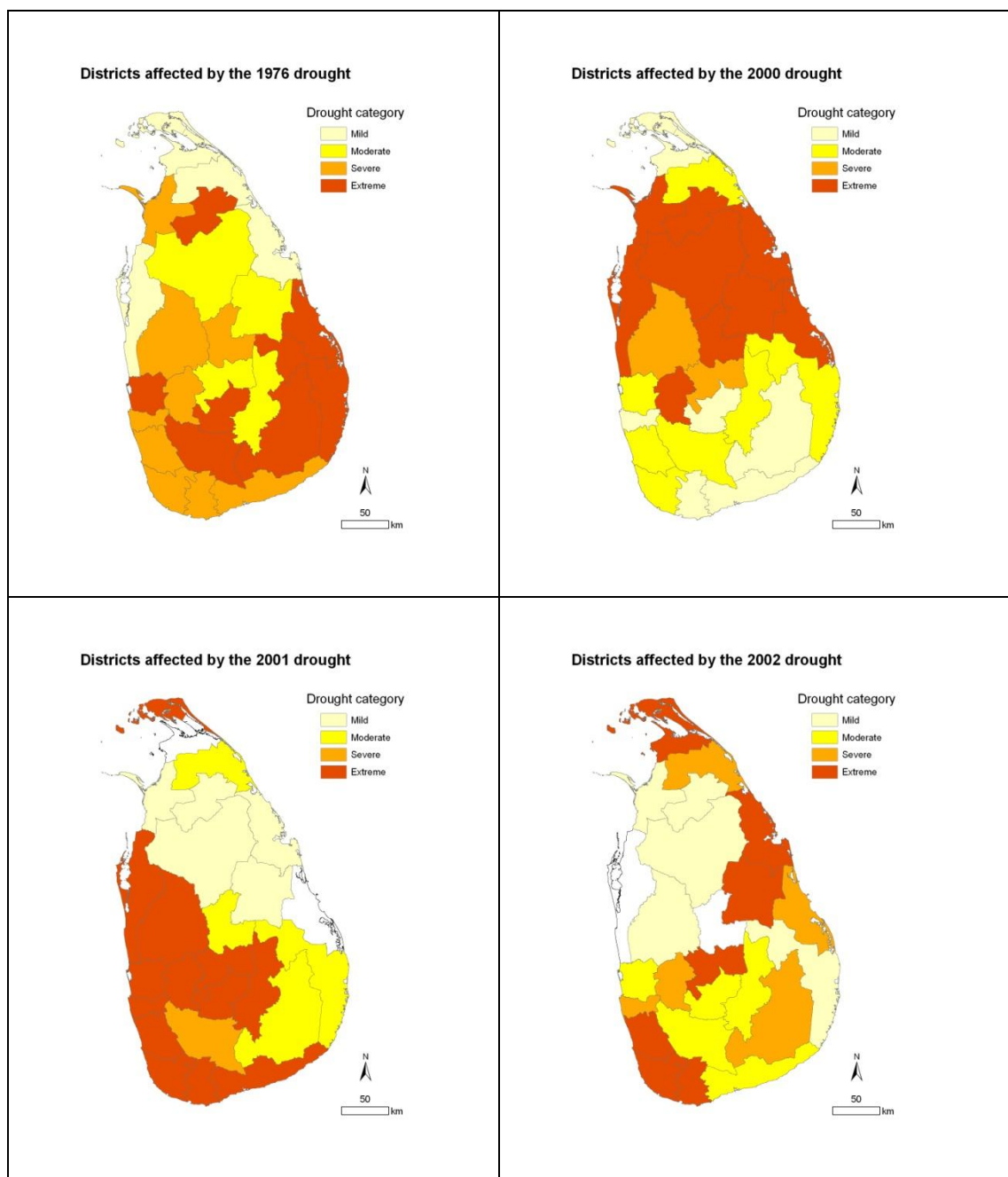


**Figure 2.4:** Drought severity category at district level for the extreme drought events of (clockwise from top left) 1976, 2000, 2001 and 2002. Colour coding is by severity level with dark orange indicating “extreme” drought, light orange indicating “mild” drought and white indicating “non-drought”.

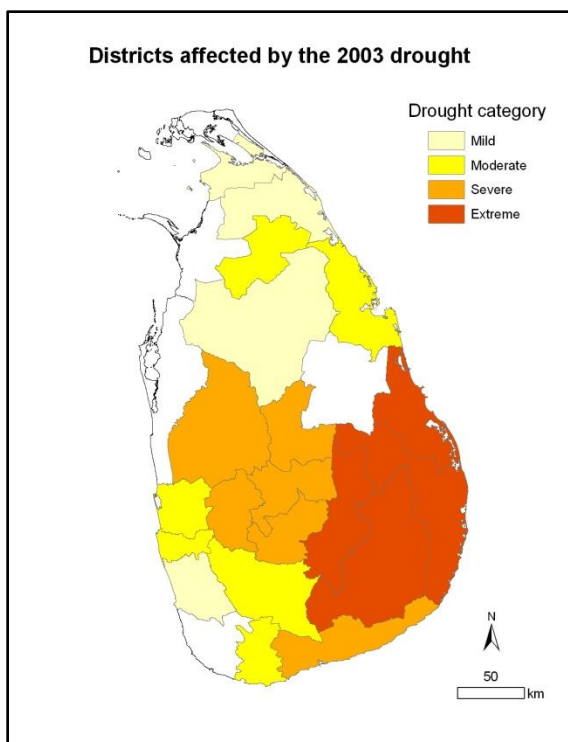


**Figure 2.5:** Drought severity categories at district level for the 2003 “severe” drought event

Moderate droughts affect far fewer districts than extreme and severe droughts. Yet, such droughts could still affect agriculture and other water sectors of water demand depending on where such droughts take place. As with the extreme and severe categories, the spatial extent of drought occurrence varies by event (see Figure 2.6).

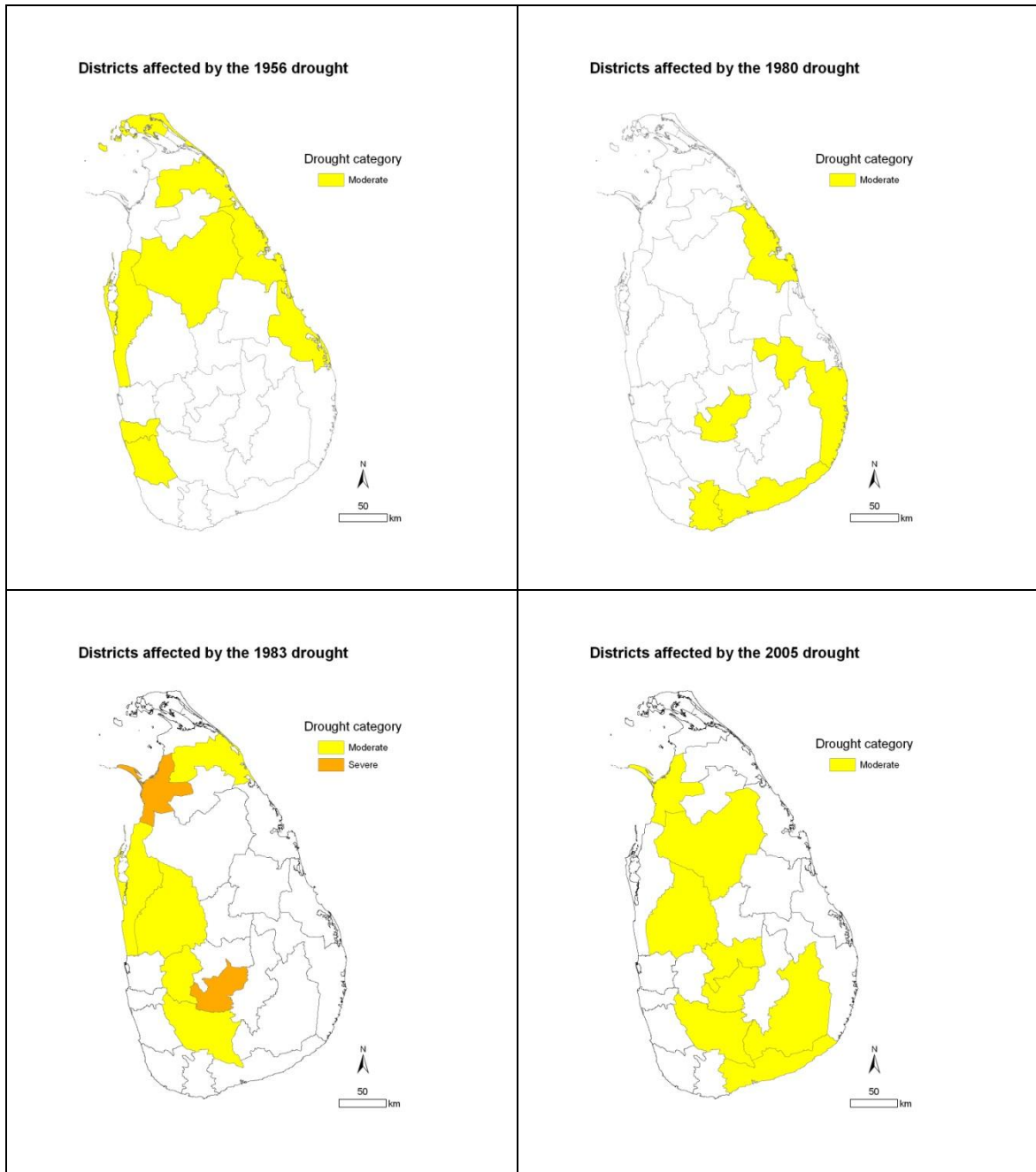


**Figure 2.6:** Districts affected by moderate droughts in (clockwise from left) 1956, 1980, 1983 and 2005

### **2.3.4: Effect of Maha droughts on rice cultivation and influence of ON and DJF rainfall on Maha drought**

#### ***2.3.4.1: Effect of Maha droughts on rice cultivation:***

The null hypothesis in the t-test undertaken to assess whether there is a significant difference in rice production between drought and non-drought years is rejected as the t-statistic exceeds the t-critical value. The result is the same using both metrics of production – i.e. total *Maha* production (*t Stat* = **2.18**) and yield per hectare for the *Maha* season (*t Stat* = **2.47**). The rejection of the null hypothesis implies that there is indeed a significant difference in *Maha* rice production and yield between years of drought and non-drought. The result is clearly evident when detrended<sup>10</sup> rice production and yield are plotted against 6-monthly SPI values (Fig. 2.7). The plot further reveals that rice production is also adversely affected in years of excess rainfall such as in the years 1963-1965, 1971-1973 and 1993.

---

<sup>10</sup> Rice production increased dramatically from the late 1970 onwards with the increase in land under rice cultivation following the development of major irrigation schemes in the Dry Zone (Annex 2).

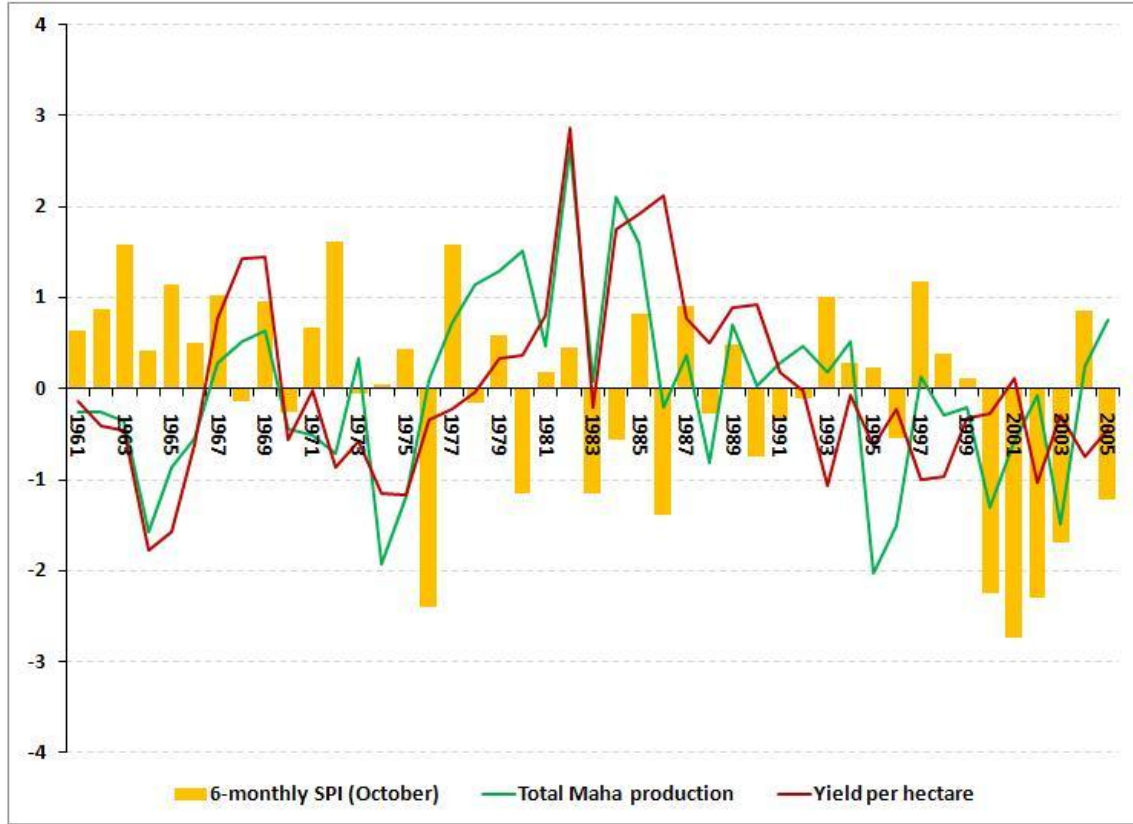


**Figure 2.7:** Detrended total Maha production and yield per hectare versus 6-monthly SPI (October)

#### 2.3.4.2: Influence of the ON and DJF rains on Maha drought:

The partial correlation between *Maha* drought and ON rainfall ( $r_{y_1}$ ) is 0.46 while the partial correlation between *Maha* drought and DJF rainfall ( $r_{y_2}$ ) is 0.15. The partial correlation between ON and DJF rainfall ( $r_{12}$ ) is -0.08. The strength of  $r_{12}$  is not significant ( $t = -0.4971$ ). This implies that we accept the null hypothesis that there is no correlation between ON and DJF rainfall. The result can be interpreted as ON rainfall being the most important driver of Maha rainfall.

A close look at the rainfall anomalies in each drought year shows that ON failure is quite common in most drought years and DJF failure occurs in some years (see Table 2.3 and Fig. 2.8). The only exception is the drought of 2002 that appears to have occurred

without negative departures in either rainfall season. This discrepancy was clarified by examining the spatial distribution of rainfall anomalies for 2002. It is a case where spatial averaging resulted in strong localized positive anomalies overriding the influence of localized negative anomalies in both the ON and DJF seasons (Fig. 2.9).

On average, the reduction in ON and DJF rainfall during extreme drought years is 125mm and 42mm; during severe drought years 109mm and 278mm; and during moderate drought years 41mm and 72mm respectively. Negative ON anomalies in the extreme and moderate categories are larger than DJF anomalies. In the single severe drought of 2003, negative DJF anomalies are stronger.

<b>Drought category</b>	<b>Years</b>	<b>Magnitude (SPI)</b>	<b>ON anomaly</b>	<b>DJF anomaly</b>
Extreme	1976	-2.4	0.27	-0.23
	2000	-2.25	-0.95	0.47
	2001	-2.73	-0.74	-0.16
	2002	-2.29	0.31*	0.45*
Severe	2003	-1.69	-0.34	-1.01
Moderate	1956	-1.03	n/a	n/a
	1980	-1.15	-0.11	-0.44
	1983	-1.15	-0.79	2.44
	1986	-1.38	-0.64	-0.57
	2005	-1.21	0.62	-0.24
Mild	1952	-0.72	n/a	n/a
	1984	-0.56	-0.54	-0.05
	1990	-0.75	-0.03	0.32
	1996	-0.55	-0.62	-1.05

**Table 2.3:** Rainfall anomalies associated with each drought event

(\*- special case of 2002; n/a – not available)

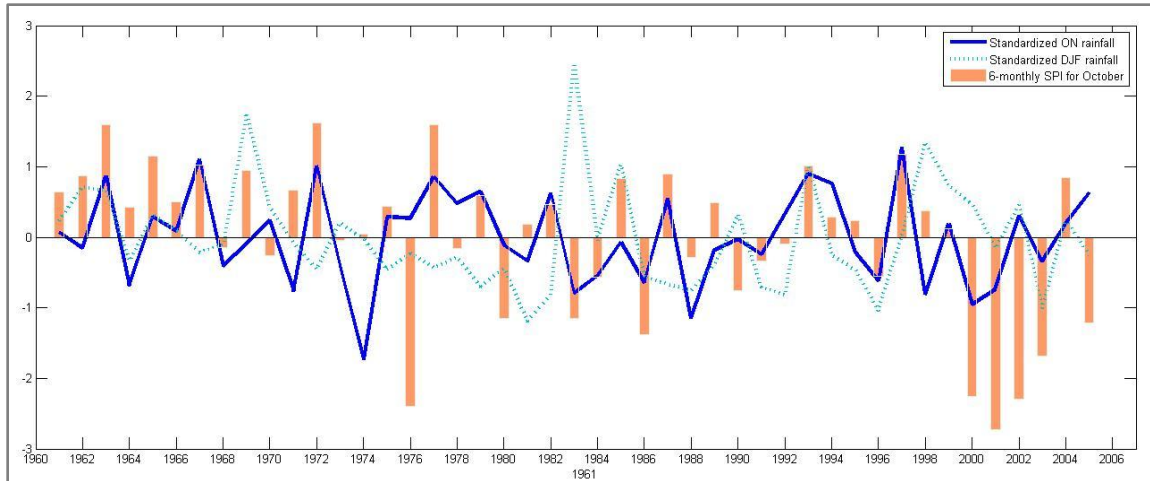


**Figure 2.8:** ON standardized anomalies (solid bright blue line) and DJF standardized anomalies (broken light blue line) plotted against 6-month SPI (solid orange bars) for October for the period 1961-2005.

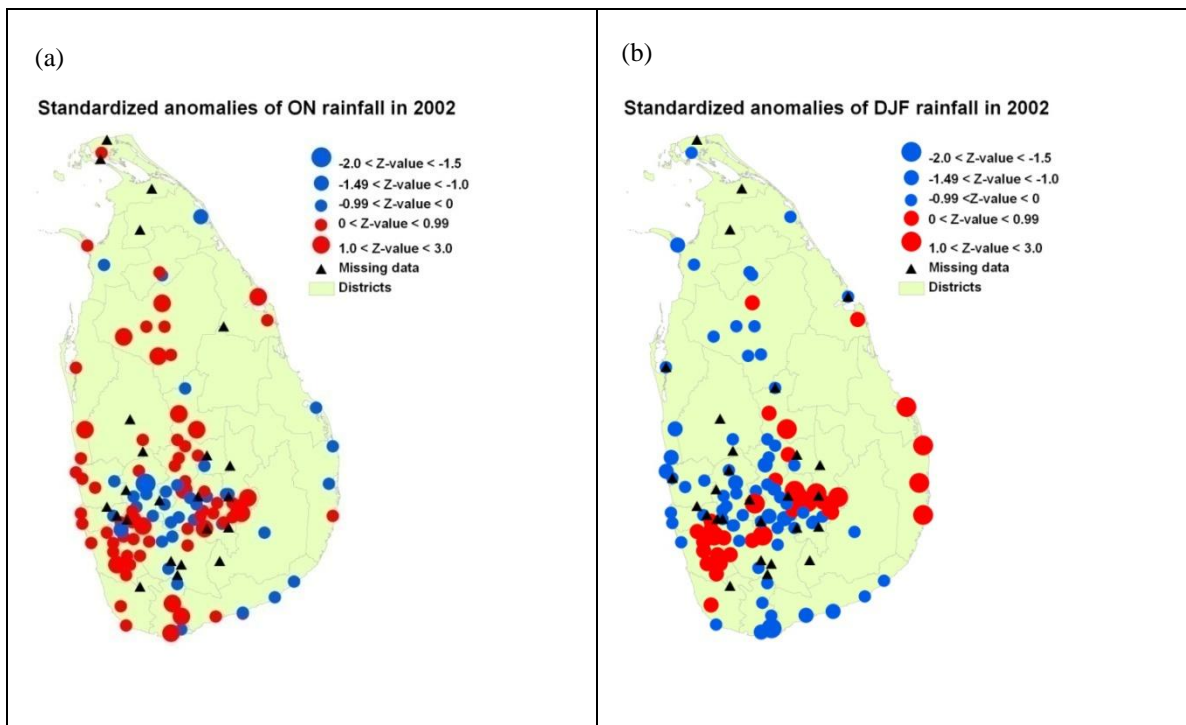


**Figure 2.9:** Standardized anomalies of ON (a) and DJF (b) rainfall in 2002. Blue circles indicate negative anomalies and red circles indicate positive anomalies

### **2.3.5: Dominant modes of variability and changes in such modes over time**

The dominant and statistically significant drought frequency at most stations is 2-8 years. The 2-8 year frequency band is clearly seen (see Figure 2.10) in the stations located in the east [Batticaloa (not shown) and Trincomalee], southeast [Badulla (not shown), Hambantota], north (Jaffna), central plains [Anuradhapura (not shown)] and the central hills [Kandy, Ratnapura, Nuwara Eliya and Bandarawela (only Kandy is shown)]. The power spectra at stations in the east (Batticaloa and Trincomalee) also display significant power in the decadal frequency band around 8-16 years – particularly post-1960. Three stations in the central hills (Kandy, Nuwara Eliya and Ratnapura) and one station in the southeast (Hambantota) also display significant frequencies in the 8-16 band around 1925-1950.

The predominant frequency band for stations along the southwestern, western and northwestern coast [Galle, Colombo, Negombo, Puttalam (not shown) and Mannar] is between 16-32 years (see Figure 2.11). In certain periods, however, some of these stations [e.g. Mannar, Galle and Puttalam (not shown)] also show significant power in the 4-8 year band. Figure 2.12 shows the spatial distribution of stations with their dominant wavelet frequencies. The hill station Nuwara Eliya also displays significant frequencies at multi-decadal timescale (30-40 years).

SPI variance in the significant 2-8 year frequency band at stations in the east (Batticaloa and Trincomalee) and in the southeast (Hambantota and Badulla) has increased from the late-1980s to the early-2000s.

Examination of spatial trends in drought occurrence for the period 1961-2005 shows that drought occurrence is increasing along the western, eastern and southeastern



region of the island (Fig. 2.13). Reasons for the increase in drought incidence and the marked increase in SPI variance at stations along the east and southeast may be related. The eastern and southeastern regions receive the most rainfall during the December-February season. Could the strength of the northeast monsoon winds be weakening due to global change as observed in a study on wind speeds over East Asia during the winter monsoon (Xu, et al., 2006)? Or could observed decreases in winter monsoonal precipitation over the Bay of Bengal attributed to regional aerosol loadings (Krishnamurti et al., 2009) be a contributing factor? A definite conclusion requires further investigation and will be addressed in future studies analyzing mean wind fields over Sri Lanka and the adjacent Bay of Bengal region.

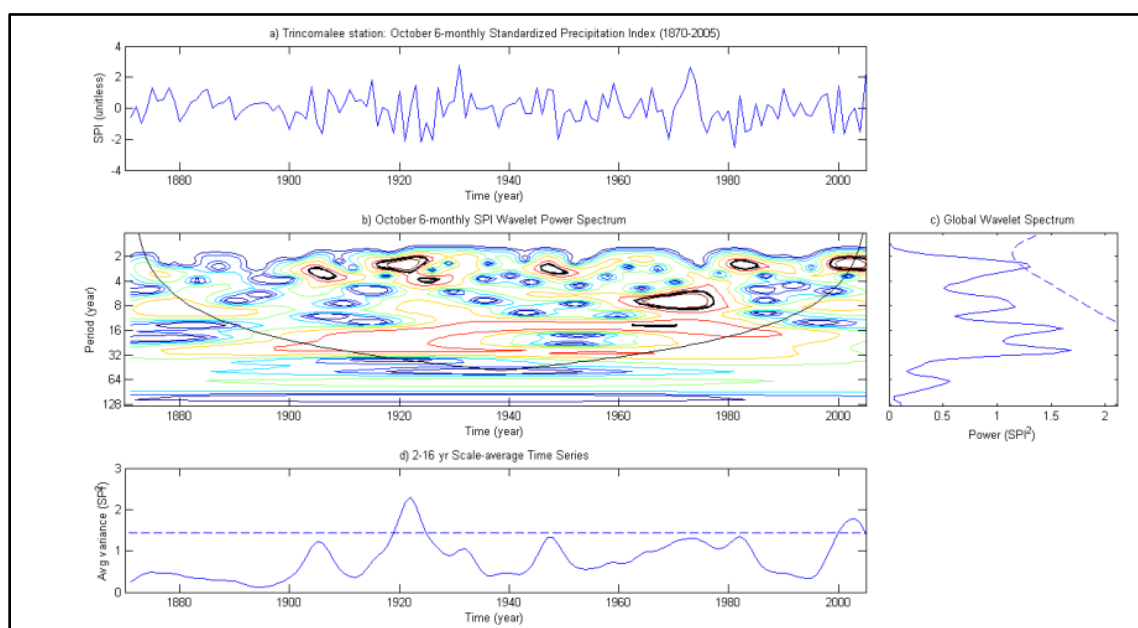


**Figure 2.10 (a):** Wavelet Transform for Trincomalee where the predominant frequency is 2-8 years. The top panel is the original SPI time series. The second panel is the Wavelet Power Spectrum (WSP) with frequencies significant at the 95% confidence level contoured in bold. The thin curved line running from left to right in the WSP is the Cone of Influence (COI) indicating the region below which edge effects distort results. The right box is the Global Wavelet Spectrum where the broken line indicates the 95% confidence level. Frequencies below the dashed line are the significant spectral peaks in the time series. The bottom panel shows the scale-average wavelet power (expressed as SPI variance) – where the scale is selected based on significant frequency bands identified from the WSP.

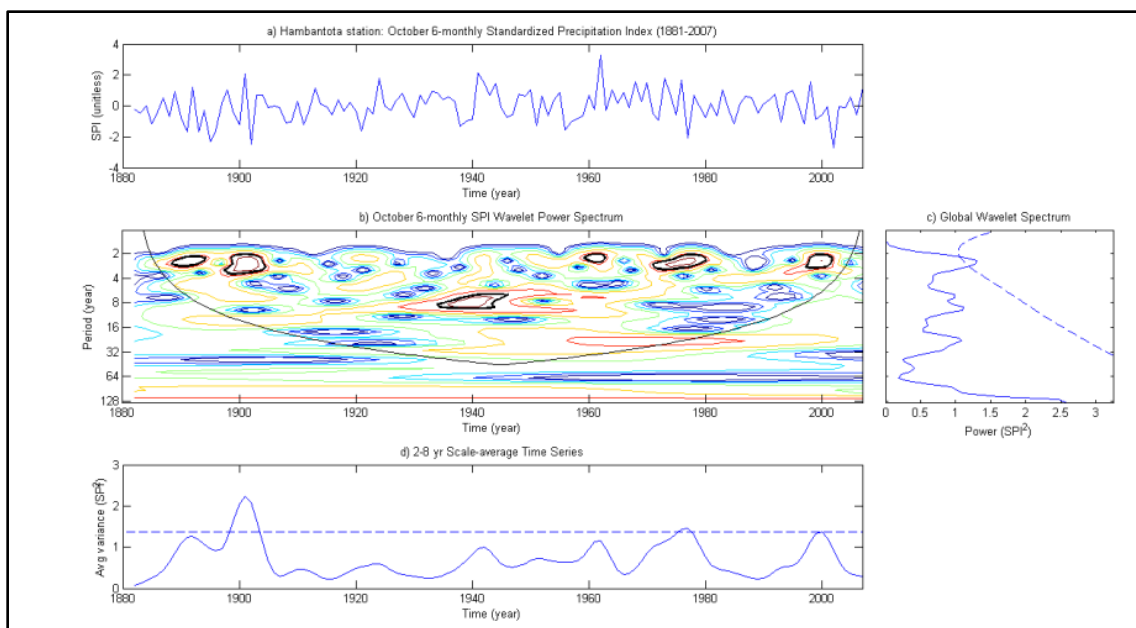


**Figure 2.10 (b):** Same as in 2.10(a) but for Hambantota

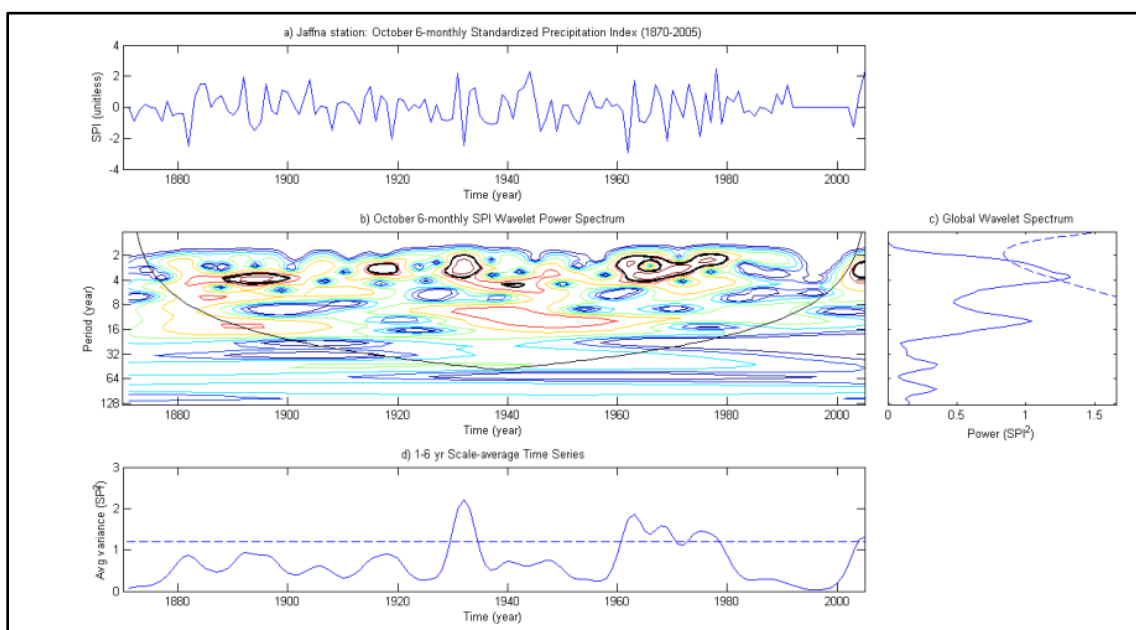


**Figure 2.10 (c):** Same as in 2.10(a) but for Jaffna

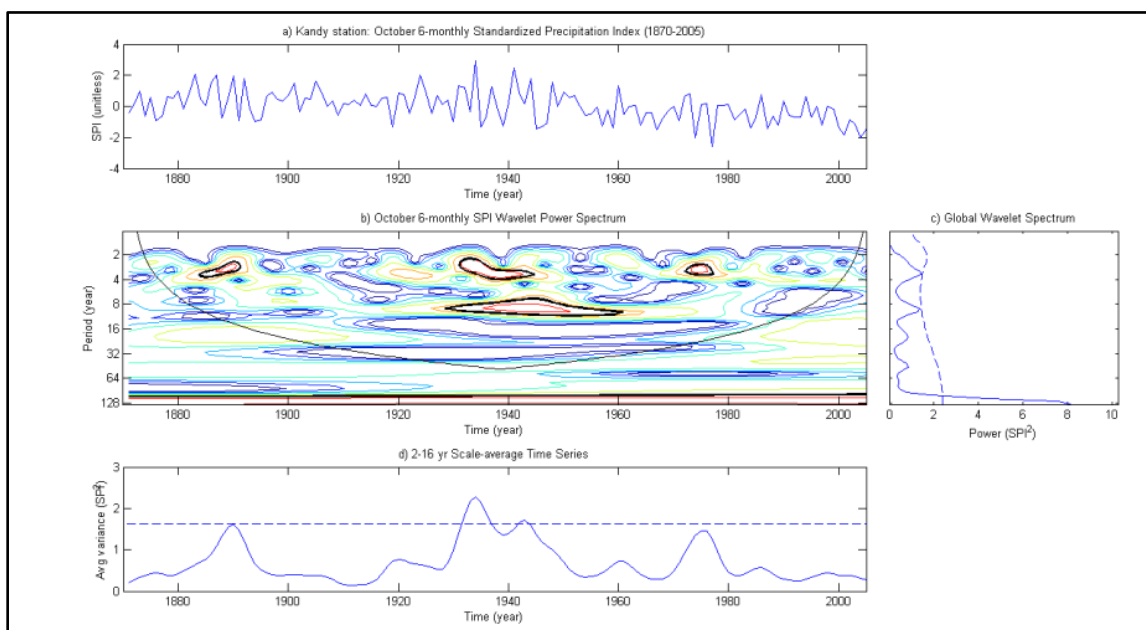


**Figure 2.10 (d):** Same as in 2.10(a) but for Kandy

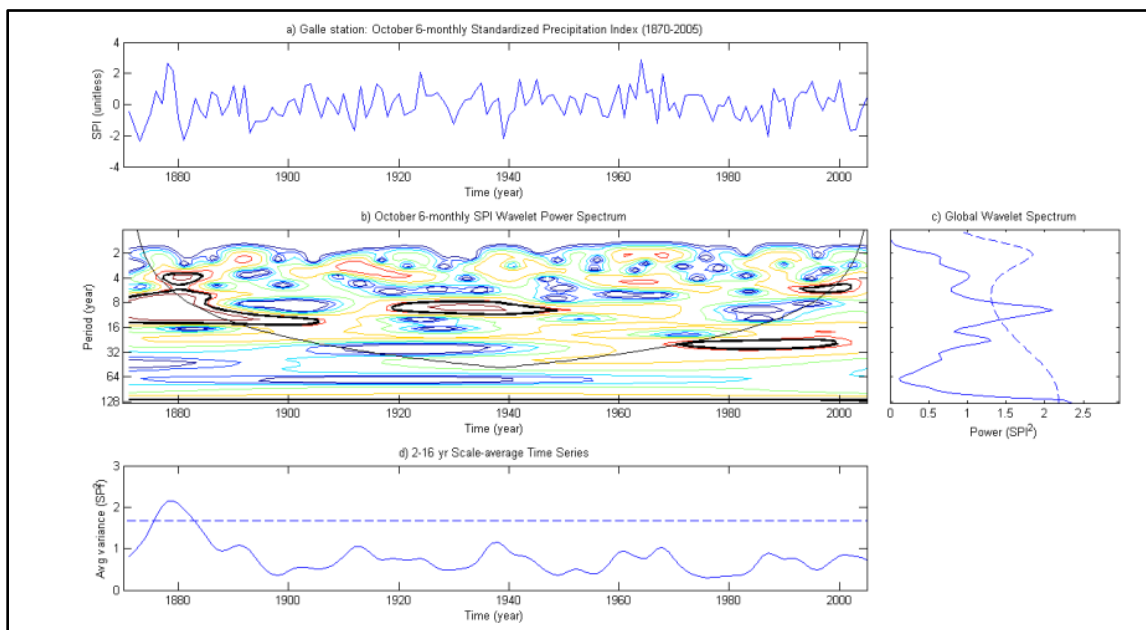


**Figure 2.11 (a):** Same as in Figure 2.10 but for Galle where the dominant frequency band is 16-32 years

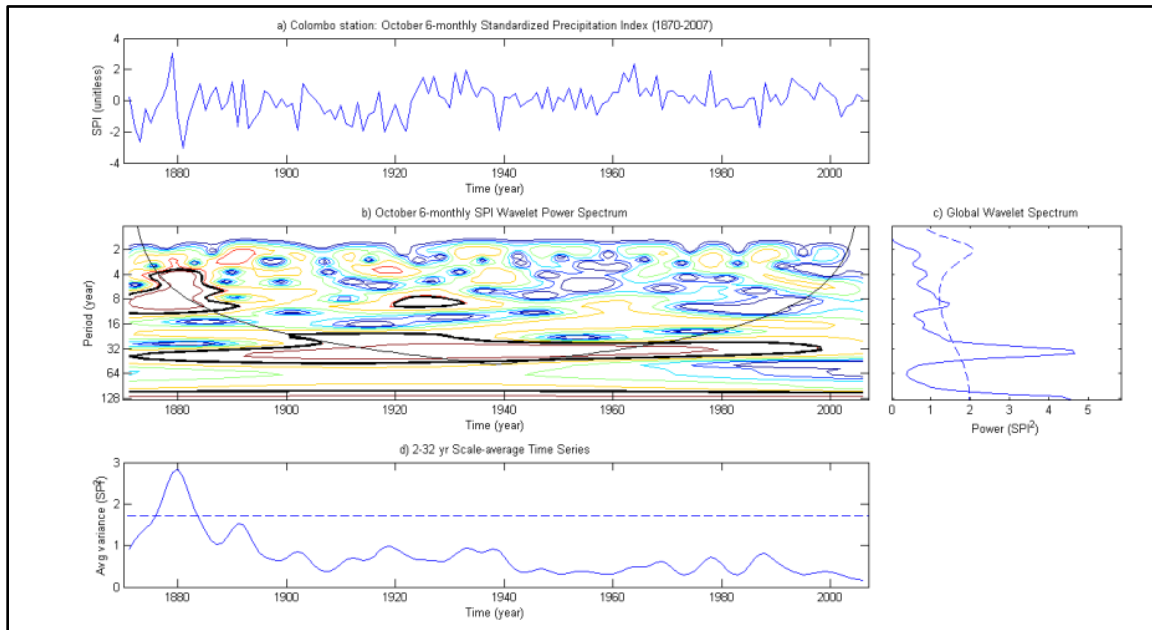


**Figure 2.11(b):** Same as in Figure 2.11(a) but for Colombo

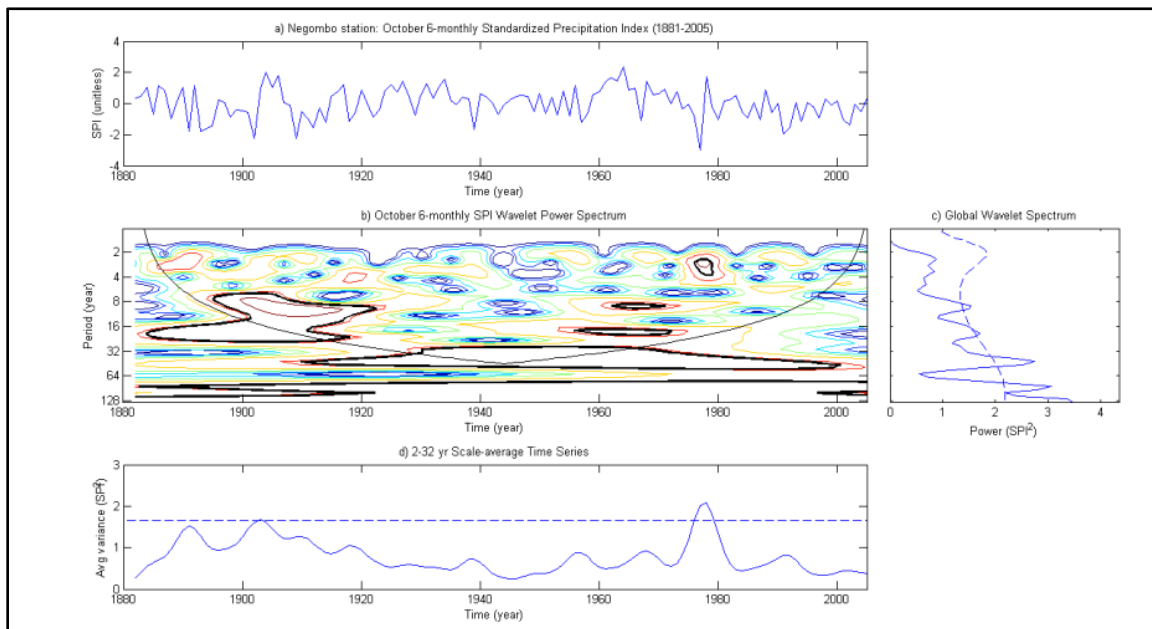


**Figure 2.11 (c):** Same as in Figure 2.11(a) but for Negombo

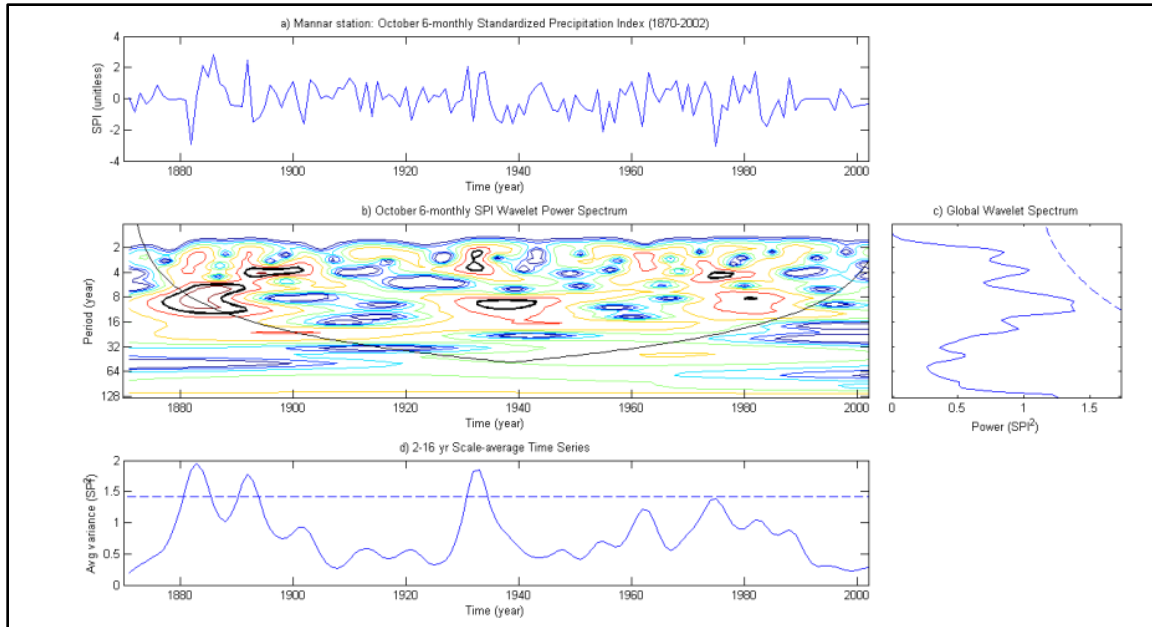


**Figure 2.11 (d):** Same as in Figure 2.11(a) but for Mannar

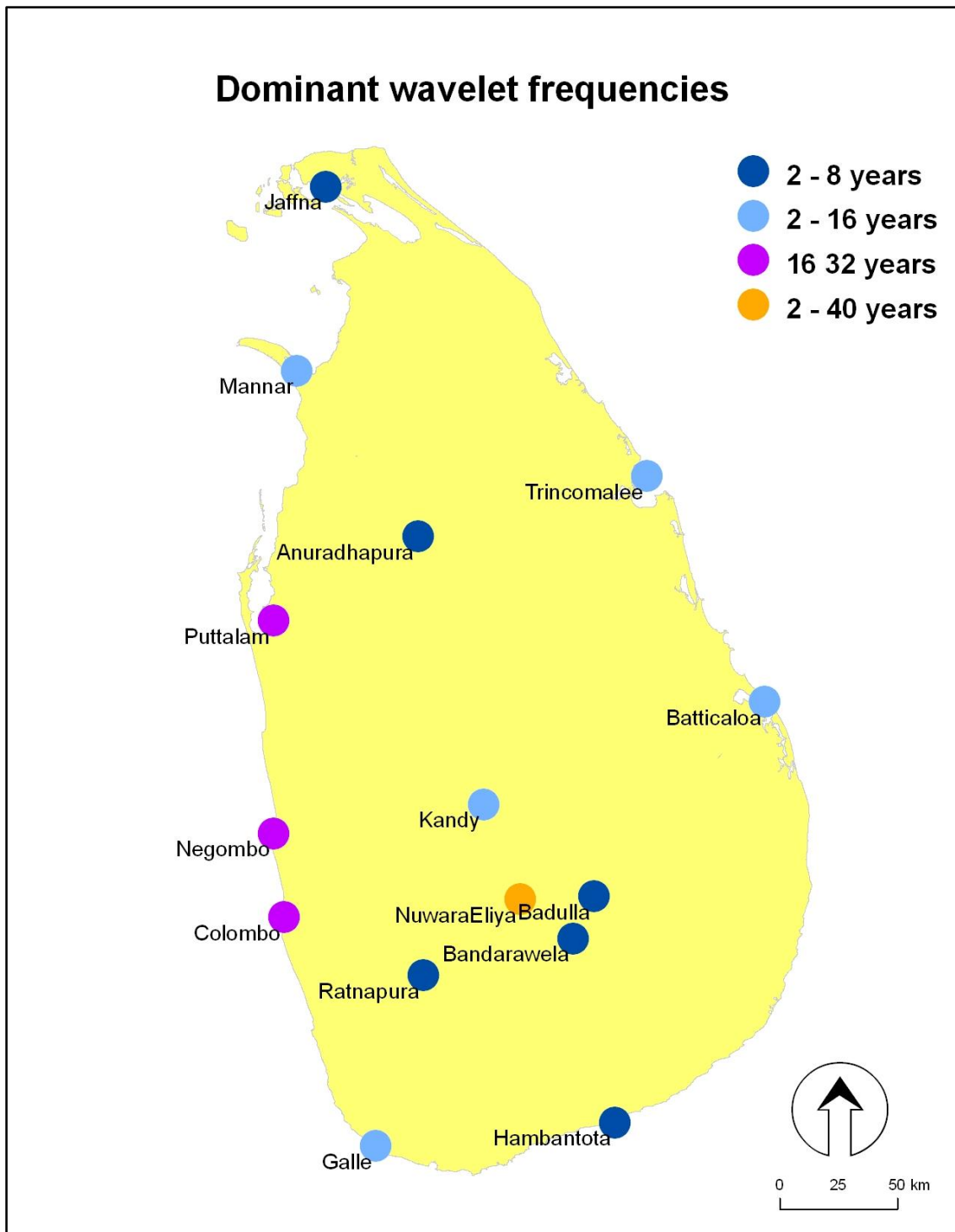


**Figure 2.12:** Dominant wavelet frequencies at stations used in wavelet transform analysis

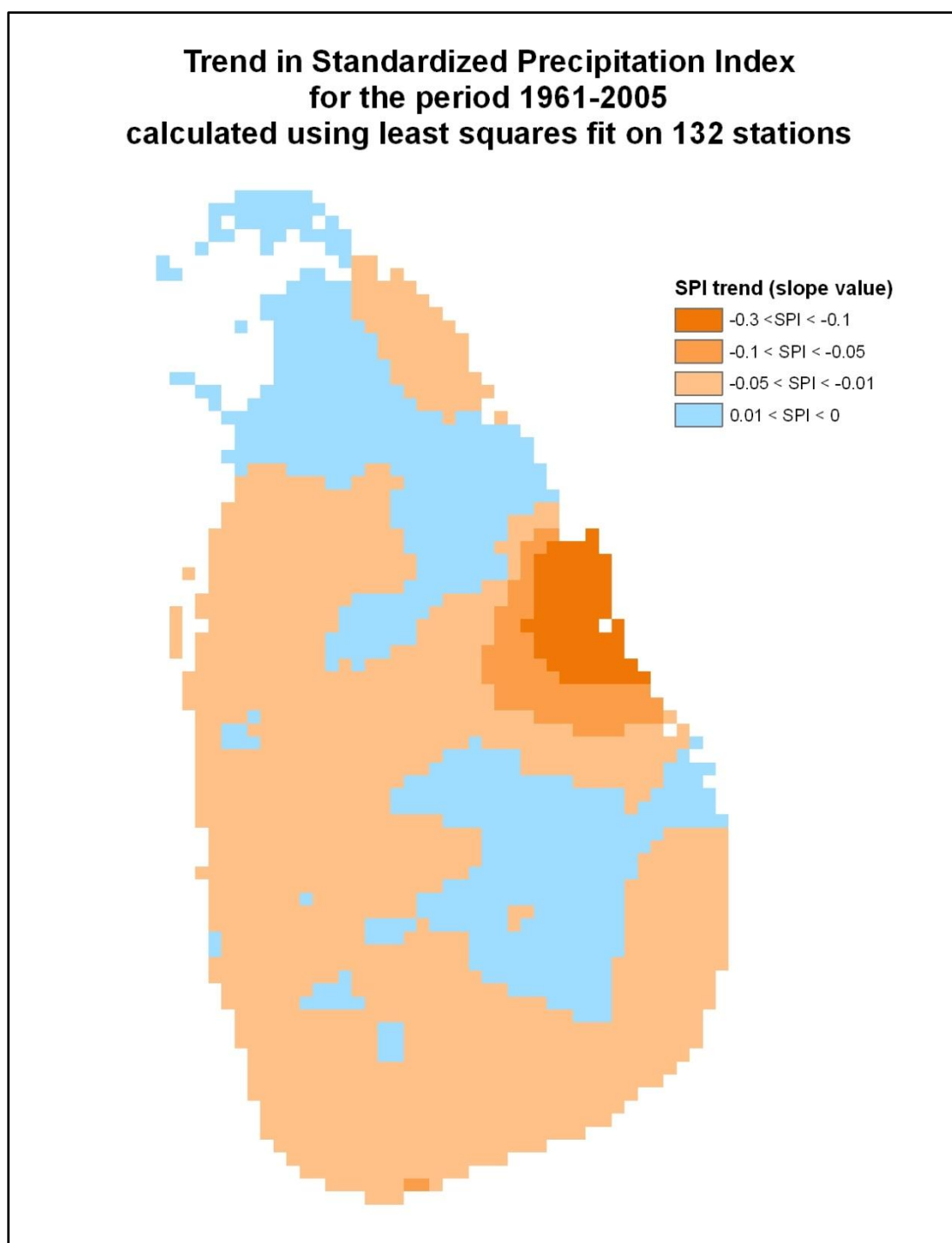


**Figure 2.13:** Interpolated map of trend in 6-month SPI for October at the 132 rain gauges. Orange depicts an increase in drought and blue depicts a decrease in drought. Trend values show changes in units of SPI per year.



## 2.4: Conclusion

Results show that there were 14 drought years and 31 non-drought years during the analysis period of 1951-2008. There is a marked increase in the occurrence of drought in the post-1975 period. Droughts of the extreme and severe category have also only all occurred in post-1975 period. Whether the increase in drought occurrence and magnitude in the post-1975 period is linked to the change in SST background state over the Indian Ocean around 1976-1977 (Terray and Dominiak, 2005), and/or to the warming of the Indian Ocean (Alory et al., 2007) requires further study. Whether there is a role for changes in land surface characteristics, such as snow cover over the Eurasian landmass, in determining the occurrence and magnitude of post-1975 drought events also requires further study.

There is no clear periodicity to drought occurrence apart from 1975-1990 when every other year appears to have been a drought year, and from 2000-2005 when droughts in the severe to extreme category occurred simultaneously. Thus, drought return periods do not appear to be a metric that could reliably be incorporated in decision-making as they do not capture actual return periods in certain categories of drought. It could well be that a longer record is required to obtain more accurate return periods. The wavelet transform provides valuable insights on the dominant modes of variability in drought occurrence. This differs from drought return periods. It provides valuable insight on the timescales of processes driving drought over Sri Lanka. Such information is useful when identifying and selecting predictors for drought forecasting.

Droughts have a significant negative impact on rice production and yield. Given the lack of clear periodicity in drought occurrence, advance knowledge of whether a

forthcoming season could be affected by drought is essential for cropping decisions and irrigation scheduling. Past drought events have not been uniform in terms of their severity and spatial extent. However, in most drought years (except for 2001), the region most affected falls within the “Dry Zone”.

The October-November (ON) convective rainfall is significantly correlated with *Maha* seasonal drought. The December-February (DJF) northeast monsoon is only weakly correlated with *Maha* seasonal drought. However, negative DJF rainfall anomalies are seen in most drought years. Therefore, the importance of the DJF season cannot be dismissed simply because its correlation with *Maha* drought is weak.

As the ON rains provide critical moisture to the growing season, advance knowledge of the likely strength of the ON rains in a forthcoming season could be invaluable to decision-making in agriculture. Failure of the DJF rains could also ruin a rice crop at the maturing stage. Advance knowledge of the strength of the forthcoming DJF rains could be critical for decisions such as (but not limited to) when, where and how much irrigation water should be released. Such knowledge could be generated through a careful study of factors (and thus potential predictors) influencing the strength of the ON and DJF rains.

Results from Wavelet Transforms on dominant modes of variability in drought incidence indicate a dominant 2-8 year frequency that is similar to the documented dominant variance in the El Niño Southern Oscillation (ENSO) (Rasmussen and Carpenter, 1982; Torrence and Webster, 1999). The 8-16 (decadal) frequency significant at certain stations is similar to the dominant variance of the Indian Ocean Dipole (IOD) (Ashok et al., 2004). Does such a similarity indicate that ENSO and IOD are controlling

factors in the occurrence of *Maha* seasonal droughts? If so, what phase of ENSO and IOD are critical? These are examples of some of the questions addressed in Chapters 3 and 4 that focus on the issue of predictability of the ON and DJF rains respectively. The multi-decadal frequency (30-40 years) observed at Nuwara Eliya may stem from precipitation changes induced by extensive deforestation in the local over the last 100-150 years. Further research is needed to establish if land change could be a driver of the multi-decadal frequency observed at this station.

Drought occurrence and variability appears to be increasing along the eastern and southeastern regions of the island. Whether such a trend could be attributed to the influence of global change on factors affecting the strength of *Maha* rainfall requires further study.

## **Chapter 3: Predictability of the October-November rains**

### **3.1: Introduction**

Several recent studies have characterized the influence of ENSO on rainfall over Sri Lanka (Rasmusson and Carpenter, 1983; Suppiah, 1996; Zubair et al., 2007). Others have addressed the influence of Indian Ocean sea surface temperatures (SSTs) and the IOD Mode (Li et al., 2003; Saji and Yamagata, 2003) on rainfall over Sri Lanka (Malmgren et al., 2007; Zubair et al., 2003). Findings of these studies relevant to understanding atmospheric factors driving rainfall during the Maha include the enhancement of boreal fall rainfall during El Niño events and positive IOD events (Rasmusson and Carpenter, 1983; and Zubair and Ropolewski, 2006); and the association of droughts in Sri Lanka with the cold phase of ENSO (Lyon et al., 2009).

These studies have not specifically delved into the predictability of drought or other climate extremes. Their focus has consistently been to explain the influence of various teleconnection mechanisms on the inter-annual variability of precipitation over Sri Lanka. Studies on the seasonal predictability of rainfall over Sri Lanka are limited and have focused primarily on ENSO-driven predictability (e.g. Suppiah, 1989; Zubair et al., 2007). The ENSO-rainfall correlation has been extended to characterize ENSO's influence on rice production (Zubair, 2002) and to predict coconut production (Pieris, et al. 2008).

These investigations provide invaluable insight into some of the atmospheric processes influencing seasonal rainfall. However, they are not directly applicable to operational planning due to two reasons. First, the predictor fields – most often SSTs in the Nino3.4 region, the SOI or the IOD mode index – do not account for all the variance

in seasonal rainfall and their associated empirical relationships are not constant through time. Many previous studies on the ENSO-monsoon coupling report epochal changes and periodic degradations in skill when using ENSO indices as the predictor fields (Rajeevan, 2001; Parthasarathy et al., 1991). While the influence of positive IOD events on rainfall over Sri Lanka has been documented (Zubair et al., 2003), the influence of negative IOD events has not been documented as yet. Negative IOD events may not necessarily have the inverse influence to positive IOD events as the influence of positive and negative phase IOD events on rainfall during the boreal fall over South Asia is asymmetric (Prasanna and Yasunari, 2008). Such findings alert us to the dangers of relying entirely on empirical predictors without understanding their underlying physical mechanisms.

Second, past studies on the predictability of seasonal rainfall over Sri Lanka have considered the months October to December (OND) as comprising a single season – often referring to it as the northeast monsoon season (Zubair and Ropelewski, 2006; Zubair et al., 2007). OND is the northeast monsoon season over southern and southeastern India. As Sri Lanka is closer to the equator than southern peninsular India, it is influenced by a transition season from October-November referred to as an “inter-monsoon”. The separation of the inter-monsoon from the monsoon season is not a new concept. Many studies on tropical climate have reported that there is such a transition season in locations in close proximity to the equator (Hastenrath 2000; Hastenrath and Polzhin, 2004). Numerous past studies on Sri Lankan climate have delineated four rainfall seasons: the first inter-monsoon (March-April); the southwest monsoon (May-September); the second inter-monsoon (October-November); and the northeast monsoon

(December-February) (Domrös, 1974; Yoshino and Suppiah, 1984). The October-November (ON) season in Sri Lanka is distinct from the northeast monsoon season (DJF). Such distinction is evident when comparing the monthly mean lower atmospheric wind field at 850hPa directly over Sri Lanka for October-November and December-February (Fig. 3.1). In October (Fig. 3.1 (a)), westerly winds prevail to the immediate south with no distinct direction to the mean wind field over the island. In November (Fig. 3.1(b)), the band of westerlies is placed further south and the mean wind field over the island has no distinct direction. Winds during December, January and February have a distinct northeasterly or easterly direction (Fig. 3.1 (c)-(d)). As useful information on processes influencing a particular rainfall season is lost if different seasons are lumped together, this study sticks to the traditional delineation of rainfall seasons over Sri Lanka as it has a consistent physical basis.

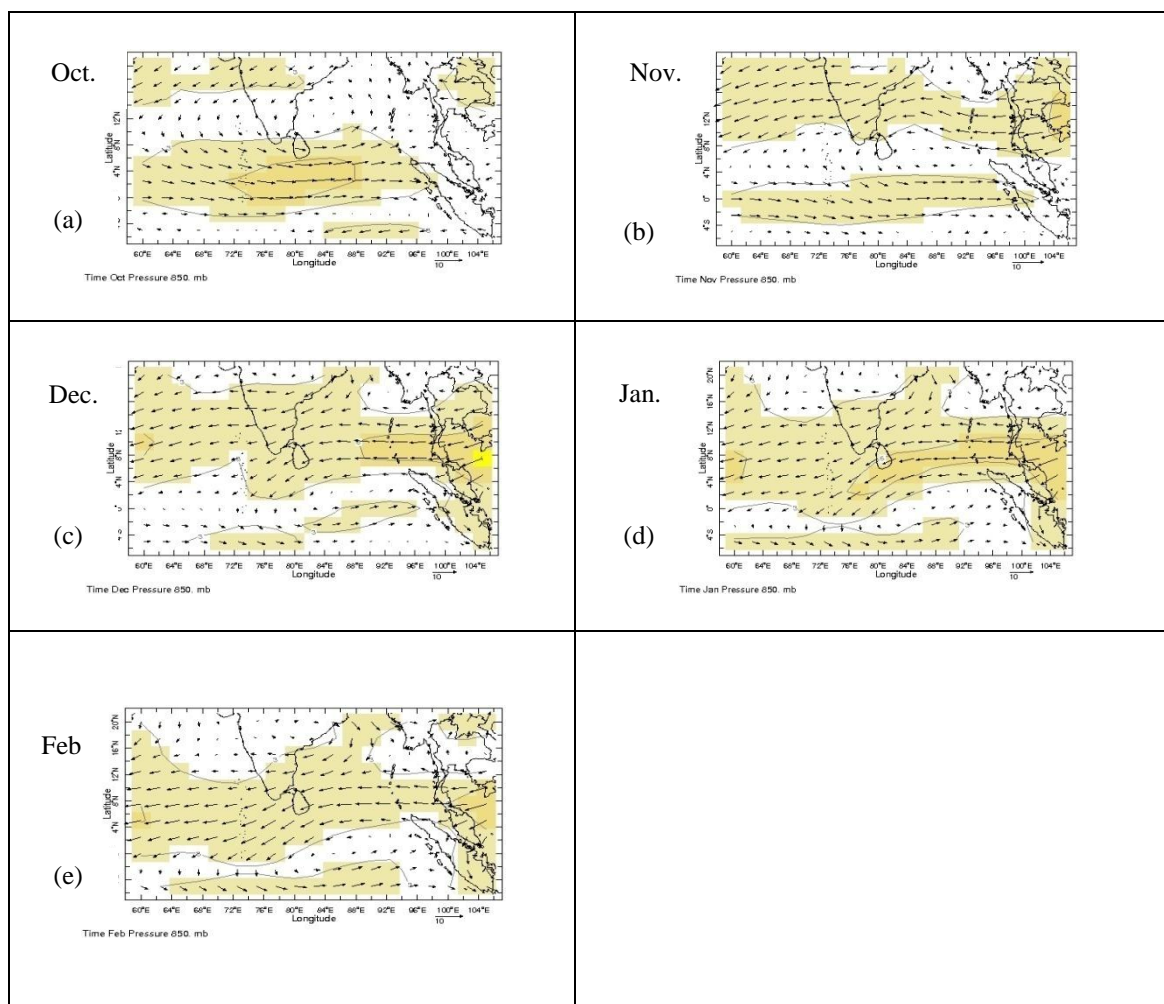


**Figure 3.1:** Mean 850hPa wind field over Sri Lanka for October, November, December, January and February from NCEP-NCAR reanalysis data for 1951-2005

The chapter seeks to elucidate the atmospheric factors that induce the failure of the ON rains. It proposes a methodology that could be adopted to forecast ON rainfall in an operational manner. Specific research questions addressed include: What atmospheric factors drive the failure of the ON rains? and, Can seasonal forecasts from GCM ensemble runs predict the failure of ON rainfall? It reports on the factors driving the failure of the October-November rains, and on the predictability of these rains using selected predictor fields generated by GCM seasonal forecasts. Chapter 4 reports on the atmospheric factors influencing DJF rainfall and its predictability.

## **3.2: Methodology and datasets used**

### ***3.2.1: Analysis of atmospheric factors influencing ON rain failure***

#### ***3.2.1.1: Datasets used:***

Daily quality-controlled rainfall data at 132 rain gauges (Fig. 2.1, Chapter 2) across Sri Lanka were obtained from the Sri Lanka Department of Meteorology for the period 1961-2005. Total ON rainfall was calculated after aggregating the daily data to monthly rainfall.

NCEP-NCAR Reanalysis (Kistler et al., 2001) data, at  $2.5^0 \times 2.5^0$  resolution, of the following fields for the period 1961-2005: September mean sea level pressure (domain:  $40^0\text{E}$ - $270^0\text{E}$  and  $30^0\text{S}$ - $45^0\text{N}$ ); October-November mean geopotential heights at 850hPa, 500hPa and 200hPa (domain:  $40^0\text{E}$ - $270^0\text{E}$  and  $30^0\text{S}$ - $45^0\text{N}$ ); and October-November mean zonal and meridional wind at 850hPa (domain:  $40^0\text{E}$ - $270^0\text{E}$  and  $30^0\text{S}$ - $45^0\text{N}$ ).

#### ***3.2.1.2: Analysis method:***

Cross-validated Canonical correlation analysis (CCA) was the method adopted to identify the large-scale atmospheric patterns influencing ON rainfall and to build the statistical downscaling model. CCA identifies a sequence of pairs of patterns in two multivariate datasets. Linear combinations of the original data are then produced by projecting the original data onto the identified patterns. New variables – known as the “canonical variates” – that maximize the interrelationships between the two data sets are then identified (Wilks, 2006, pg. 509).



CCA is used as a purely statistical forecasting technique if one of the data fields (e.g. the  $x$  or the predictor) is observed prior to the other field (e.g. the  $y$  or the predictand) (Von Storch and Zwiers, 2002; Wilks, 2006). Such application of CCA has been undertaken in the forecasting of SSTs (Landman and Mason, 2001), in the prediction of seasonal temperatures over land (Shabbar and Barnston, 1996) and in the prediction of ENSO episodes (Barnston and Ropelewski, 1992). When using CCA for forecasting purposes, a simple linear regression model is constructed that relates the predictand canonical variates  $w_m$  to the predictor canonical variates  $v_m$  (Wilks, 2006).

$$w_m = \hat{\beta}_{0,m} + \hat{\beta}_{1,m}v_m$$

Where,

$m = 1, 2, \dots, M$  ( $M$  – the number of canonical pairs)

For the purposes of this study, the original predictor and predictand fields are filtered using Empirical Orthogonal Function (EOF) analysis prior to performing CCA on a subset<sup>11</sup> of the EOF modes (Barnett and Preisendorfer, 1987; Bretherton et al., 1992). EOF is a data compression technique such that a dataset containing a large number of variables is reduced to a dataset containing fewer new variables. The new variables are linear combinations of the original variables chosen in such a manner that the new linear combinations represent the highest possible proportion of variability found in the original dataset. If there are multiple observations of a  $(K \times 1)$  data vector  $x$ , EOF finds  $(M \times 1)$  vectors  $u$  whose elements are linear combinations of the elements of the  $x_s$  that contain most of the information of the original collection of  $x_s$ . The components or new variables are defined by the eigenvectors of the covariance matrix of  $x$ ,  $[S]$ . The  $m^{th}$

---

<sup>11</sup> The subset is usually composed of just the leading EOF modes accounting for over 90% of the variance in the datasets.

orthogonal function (principal component),  $u_m$  is obtained as the projection of the data vector  $x'$  (data anomalies) onto the  $m^{\text{th}}$  eigenvector  $e_m$  such that:

$$U_m = e_m^T x'$$

or

$$U_m = [E]^T x'$$

Where,  $[E]$  is a square matrix with  $K$  eigenvector columns (Wilk, 2006, pg. 463-464).

The first few components – i.e. vectors  $u$  – contain the largest fraction of the variance of the original dataset. Most often, the first 2-3 components account for approximately 99% of the variance of the system (von Storch and Zwiers, 1999). Each consecutive component is constrained to be orthogonal to the previous component.

Cross-validation is a technique used to reduce the problem of over-fit or artificial skill (Barnston and van den Dool, 1993). A portion of the dataset is left out when building the forecast model<sup>12</sup>. The forecast is then verified using the portion left out. The number of data points that could be omitted ranges from 1 (referred to as “leave-one-out-cross-validation”) to half the sample size (Barnston and van den Dool, 1993). A training period of 45 years (1961-2005) and a cross-validation window of 3 years were used in this study. Thus, at each 3-year step, the 3 consecutive years are omitted from the training period. Next, the forecast model is completely reconstructed and the forecast is generated for the middle year – i.e. the second year – in the years omitted from the training period. The process is repeated for each in the training dataset. The predictor

---

<sup>12</sup> The Climate Predictability Tool (CPT) - <http://iri.columbia.edu/outreach/software/index.html> - developed at the International Research Institute for Climate and Society (IRI), Columbia University, was used to run construct the statistical prediction model based on CCA. The tool has three analysis options: CCA, Principal Components Regression and Multiple Linear Regression. It builds statistical prediction models based on one of these three analysis techniques.

fields tested were the NCEP-NCAR reanalysis fields mentioned above (section 2.1.1) and the predictand was total ON rainfall at the 132 rain gauges.

The strength of the predictor fields were assessed based on the overall goodness-of-fit between the cross-validated forecasts and the observation time series. Goodness-of-fit is a measure presenting an average correlation between the cross-validated forecasts and the observation time series. The measure is reported for every possible combination of predictor and predictand modes. When the goodness-of-fit value is closer to 1 the correlation between the predictor and predictand fields is stronger. The optimum predictor field was selected after several iterations of varying predictor domains to identify the predictor and relevant domain that had the most influence on ON rainfall.

The optimum predictor field was the contemporaneous (ON) zonal wind at 850hPa (referred to hereafter as U850) within the domain 40°E-105°E and 5°S-15°N. Studies note the presence of a zonal circulation cell with strong lower atmospheric westerlies that drive an eastward equatorial jet (Wyrtki Jet) in the equatorial Indian Ocean region during the monsoon transition months of April-May and October-November (Hastenrath, 2000; and Hastenrath and Polzin, 2003 and 2004). Therefore, the selection of U850 as a potential predictor of the ON rains has a physical basis. Temporal composites of the U850 pattern in drought years associated with the failure of ON rainfall (Table 2.5, Chapter 2) were prepared to identify U850 wind characteristics in such years.

The ON season receives most of its rainfall from tropical depressions and cyclones – most of which originate in the Bay of Bengal (Suppiah, 1996). Rainfall is distributed throughout the island during this season (Yoshino and Suppiah, 1984). The U850 has a significant negative correlation (blue region in Fig. 3.2) with ON rainfall and

thus appears to influence factors – such as vorticity at 850hPa, vertical velocity at 500hPa and the vertical shear of the mean zonal wind (difference in wind speed between 200hPa and 850hPa) – driving convection over Sri Lanka during this season. The interplay between these factors in drought years was studied using composite analysis on NCEP-NCAR reanalysis data of these fields. Low-level vorticity and vertical shear of the mean zonal winds were selected as factors influencing convection, as their influence on tropical cyclogenesis has been reported (Frank and Roundy, 2006; and Bessafi and Wheeler, 2006). Mid-atmospheric (500hPa) vertical velocity was selected as it has previously been used to study tropical convection in conjunction with the low-level vorticity and zonal wind shear fields (Hastenrath and Polzin, 2004).

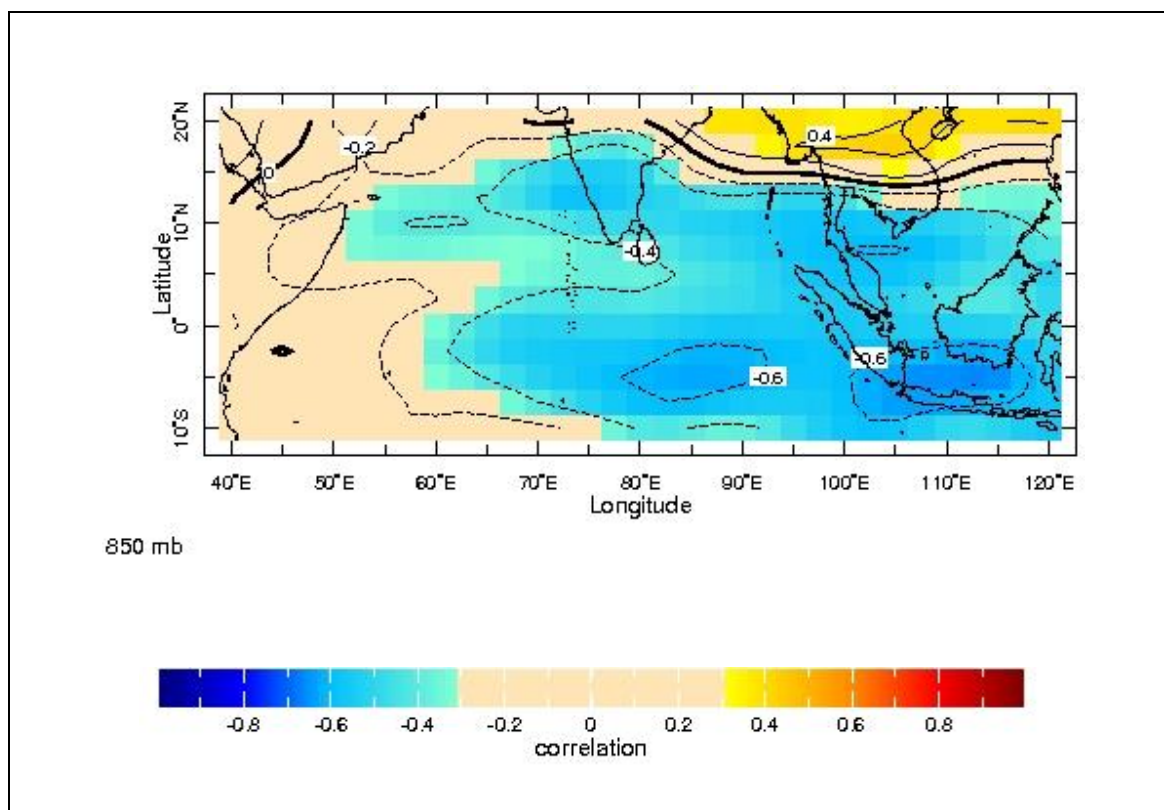


**Figure 3.2:** Correlation between zonal winds at 850hPa and mean ON rainfall over Sri Lanka. Broken lines show regions negatively correlated, and solid lines show regions positively correlated, with ON rainfall. Blue (negative correlation) and orange (positive correlation) shading depict correlation significant at the 95% confidence level. The contour interval is 0.2 correlation units.

### ***3.2.2: Assessment of the predictability of ON rain failure***

#### ***3.2.2.1: Datasets used:***

Retrospective forecasts of U850, issued with one month's lag in September, were obtained from archives of experimental forecasts carried out at the IRI using the ECHAM4.5 AGCM (Roeckner et al., 1996) forced with persisted SST anomalies (ECHAM\_PSST) and constructed analogues of SST anomalies (ECHAM\_CA) (Li and Goddard, 2005) and from the National Centers for Environmental Prediction (NCEP) fully coupled Climate Forecast System (CFS) GCM (Saha et al., 2006). September was selected as the month when the forecast is issued as it is in September that the Department Agriculture of Sri Lanka holds the 'Seasonal Conference' at which decisions on what variety and extent of rice and other annual crops should be planted during the oncoming *Maha* season are made. Thus, the forecast of ON U850 – and hence expected ON rainfall – can be made with a lag of one month. The time-lag of one month is, therefore, useful for operational purposes.

The ECHAM4.5 is a spectral model with a triangular truncation at wave number 42 (T42) – equivalent to approximately 2.8°degrees in the horizontal and 18 levels in the vertical (Li and Goddard, 2005). The ECHAM\_PSST retrospective forecasts for the period 1968-2002 were produced using a 12-member ensemble with persisted anomalies of the SSTs as boundary forcing. These boundary conditions are generated by persisting the observed SST anomalies of the month preceding the forecast period and adding it to the evolving annual cycle of climatological SSTs (Li and Goddard, 2005). The ECHAM\_PSST retrospective forecasts have a lead time of 5 months. Monthly ECHAM\_PSST retrospective forecasts from January 1968 to June 2003 are archived at:

<http://iridl.ldeo.columbia.edu/expert/SOURCES/.IRI/.FD/.ECHAM4p5/.Forecast/.psst/.ensemble12/.MONTHLY/>. The ECHAM\_CA retrospective forecasts for the period 1957 to July 2008 were produced using a 24 member ensemble with constructed analogues (van den Dool, 1994) of SSTs over the tropical oceans as boundary forcing (Li and Goddard, 2005). The ECHAM\_CA forecasts have a lead time of 7 months. Monthly ECHAM\_ca retrospective forecasts from January 1957 to July 2008 are archived at [http://iridl.ldeo.columbia.edu/expert/SOURCES/.IRI/.FD/.ECHAM4p5/.Forecast/.ca\\_sst/.ensemble24/.MONTHLY/](http://iridl.ldeo.columbia.edu/expert/SOURCES/.IRI/.FD/.ECHAM4p5/.Forecast/.ca_sst/.ensemble24/.MONTHLY/).

The CFS is a fully-coupled ocean-land-atmosphere seasonal climate prediction system. The atmospheric component is the NCEP GFS model with a spectral triangular truncation at wave number 62 (T62) – equivalent to an approximately 200km Gaussian grid. It has 64 vertical layers. The ocean is represented by the GFDL Modular Ocean Model version 3 (MOM3) with a latitudinal domain from 74°S to 64°N. The zonal resolution is 1°. The meridional resolution is 1/3° between 10°S and 10°N and gradually increases towards the tropics and remains fixed at 1° poleward of 30°S and 30°N (Saha et al., 2006). There are 40 vertical levels. The vertical resolution from the surface to 240m depth is 10m and increases to a maximum of 511m downward of 240m (Saha et al., 2006). Retrospective forecasts from 1981 to the present were generated using a 15-member ensemble. The CFS forecasts have a lead time of 9 months. Monthly CFS retrospective forecasts from January 1981 to December 2008 are archived at <http://iridl.ldeo.columbia.edu/expert/SOURCES/.NOAA/.NCEP/.EMC/.CFS/.MONTHLY/>.

The predictand dataset used was ON rainfall at the 132 rain gauges (mentioned in section 2.1.1).

### **3.2.2.2: Analysis method:**

The statistical forecasting model was constructed with Model Output Statistics (MOS)<sup>13</sup> using CCA (same as in section 2.1.2).

The skill in predicted precipitation at the rain gauges was measured using Pearson's moment correlation (Wilks, 2006, pg.50). Strength of the correlation represents the degree to which predicted precipitation matches the observed. Skill in predicted tercile (whether below-, above- or near-normal) precipitation was measured using the Hit Skill Score (Baigorria et al., 2008) where:

$$\text{Hit Skill Score} = \frac{\text{No. correct} - \text{No. expected correct}}{\text{No. of forecasts} - \text{No. expected correct}} \times 100\%$$

The HSS is a measure of the percentage of times, beyond that expected by chance, the tercile forecast category corresponds to the observed category. The Hit Skill Score (HSS) has a range from -100% (complete lack of predictability) to +100% (maximum predictability).

Tercile forecast probabilities in years of known drought was the metric used to assess whether seasonal forecasts from the GCMs could predict ON rain failure.

---

<sup>13</sup> The term Model Output Statistics (MOS) is used to refer to statistical downscaling performed using model generated output as predictor variables.

### 3.3: Results

#### 3.3.1: Atmospheric dynamics driving failure of the October-November rains

Anomalously strong contemporaneous zonal winds at 850hPa, in the domain 5°S-15°N and 60°E-105°E (hereafter referred to as the central Indian Ocean) suppress convection over Sri Lanka during the ON season (Fig. 3.3).

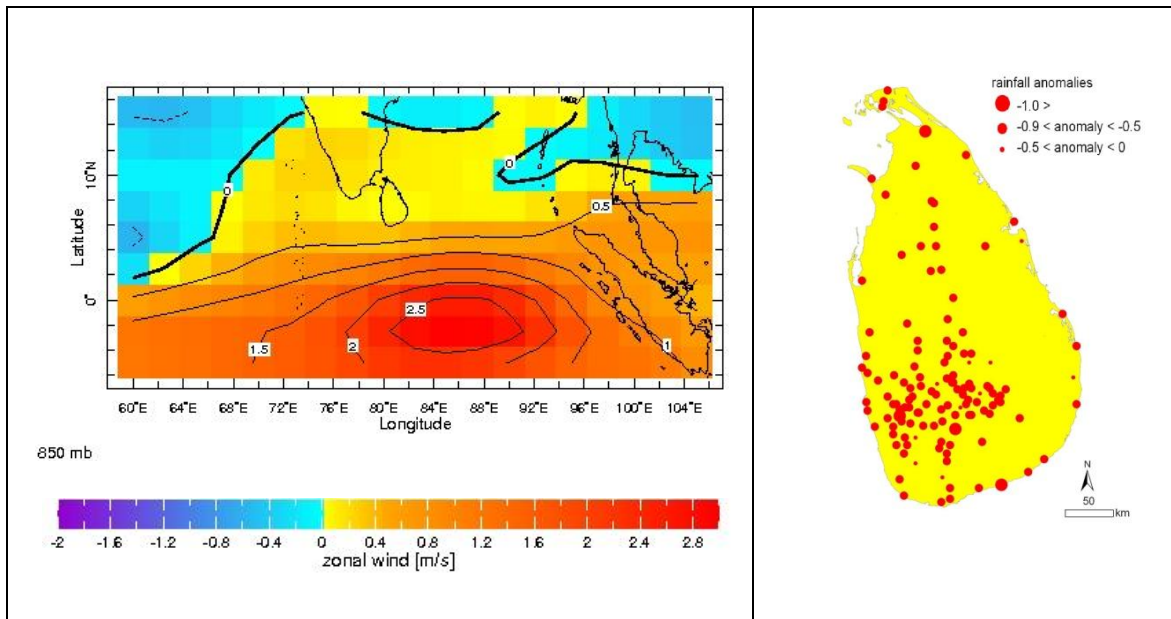


**Figure 3.3:** Temporal composites of the October-November (contemporaneous) U850 field (left) and associated negative anomalies in mean ON rainfall over Sri Lanka in years when ON rainfall failed (right)

In years when the zonal winds are anomalously strong, a strong vertical shear of the mean zonal wind, weak low-level vorticity, and anomalously low mid-tropospheric vertical velocity act in concert to suppress convection over Sri Lanka (Fig. 3.4).



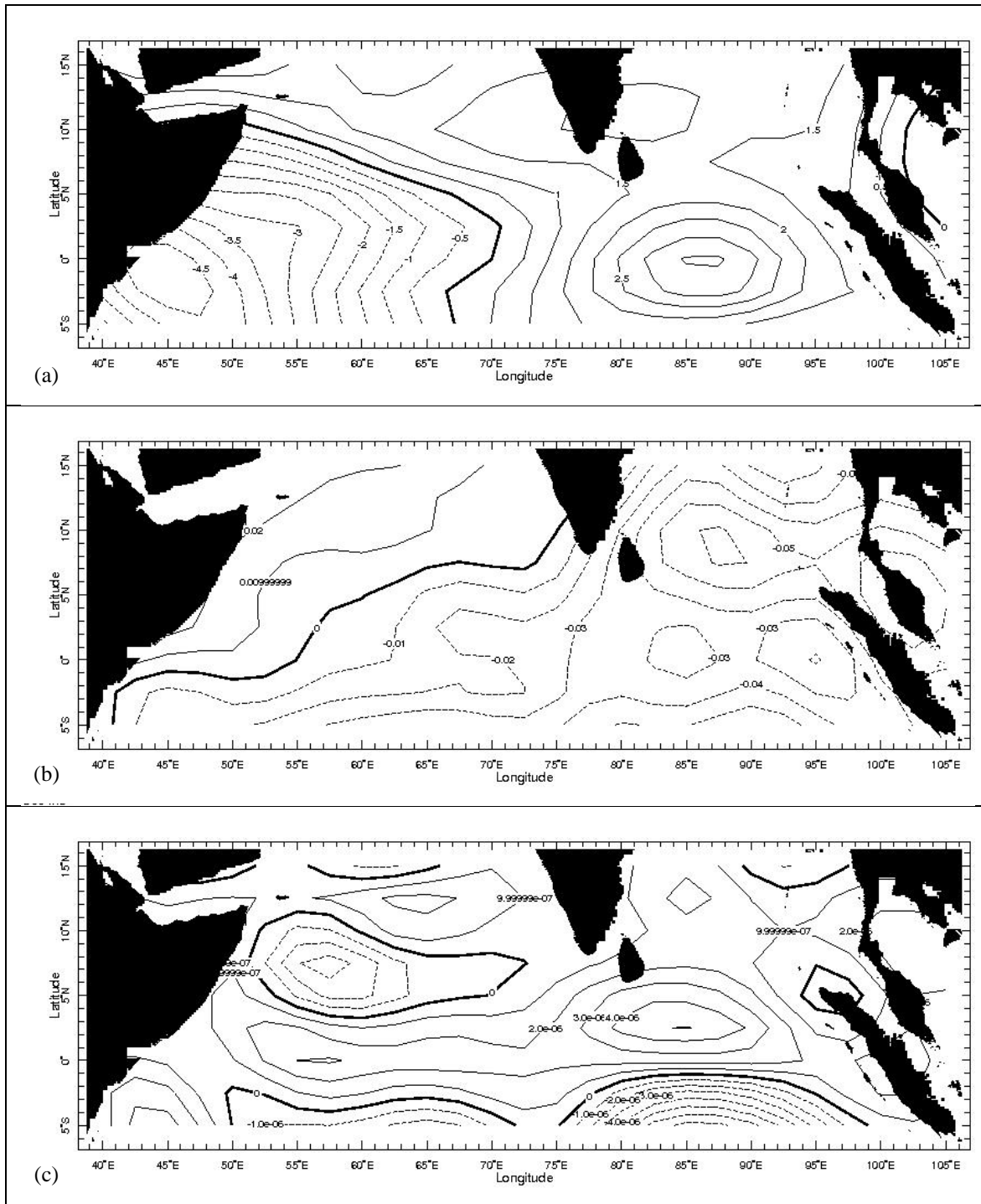


**Figure 3.4:** Temporal composites of October-November anomalies of the vertical shear of the zonal wind (a), vertical velocity at 500hPa (b) and relative vorticity at 850hPa (c) in years when ON rainfall failed

The strength of the contemporaneous U850, over the central Indian Ocean, in drought years is often (but not always) in sync with the high phase of the Southern Oscillation (SO) (Fig 3.5). This corroborates prior investigations that have noted that the equatorial westerlies are often strengthened during the high phase of the SO (Hastenrath 2000; Hastenrath and Polzin, 2003; and Suppiah, 1989) and that there is a strong negative correlation between ON rainfall and the SOI (Suppiah, 1997). Zonal wind anomalies in the Indian Ocean are also strongly coupled to the IOD Mode (Saji et al., 2003; Ashok et al., 2004) that matures in the months September to October. Most years of anomalously strong zonal winds coincide with negative IOD events (Fig. 3.5). However, as with the SOI, the relationship is not constant.

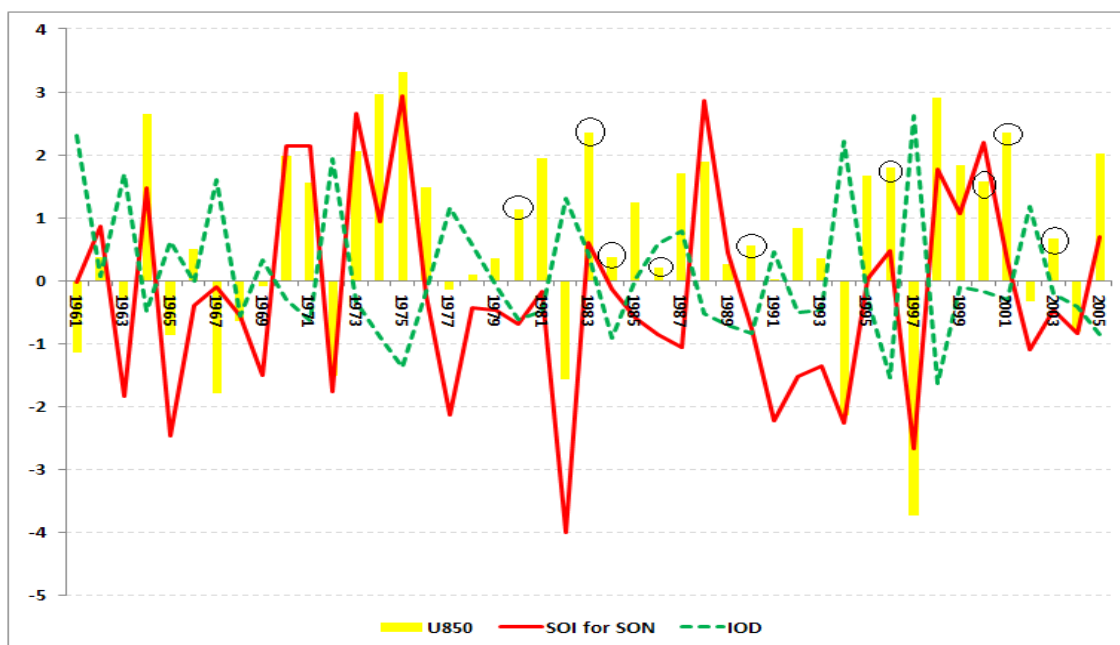


**Figure 3.5:** Mean October-November U850 for the domain  $5^{\circ}\text{S}$ - $15^{\circ}\text{N}$  and  $60^{\circ}\text{E}$ - $105^{\circ}\text{E}$  (yellow bars); mean SOI for September-November (red line); the Indian Ocean Dipole mode index (dashed green line) calculated as the standardized difference between the spatial mean SST over the western ( $50^{\circ}\text{E}$ - $70^{\circ}\text{E}$  and  $10^{\circ}\text{S}$ - $10^{\circ}\text{N}$ ) and eastern ( $90^{\circ}\text{E}$ - $110^{\circ}\text{E}$  and  $10^{\circ}\text{S}$ - $0^{\circ}\text{S}$ ) Indian Ocean (Vinayachandran et al., 2002); and years when ON rainfall anomalies were negative (black circles above yellow bars)

### ***3.3.2: Predictability of the October-November season***

All three GCMs were able to capture quite well the leading canonical mode of the zonal wind associated with ON rain failure/enhancement (Fig. 3.6) as identified in the diagnostic analysis (section 3.1). The pattern of the spatial loadings of the zonal wind field in the CFS (Fig. 3.5 (c)) matches the observed pattern (Fig. 3.3 (left)) better than the two versions of the ECHAM4.5.

Pearson's correlation skill values were significant at the 95% confidence level in the southern, southeastern and west-central regions of the island for the two versions of the ECHAM4.5 (Fig. 3.7(a) and (b)). The ECHAM4.5\_PSST also had a region of significant skill in the north-central region. Skill values for the CFS were not significant (Fig. 3.7(c)) and many stations in the southwestern region recorded negative correlation values not seen in the two versions of the ECHAM4.5.

The average and maximum Hit Skill Scores (HSS) for the downscaled forecasts from all three GCMs were 20% and 45% respectively. Figure 3.8 shows examples of time series of observed versus predicted precipitation at a station with an average HSS (Fig. 3.8(a)) and at a station with an HSS in the 90<sup>th</sup> percentile (Fig. 3.8(b)). Of the 132 stations used in the analysis, the percentage of stations with no skill ( $HSS \leq 0$ ) was 9% in the ECHAM4.5\_PSST, 14% in the ECHAM4.5\_CA, and 17% in the CFS. Stations with no skill in the two versions of the ECHAM4.5 were located along the western coastal region while some of the stations with no skill in the CFS were located in the interior of the island.

Forecast skill in rice cultivation areas in the central, north-central, southern and southeastern parts of the country is promising. Skill over rice cultivation areas in the east

is limited. Overall, the two versions of the ECHAM4.5 have better skill over the rice cultivation area than the CFS.

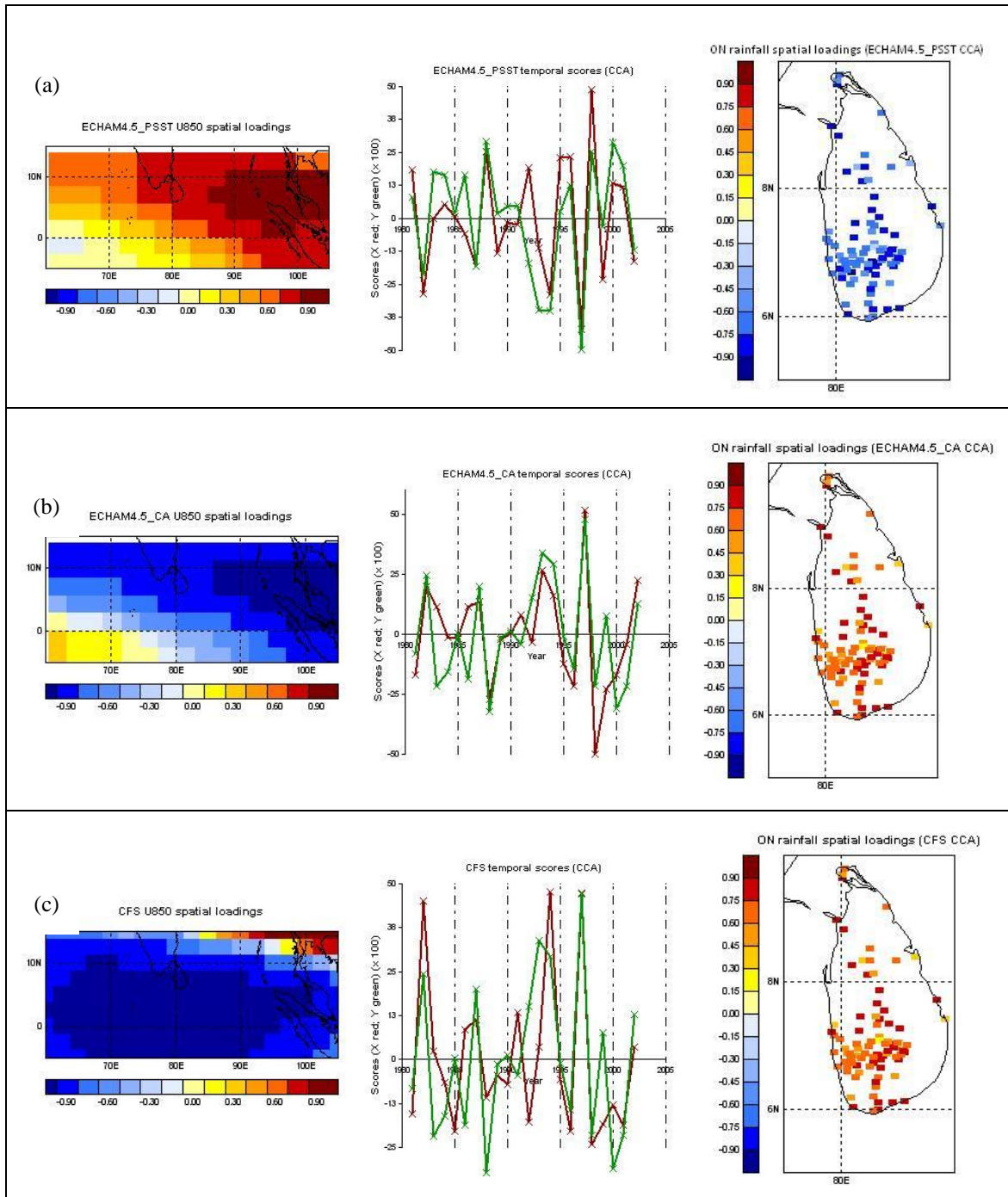


**Figure 3.6:** Leading canonical modes and associated temporal scores of the spatial loadings for the ECHAM4.5\_PSST (a); the ECHAM4.5\_CA (b); and the CFS (c). Red in the spatial loadings of U850 spatial loadings and ON rainfall anomalies indicates positive anomalies and blue indicates negative anomalies. The red line in the temporal scores depicts the predictor and the green line depicts the predictand.

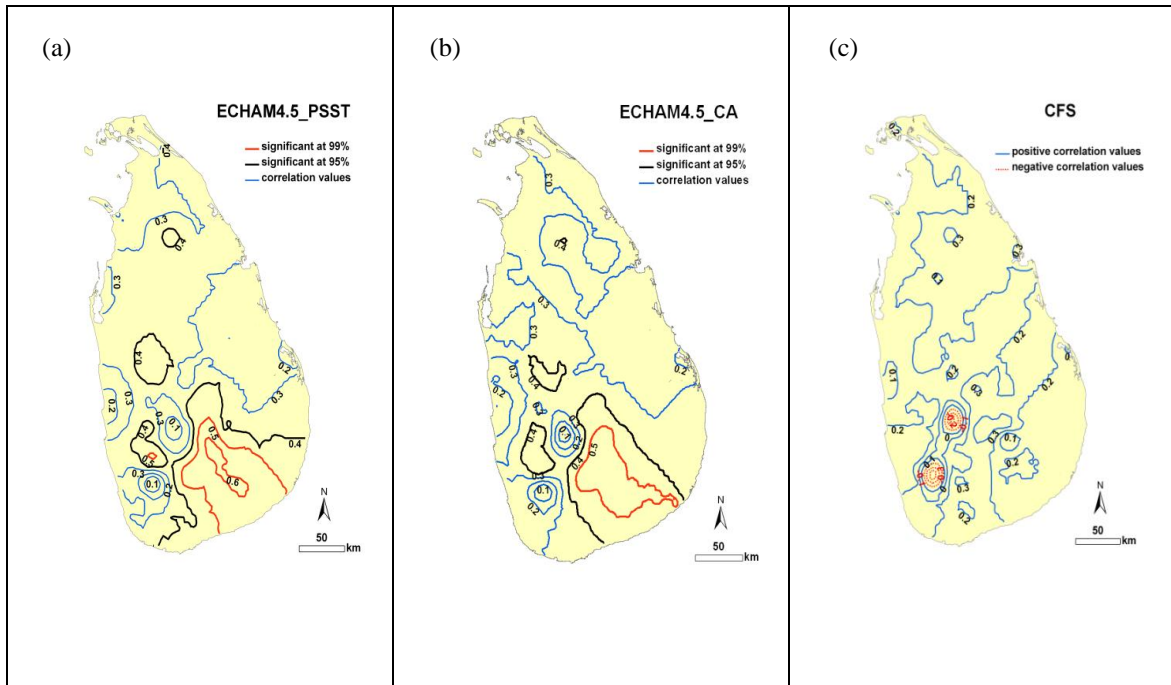


**Figure 3.7:** Pearson's correlation skill maps for the ECHAM4.5\_PSST (a); the ECHAM4.5\_CA (b); and the CFS (c). Contour interval is 0.1 correlation units. Correlation values significant at the 95% confidence level are depicted as solid black lines and correlation values significant at the 99% confidence level are depicted as solid red lines.

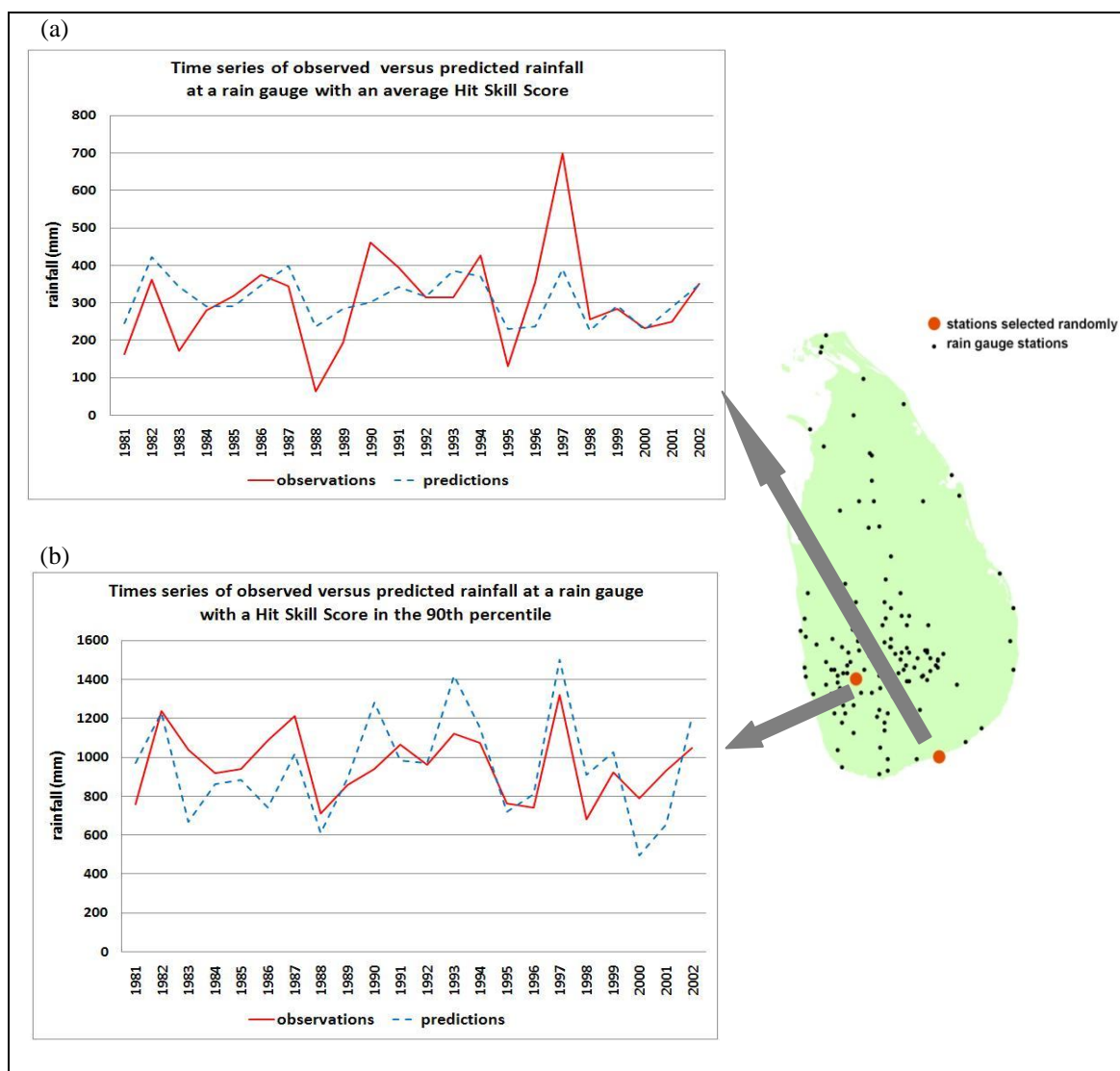


**Figure 3.8:** Examples of predicted (from ECHAM4.5\_PSST) versus observed rainfall at rain gauge stations with an average Hit Skill Score (a) and at a station with a Hit Skill Score in the 90<sup>th</sup> percentile (b). Filled orange circles in the map of rain gauge stations (right) show the location of the stations selected randomly.

The ECHAM4.5\_PSST and the CFS had their tercile probability forecasts for ON rainfall weighted towards the below-normal category in the years of extreme drought when ON rainfall anomalies were below normal (i.e. 2000 and 2001). An example of the tercile probability forecast for ON rainfall in 2001 from the CFS clearly shows weighting of the probabilities towards the below-normal category (Fig. 3.9). The tercile probability forecast of the ECHAM4.5\_CA got the tercile forecast for 2000 correct but was weighted towards the above-normal category in 2001. None of the GCM ensemble predictions was able to get the tercile forecast for ON rainfall in moderate drought years correct (Table 3.1).

<i><b>Drought category</b></i>	<i><b>Years</b></i>	<i><b>ECHAM4.5_PSST</b></i>	<i><b>ECHAM4.5_CA</b></i>	<i><b>CFS</b></i>
Extreme	2000	BN (correct)	BN (correct)	BN (correct)
	2001	BN (correct)	AN (wrong)	BN (correct)
Moderate	1983	AN (wrong)	AN (wrong)	AN (wrong)
	1986	AN (wrong)	AN (wrong)	AN (wrong)

**Table 3.1:** Summary of tercile probability forecasts of ON rainfall from the two versions of the ECHAM4.5 and the CFS. BN refers to below-normal and AN refers to above-normal.

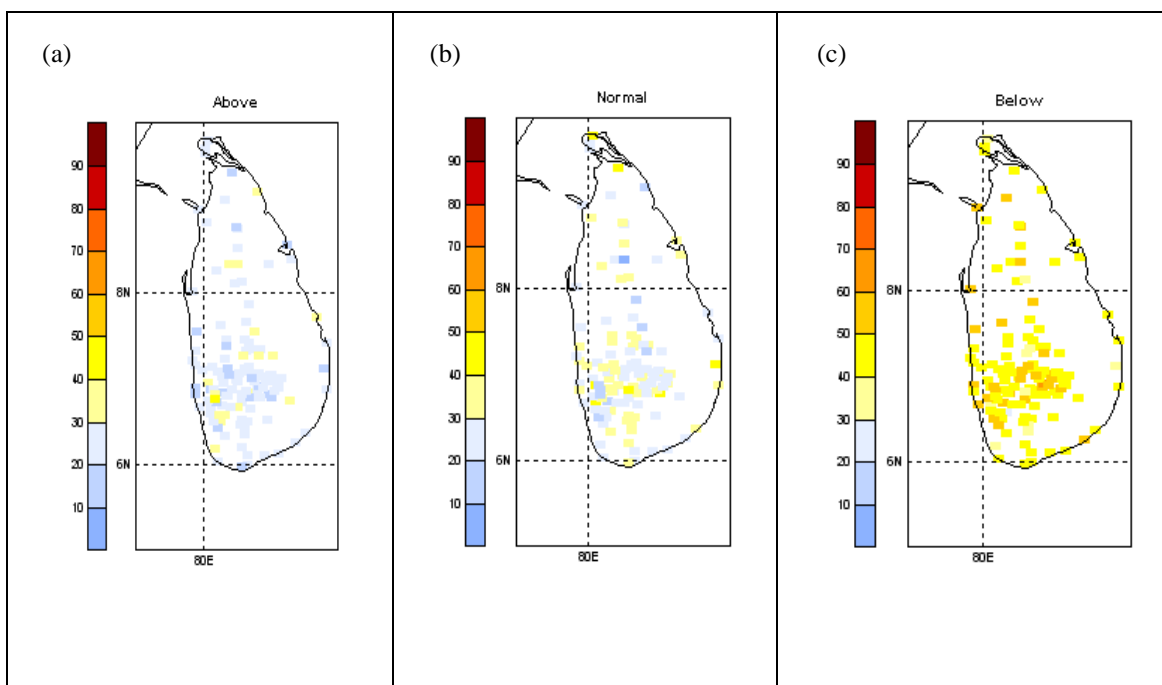


**Figure 3.9:** Tercile probability forecasts of ON rainfall in 2001 generated from the CFS depicting the above-normal (a), near-normal (b) and below-normal (c) categories. Blues indicates lower probabilities and reds indicate higher probabilities.

### 3.4: Conclusion

The study finds that the strength of the contemporaneous zonal (westerly) winds at the 850hPa level over the domain  $60^{\circ}\text{E}$ - $105^{\circ}\text{E}$  and  $5^{\circ}\text{S}$ - $15^{\circ}\text{N}$  controls October-November precipitation over Sri Lanka. Drought occurs when anomalously strong zonal winds over the central Indian Ocean suppress convection over Sri Lanka. The exact reason for the strengthening of the westerly zonal winds is as yet unclear. It could be a consequence of strong summer monsoon winds increasing upwelling along the east African coast and thus setting up a marked SST gradient between the eastern and western Indian Ocean. Results show that in some years the anomalous strengthening of the zonal winds can be attributed to La Niña events and negative IOD events. 1983 and 2000 were two *Maha* drought years – coinciding with La Niña events – when only October-November rainfall,



and not December-February rainfall, failed. December-February rainfall was above normal in those two years. Whether ENSO leads IOD influence on the zonal wind or vice versa, or whether both simply act in concert, is as yet unclear. The reason for there being years when the zonal winds are strong without either of these phenomena exerting a discernible influence is also unclear.

It is evident that the zonal wind field is consistently above normal in years when ON rainfall is below normal. This alone is an improvement on predictions relying on indices of the Southern Oscillation or the IOD given that the influences of those modes are not consistent through time.

Droughts associated with the failure of ON rainfall can be predicted on an operational basis using GCM predicted fields of ON U850 issued in September of a given year. Statistically significant forecast skill was observed over the rice cultivation areas of the southern, southeastern, central and north-central portions of the island in the two versions of the ECHAM4.5. Therefore, estimates of expected rainfall at station-level from the two versions of the ECHAM4.5 can be utilized to aid specific decisions on the variety and extent of rice to be planted in these areas. Tercile forecasts from the CFS and the ECHAM4.5\_PSST can be consulted to predict whether the upcoming Maha season is likely to be susceptible to drought.

## **Chapter 4: Predictability of the December-February rains**

### **4.1: Introduction**

The December-February (DJF) northeast monsoon season coincides with the Asian winter monsoon. The northeast monsoon brings rainfall to the eastern seaboard and the eastern slopes of the central hills of Sri Lanka (Suppiah, 1989).

The Asian monsoon system dominates the tropics and sub-tropics of the entire eastern hemisphere (Wang, 2006). It is a coupled land-ocean-atmosphere phenomenon where the Pacific and the Indian Oceans and the Eurasian continent play significant roles (Bamzai and Shukla, 1999). It is driven by a combination of land-sea temperature contrast and latent heat release (Ramage, 1971). The land-sea contrast fueling the Asian summer monsoon sets in with the advent of spring as the Asian landmass and adjacent air column warm to a temperature higher than that of the surrounding oceans (Barnett et al., 1989). A land-to-sea surface circulation takes place in the boreal winter when the oceans south of the Asian landmass warm with the southward migration of the of the inter-tropical convergence zone (ITCZ). The winter-time land-to-sea circulation is known as the Asian winter monsoon.

The winter monsoon over South Asia has received little emphasis in prediction studies compared to the extensive research undertaken to predict the South Asian summer monsoon and the East Asian winter monsoon.

As with predictability studies on the October-November (ON) season, past research on the South Asian winter monsoon has focused on ENSO driven predictability. Findings of such studies of potential relevance to assessing predictability of the DJF rains over Sri Lanka are: El Niño events strengthen northeast monsoonal rainfall over

Southeast India and Sri Lanka (Kumar et al., 2007; Zubair and Ropelewski, 2006); the correlation between El Niño and northeast monsoonal rainfall has been strengthening since the mid-1970s (Kumar et al., 2007); and that DJF rainfall over Sri Lanka has a significant negative correlation with the Southern Oscillation Index (SOI) for August-October (ASO) (Suppiah, 1989). A study characterizing the influence of the Indian Ocean Dipole Mode (IODM) on the northeast monsoon, finds that the positive (negative) phase enhances (decreases) the total northeast monsoon over southern and southeastern India (Kripalani and Kumar, 2004). Another study proposes the use of mean upper air temperatures for September as potential predictors of winter monsoonal precipitation over stations in southern India (Kumar et al., 2004).

Apart from the study that finds a significant negative correlation between DJF rainfall over Sri Lanka and the SOI (Suppiah, 1989), all the above consider October-December (OND) as the season when the northeast monsoon prevails. Chapter 3 discusses reasons why such delineation is not useful for studies on the seasonal predictability of rainfall over Sri Lanka.

Correlation between standardized anomalies of DJF rainfall at the 132 rain gauges with the SOI for ASO for the period 1961-2004 shows that the relationship established by Suppiah (1989) is neither significant nor consistent (Fig. 4.1). It is evident that there are years when DJF rainfall is suppressed during SOI negative (i.e. El Niño) years and enhanced during SOI positive (i.e. La Niña) years. As discussed in Chapter 3, this result confirms that epochal changes in the relationship between SOI versus seasonal rainfall render its use as a potential predictor of DJF rainfall questionable.

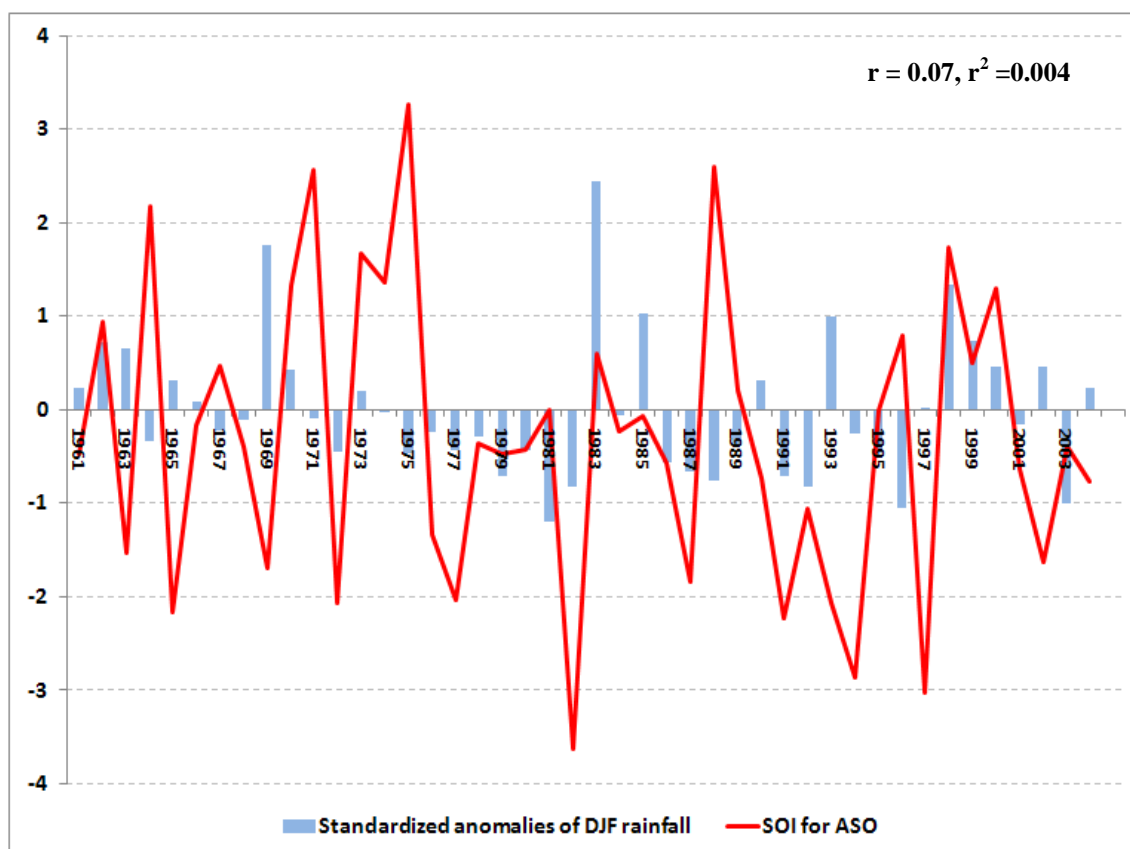


**Figure 4.1:** Plot of standardized anomalies of mean DJF rainfall (blue bar) at a 132 rain gauges versus August-September (ASO) mean value of the Southern Oscillation Index (SOI) (red line) for the period 1961-2004. Values on the y-axis are units of standardized anomalies.

The influences of baroclinic developments in the mid- and higher latitudes have a larger influence on equatorial regions during the Asian winter monsoon than during the summer monsoon (Chang, 2005). Thus, many factors, such as the influence of the Siberian High, snow cover anomalies over Eurasia, cold surge dynamics, etc., could potentially influence the strength of the northeast monsoon over Sri Lanka. Unfortunately, prior research has not examined the potential impact of such factors in detail. The only reference to the potential influence of the Eurasian landmass on DJF rainfall refers to dry conditions prevailing throughout the island when airstreams travelling southwards from the subtropical anticyclonic ridge in the Northern Hemisphere

have a larger proportion of their trajectories over the Indian subcontinent (JayaMaha, 1975).

This chapter seeks to elucidate the atmospheric factors that induce failure of the DJF rains. It examines the potential for forecasting DJF rains in an operational manner. Specific research questions addressed include: What atmospheric factors drive the failure of the DJF rains?; and Can seasonal forecasts from GCM ensemble runs predict the failure of DJF rainfall? It reports on the factors driving the failure of the DJF rains, and on the predictability of these rains using selected predictor fields generated by GCM seasonal forecasts.

## **4.2: Methodology and datasets used**

### ***4.2.1: Analysis of atmospheric factors influencing DJF rain failure***

#### ***4.2.1.1: Datasets used:***

Total DJF rainfall was calculated by aggregating daily quality-controlled data for the months December-February at the 132 rain gauges (mentioned in Chapter 2 and Chapter 3) for the period 1961-2004.

NCEP-NCAR Reanalysis (Kistler et al., 2001) data, at  $2.5^0 \times 2.5^0$  resolution, of the following fields for the period 1961-2004: Monthly and two- and three-month averages of mean sea level pressure (domain:  $40^{\circ}\text{E}$ - $270^{\circ}\text{E}$  and  $30^{\circ}\text{S}$ - $80^{\circ}\text{N}$ ) for the months September to February; November, December and December-February mean geopotential heights at 850hPa, 500hPa and 200hPa (domain:  $40^{\circ}\text{E}$ - $270^{\circ}\text{E}$  and  $30^{\circ}\text{S}$ - $50^{\circ}\text{N}$ ); and December-February mean zonal and meridional winds at 850hPa, 500hPa and 200hPa (domain:  $70^{\circ}\text{E}$ - $105^{\circ}\text{E}$  and  $0^{\circ}\text{N}$ - $30^{\circ}\text{N}$ ). Vertical wind shear (i.e. the difference in

wind speeds between 850hPa and 200hPa) of the zonal and meridional components of the mean December-February wind was also tested as a potential predictor variable.

#### ***4.2.1.2: Analysis method:***

Cross-validated canonical correlation analysis (section 3.2.1.2, Chapter 3), with a training period of 44 years (1961-2004) and a cross-validation window of 3 years, was the analysis technique used to identify the large-scale atmospheric patterns influencing DJF rainfall and to build the statistical downscaling model.

The optimum predictor field was the contemporaneous (December-February) vertical shear of the mean meridional wind (referred to hereafter as  $V_s$ ) in the domain 80°E-90°E and 0°N-20°N.  $V_s$  has not previously been suggested as a predictor of the strength of the northeast monsoon over Sri Lanka. However, an index known as the Monsoon Hadley Circulation Index (MHI) – based on the area averaged mean  $V_s$  for the months June-September – has been suggested as an index to measure the strength of the South Asian summer monsoon (Goswami et al., 1999; Wang and Fan, 1999).

Precipitation during the northeast monsoon is primarily in the form of waves in the easterly air stream, cyclonic wind circulations and convection (de Silva, 1997). Unlike the October-November season, the DJF season is not a convective storm season. It, thus, falls within the “rains” category of monsoonal precipitation characterized by Ramage (1971). A strong vertical shear of the mean meridional wind is conducive for the prevalence of such a “rains” regime.

## **4.2.2: Assessment of predictability of DJF rain failure**

### ***4.2.2.1: Datasets used:***

Retrospective forecasts of  $V_s$ , issued with one month's lag in November, from archived experimental hindcasts from the ECHAM4.5\_PSST, the ECHAM4.5\_CA and the NCEP CFS (see section 3.2.2.1, Chapter 3 for a description of these GCM ensembles) for the period 1961-2004. The predictand dataset used was DJF rainfall at the 132 rain gauges from 1961-2004.

### ***4.2.2.2: Analysis method:***

The statistical forecasting model was constructed with Model Output Statistics (MOS) using CCA (same as in section 4.2.1.2). The skill in predicted precipitation at the rain gauges was measured using Pearson's moment correlation. Skill in predicted tercile (whether below-, above- or near-normal) precipitation was measured using the Hit Skill Score (see section 3.2.2.2 in Chapter 3). Tercile forecast probabilities in years of known drought was the metric used to assess whether seasonal forecasts from the GCMs could predict DJF rain failure.

## **4.3: Results**

### ***4.3.1: Atmospheric dynamics driving the failure of December-February rainfall***

An anomalously weak contemporaneous (DJF) vertical shear of the mean meridional wind ( $V_s$ ), in the domain 80°E-90°E and 0°N-20°N, suppresses rainfall over Sri Lanka. The reduction in rainfall is marked in the northern, north central, southeastern and western parts of the country (Fig. 4.2).

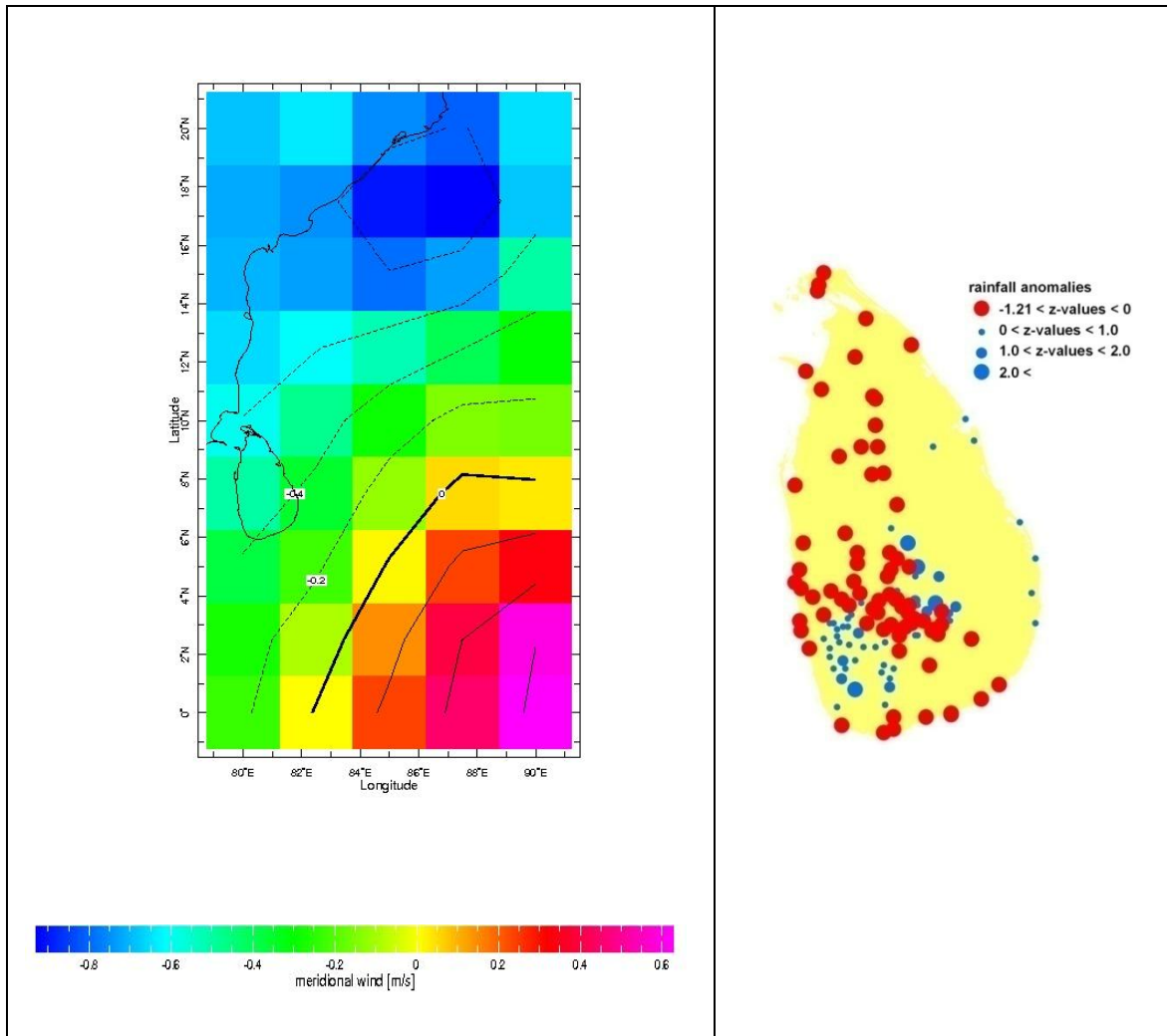


**Figure 4.2:** Temporal composites of the December-February (contemporaneous)  $V_s$  field (left) and associated negative anomalies in mean DJF rainfall over Sri Lanka (right) in the drought years 1976, 1980, 1984, 1986, 1996, 2001 and 2003 when DJF rainfall was below normal. Blues indicate negative  $V_s$  anomalies and reds indicate positive anomalies.

The exact reason for the reduction in wind shear in the years when the DJF rains failed is unclear. A comparison of mean wind field at 850hPa in drought years with climatology shows that the wind stream flowing towards Sri Lanka from the northern Bay of Bengal region is weakened or non-existent in drought years. (Figure 4.3).



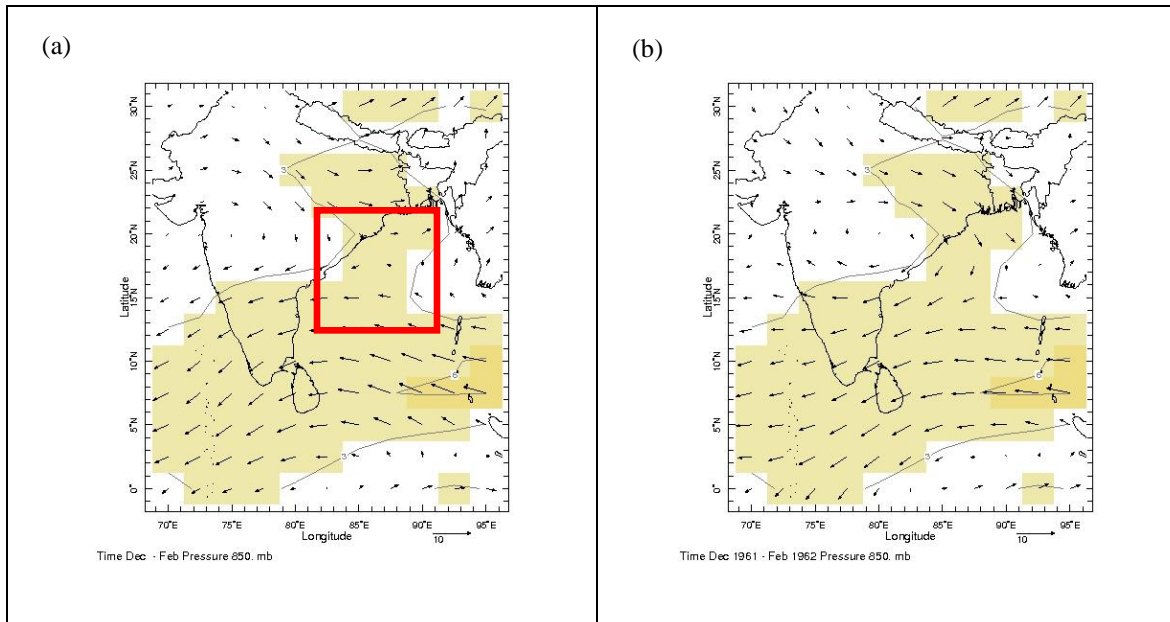


**Figure 4.3:** Mean December-February wind vector at 850hPa in drought years (a) and mean DJF wind vector (1961-2004) (b). Red square in (a) denotes region where the wind stream weakens in drought years.

An examination of  $V_s$  in drought years over a larger domain showed a broad region of reduced  $V_s$  along eastern and southeastern Asia (Fig. 4.4).

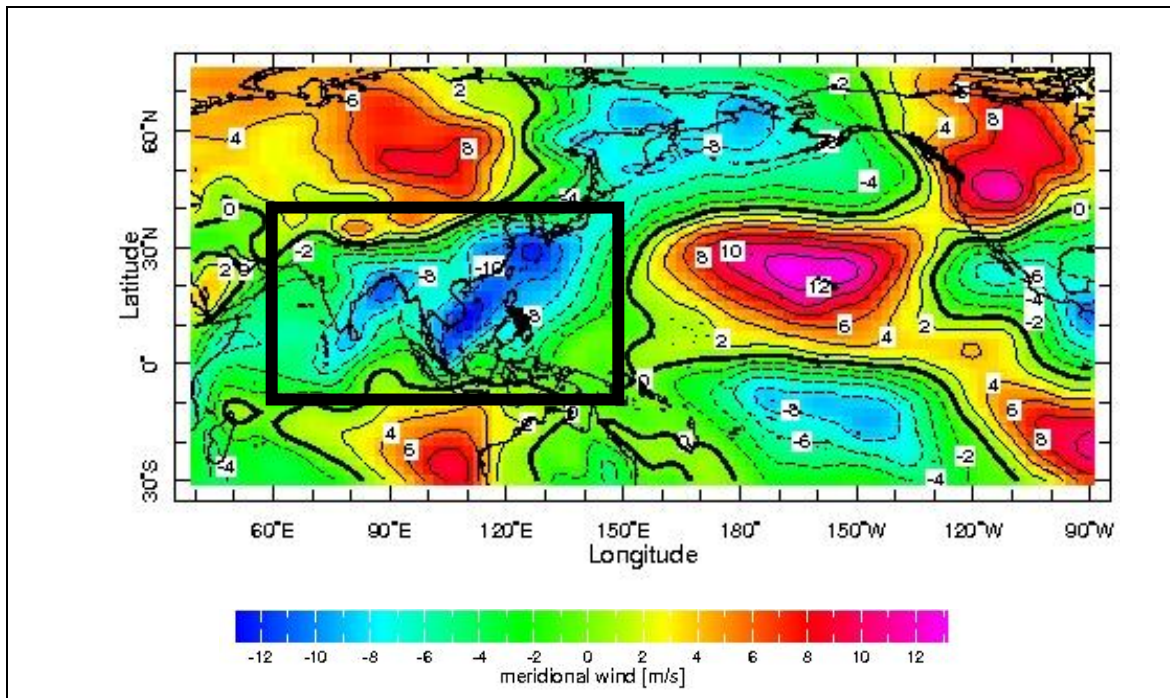


**Figure 4.4:** Same as in 4.2 but for the domain 40°E-270°E and 30°S-65°N. Blues indicate negative  $V_s$  anomalies and red indicate positive anomalies. The black box encloses the broad region of reduced  $V_s$ .

Literature on the East Asian Winter monsoon (DJF) was consulted to find out if factors affecting the strength of the East Asian Winter monsoon could influence the strength of the wind anomalies near Sri Lanka. The connection between the Asian winter monsoon and the northeast winter monsoon over Sri Lanka is evident in terms of the extent of the convective activity and the mean climatological wind fields for DJF. Deep convection occurs near the Maritime Continent during the boreal winter (DJF). Such deep convection extends into the eastern Indian Ocean. Northeasterly winds blowing towards the South China Sea are deflected to the west and south by the topography of the Malayan Peninsula and Sumatra. Such a deflection results in easterly winds extending into the Bay of Bengal (Chang et al., 2005).

Factors influencing the strength of convection in the Maritime continent include: the Borneo Vortex<sup>14</sup>, northeast cold surges and the Madden Julian Oscillation<sup>15</sup> (Chang et al, 2005). The relative position of the Siberian High and the convective heat source over the Maritime Continent affect the penetration of transient cold surges<sup>16</sup> during the winter season (Zhang et al., 1997). Such surges are significantly correlated with anomalies in the zonal and meridional components of lower-tropospheric winds. Such anomalies extend into the Bay of Bengal and the eastern Indian Ocean (Compo et al., 1999) through modification of the strength and relative location of the Borneo Vortex. The presence of surges strengthen the Borneo Vortex, shift it westward and induce enhanced convection along the west coast of Borneo and the South China Sea. The MJO decreases the

---

<sup>14</sup> The Borneo Vortex is defined as a closed counterclockwise circulation of the 925hPa wind within the domain 107.5°E- 117.5°E and 2.5°S-7.5°N (Chang et al., 2005).

<sup>15</sup> The Madden Julian Oscillation (MJO) is the dominant mode of intra-seasonal variability in the tropical troposphere (Madden and Julian, 1971).

<sup>16</sup> Cold surges are characterized by a sharp drop in temperature, an increase in surface pressure and a strengthening of the northerly winds in the region of East Asia (Compo, et al., 1999).

frequency of cold surges and the number of days that the Bornex Vortex prevails (Chang, et al., 2005).

Thus, it appears that cold surge dynamics, the Siberian High, the MJO and the relative location of the Borneo Vortex, and the interplay between each of these, could influence the strength of the northeast monsoon over Sri Lanka. Whether anomalies in  $V_s$  are a direct manifestation of the influence of such factors needs further investigation. Such investigation requires studying sub-monthly (i.e. weekly or daily) data as opposed to the monthly fields used in this study.

#### ***4.3.2: Predictability of the December-February season***

The three GCMs were able to capture the leading canonical mode of  $V_s$  associated with DJF rain failure (Fig. 4.5) as identified in the diagnostic analysis. However, only the prediction using forecast  $V_s$  fields from the ECHAM4.5\_CA had skill<sup>17</sup>.

The literature on experimental forecasts generated using prescribed sea surface temperature anomalies to force the ECHAM4.5 AGCM shows that seasonal prediction skill for the ECHAM4.5\_CA is better than the ECHAM4.5\_PSST during the January-March season (Lee and Goddard, 2005). Coupled models have deficiencies in representing atmosphere-land interaction and have only moderate prediction skill in the Asian-Australian monsoon region (Wang et al., 2008). Whether these are the reasons why the ECHAM4.5\_PSST and the full-coupled CFS had no skill in predicting the DJF season needs further investigation.

Pearson's correlation skill values of the downscaled precipitation from the ECHAM4.5\_CA were significant at 95-99% confidence levels in northern, north central

---

<sup>17</sup> The prediction model run with forecast fields from the ECHAM4.5\_PSST and the NCEP CFS had negative goodness-of-fit.

and eastern parts of the island (Fig. 4.6). Negative correlation values are concentrated in the western and southwestern region. The average and maximum Hit Skill Score (HSS) was 11% and 45%. Figure 4.7 shows examples of time series of observed versus predicted precipitation at a station with an average HSS (Fig. 4.7(a)) and at a station with an HSS in the 90<sup>th</sup> percentile (Fig. 4.7(b)). Fourteen percent of the 132 stations used in the analysis had no skill ( $HSS \leq 0$ ). All these stations were located within the southwestern region of the island (not shown). Forecast skill in rice cultivation areas in the eastern, central and north-central parts of the country is promising. Skill over the rice cultivation areas in the south and southeast is limited.

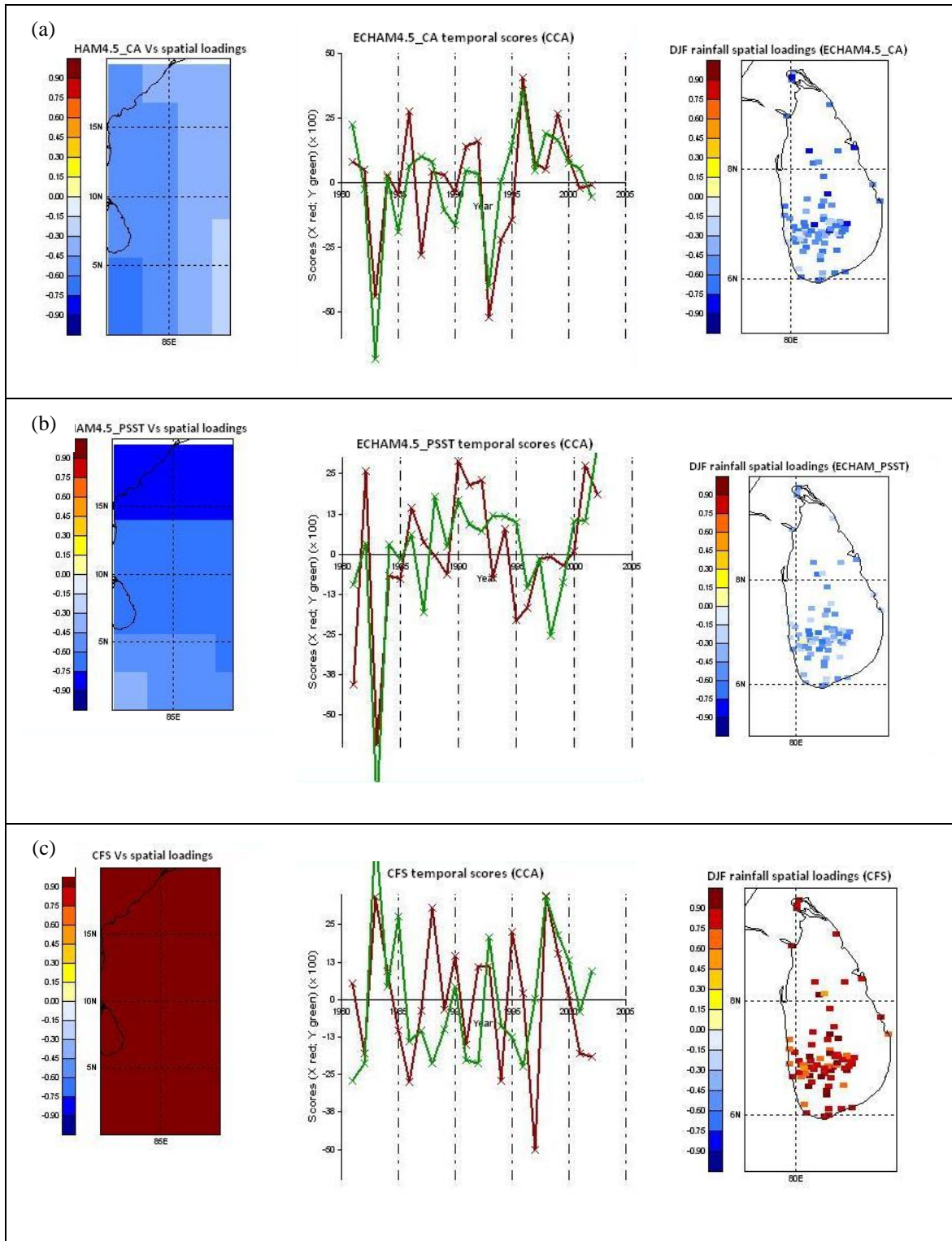


**Figure 4.5:** Leading canonical modes and associated temporal scores of the spatial loadings for the ECHAM4.5\_CA (a); the ECHAM4.5\_PSST (b); and the CFS (c). Red in the spatial loadings of  $V_s$  and DJF rainfall anomalies indicates positive anomalies and blue indicates negative anomalies. The red line in the temporal scores depicts the predictor and the green line depicts the predictand.

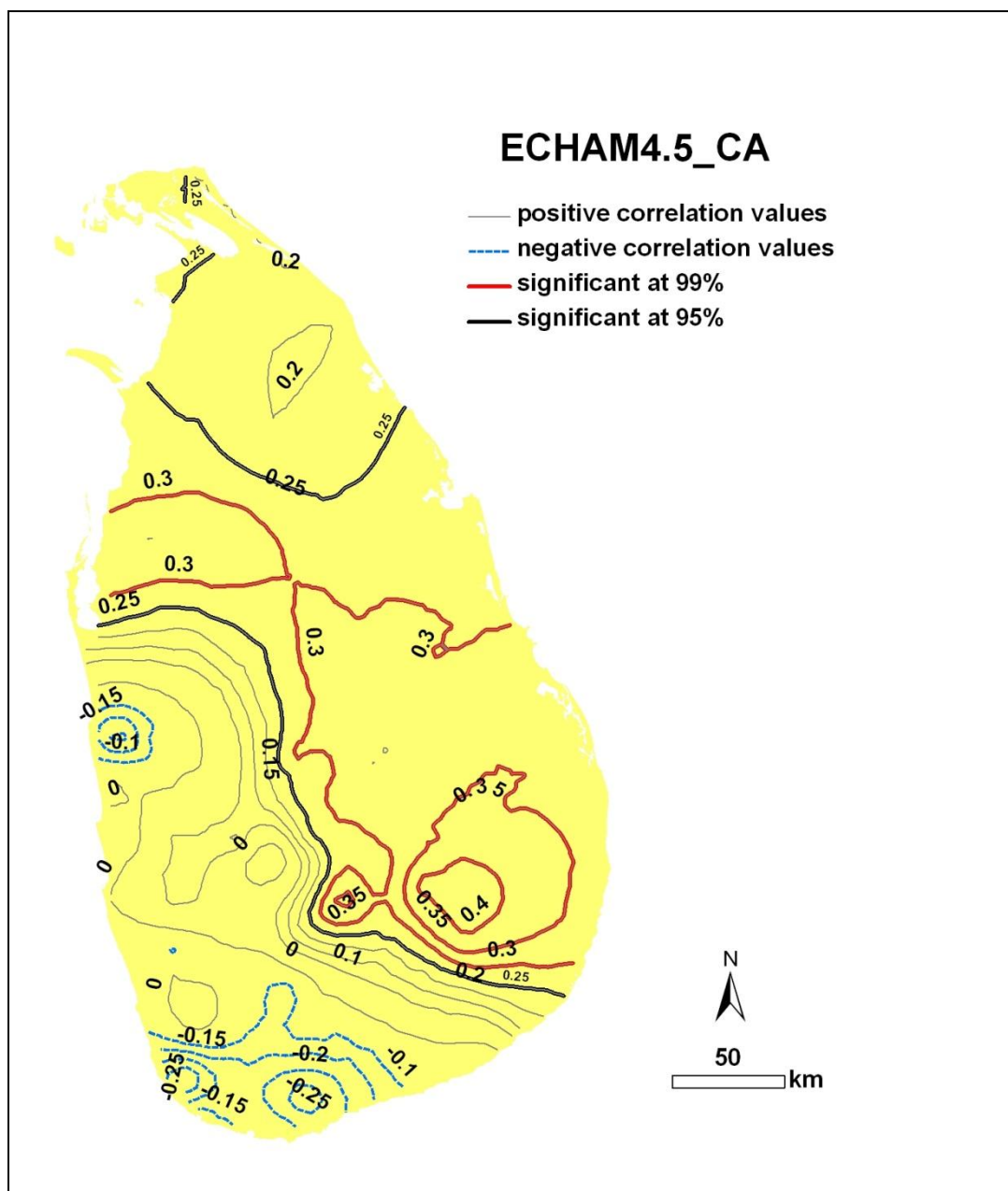


**Figure 4.6:** Pearson's correlation skill maps for the ECHAM4.5\_CA. Contour interval is 0.05 correlation units. Correlation values significant at the 95% confidence level are depicted as solid black lines and correlation values significant at the 99% confidence level are depicted as solid red lines. Broken blue lines depict values of negative correlation. Thin grey lines depict positive correlation values that are not statistically significant.



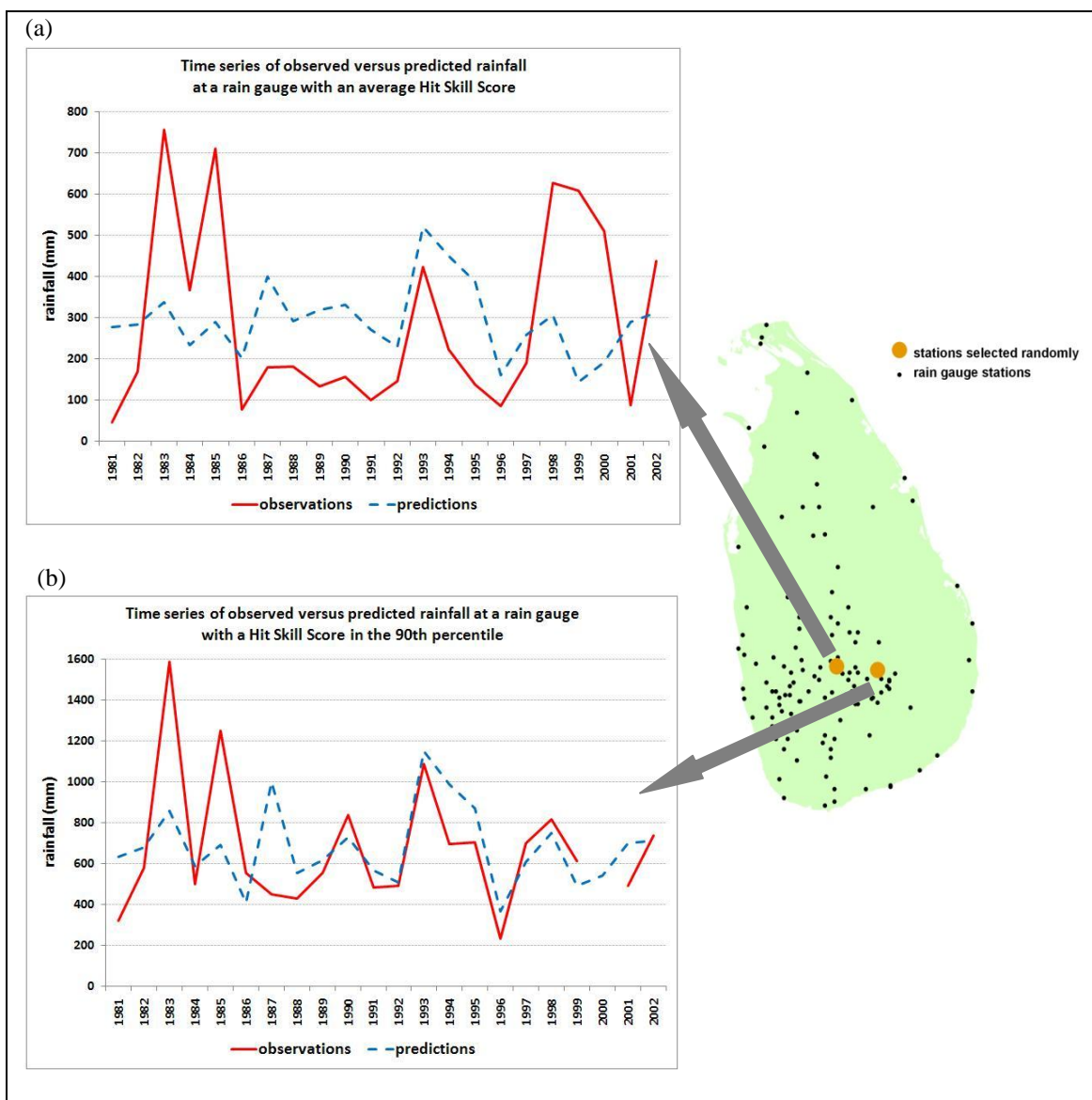


**Figure 4.7:** Examples of predicted (from ECHAM4.5\_CA) versus observed rainfall at rain gauge stations with an average Hit Skill Score (a) and at a station with a Hit Skill Score in the 90<sup>th</sup> percentile (b). Filled orange circles in the map of rain gauge stations (right) show the location of the stations selected randomly.

The tercile forecast for DJF rainfall for the year 2001 (extreme drought) was ambiguous because no category was clearly weighted (Fig. 4.8). The tercile forecast for 1986 (moderate drought) was correct. (Table 4.1).

<i>Drought category</i>	<i>Years</i>	<i>ECHAM4.5_ca</i>
Extreme	2001	Ambiguous
Moderate	1986	BN (correct)

**Table 4.1:** Summary of tercile probability forecast of DJF rainfall from the ECHAM4.5\_CA. BN refers to below-normal

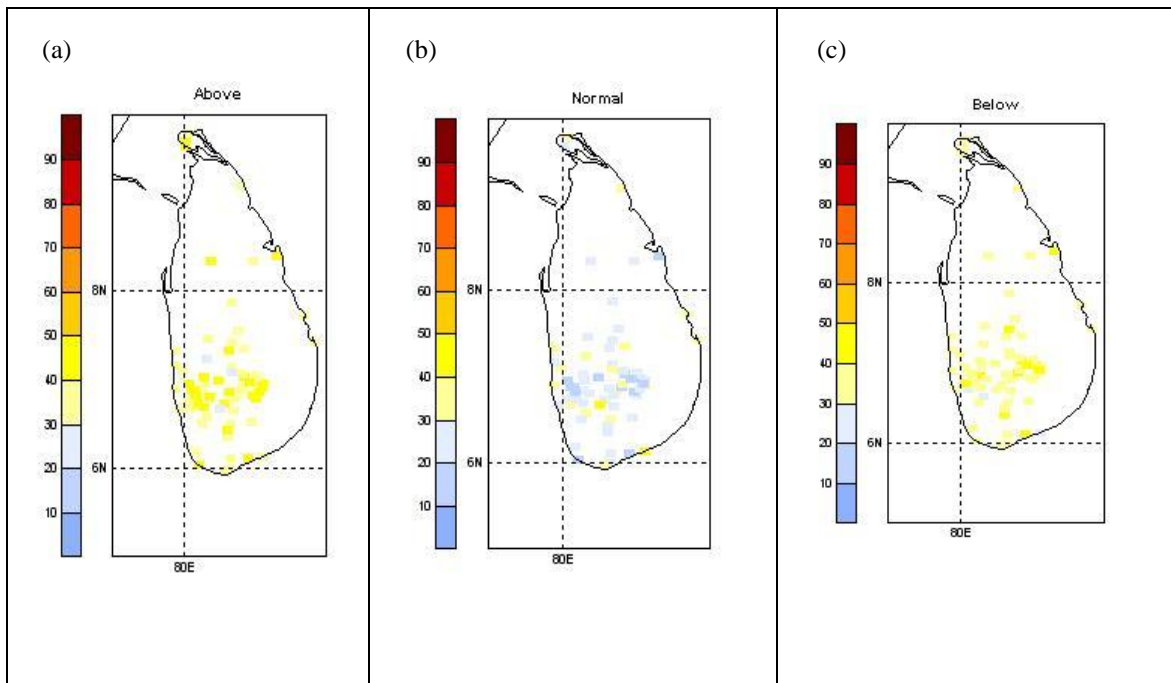


**Figure 4.8:** Tercile probability forecasts of DJF rainfall in 2001 generated from the ECHAM4.5\_CA depicting the above-normal (a), near-normal (b) and below-normal (c) categories. Blues indicates lower probabilities and reds indicate higher probabilities.



#### 4.4: Conclusion

The vertical shear of the contemporaneous (December-February) meridional wind ( $V_s$ ), in the domain  $80^{\circ}\text{E}$ - $90^{\circ}\text{E}$  and  $0^{\circ}\text{N}$ - $20^{\circ}\text{N}$ , controls DJF rainfall over Sri Lanka. DJF rainfall is suppressed when  $V_s$  is anomalously low and vice versa. A reduction in  $V_s$  decreases the passage of storm-bearing weather systems reaching Sri Lanka. Reasons for the variability in the strength of  $V_s$  are as yet unclear. Studies on the East Asian Winter monsoon indicate that factors such as the Siberian High, cold surges, the Borneo Vortex and the Madden Julian Oscillation influence DJF convection over the Maritime Continent, the Eastern Indian Ocean and the Bay of Bengal. Whether such factors play a role in determining the strength of  $V_s$  and, hence, the northeast monsoon over Sri Lanka needs further investigation.

In the La Niña years of 1983 and 2000, DJF rainfall showed positive anomalies while ON rainfall had negative anomalies. These are two *Maha* drought years when DJF rain failure was not a contributory factor. La Niña episodes are known to strengthen the Siberian High, increase the number of cold surges reaching the South China Sea and increase the number of days when the Borneo Vortex prevails (Zhang et al., 1997). Whether the influence of La Niña on DJF rainfall is manifest via the former's modulation of the strength of the Siberian High, cold surges, etc., is an area that requires further investigation.

Droughts associated with the failure of DJF rainfall can be predicted with a month's lead time using forecast fields from the ECHAM4.5 forced with constructed analogues of sea surface temperature anomalies. Statistically significant prediction skill was observed over the rice cultivation regions in the eastern, central and north-central

parts of the island. Forecasts of expected rainfall at stations in such locations could be consulted to determine whether drought conditions might affect rice crops at their maturing stage. Such information could guide decisions on changes to irrigation scheduling and advisories on the need to adopt mulching techniques in the advent of imminent water stress.

## **Chapter 5: Monitoring moisture conditions on the ground in near-real time**

### **5.1: Introduction**

Chapters 3 and 4 focused on the predictability of total season precipitation for the October-November and December-February seasons. Rainfall prediction provides an indication of whether the coming season in its entirety will be above-, below- or near-normal. Such predictions are of potential use to pre-season decisions on the extent and variety of crops that should be planted. However, pre-season information alone is not sufficient. Knowledge on how a season – particularly moisture stress – evolves is critical for farmers and agricultural extension officers tasked with monitoring crop development. Such information on where moisture stress, and hence drought, may be developing is needed to launch protective measures such as mulching or increasing releases of irrigation water.

Soil moisture, a key component of the hydrological cycle, controls the partitioning of water and energy fluxes (Teuling, et al., 2007). It determines whether latent or sensible heat fluxes dominate over a particular location. The importance of soil moisture in drought monitoring stems from its role in land surface feedback processes. Ideally the spatio-temporal variability of soil moisture would be monitored to identify locations that are most susceptible to drought incidence in the event of below-normal precipitation over Sri Lanka. Unfortunately, there is no gauge network dedicated to measuring soil moisture in Sri Lanka<sup>18</sup>. Soil moisture products derived from passive microwave remotely sensed data – such as from the Advanced Microwave Scanning Radiometer (AMSR-E) sensor (Njoku et al., 2003) – could be used in the absence of

---

<sup>18</sup> Personal communication with Prof. R.B. Mapa (7 August 2007), Department of Soil Science, Faculty of Agriculture, University of Peradeniya, Peradeniya, Sri Lanka.

ground-based measurements. However, the coarse spatial resolution (25km) of such soil moisture products, and the limited ability of microwave sensors to penetrate further than the surface skin of a soil layer, renders passive microwave soil moisture products of marginal use in drought monitoring.

Indices using remotely sensed data acquired in the optical, near-infrared and thermal wavelengths, have been widely used to monitor drought from space (Kogan, 1997 and references therein; Karnieli et al., 2010; Thenkabail et al., 2004). Vegetation indices – particularly the Normalized Difference Vegetation Index (NDVI)<sup>19</sup> – have commonly been used for drought monitoring, as vegetation state and cover are affected by droughts (Karnieli et al., 2010 and references therein). However, such indices alone are not sufficient to detect drought onset (Wan, 2004a; Thenkabail et al., 2004) as vegetation has a lagged response to drought and thus cannot detect the commencement of drought events (Park et al., 2004).

Land Surface Temperature (LST) represents the instantaneous state of the energy flux from a land surface and has an empirically-established negative relationship with ground-based soil moisture measurements (Park et al., 2004). LSTs derived from remotely sensed data in the thermal infrared wavelengths (8-14µm) provide valuable

---

<sup>19</sup> The NDVI is the difference between reflectance in the visible and infrared wavelengths (Tucker et al., 1979) and is represented as:

$$NDVI = \frac{\rho_R - \rho_{NIR}}{\rho_R + \rho_{NIR}}$$

where,

$\rho$ - reflectance;  $R$ = red portion of the electromagnetic spectrum; and  $NIR$ - infrared portion of the spectrum.

The physical interpretation of NDVI is the difference between maximum absorption of reflectance in the visible wavelengths due to chlorophyll pigments and maximum reflectance in the infrared wavelengths due to leaf cellular structure (Tucker et al., 1979). The NDVI ranges from -1 to +1 with negative values indicating unhealthy vegetation and vice versa.

information on the status of soil moisture because evapotranspiration affects land-surface temperature (Anderson et al., 2007).

Drought indicators that combine vegetation state and land surface temperature state have been developed based on the assumptions that optical, infrared and thermal bandwidths are complementary in characterizing phenomena at the land surface, (Karnieli et al., 2010).

The Vegetation Temperature Condition Index (VTCI) is one such indicator, integrating remotely sensed surface reflectance and thermal properties to monitor drought (Wang et al., 2001; Wan et al., 2004a). The VTCI is defined as the ratio of the LST difference among pixels with a specific NDVI value in an area large enough to provide wide ranges of NDVI and soil moisture at the surface (Wang et al., 2001; Wan et al., 2004a). It is expressed mathematically as:

$$VTCI = \frac{LST_{NDVIi.max} - LST_{NDVIi}}{LST_{NDVIi.max} - LST_{NDVIi.min}}$$

where:

$$LST_{NDVI.max} = a + bNDVI_i$$

$$LST_{NDVI.min} = a' + b'NDVI_i$$

where,

$LST_{NDVI.max}$  and  $LST_{NDVI.min}$  – maximum and minimum LSTs of pixels with the same  $NDVI_i$  value

$LST_{NDVIi}$  – LST of a pixel with NDVI value  $NDVI_i$

$a, b, a', b'$  - Coefficients determined from the LST-NDVI scatterplot

The LST-NDVI scatterplot has a triangular shape (Figure 5.1) if it is drawn from a study site providing a range of NDVI and surface moisture conditions ranging from wilting point to field capacity (Carlson et al., 1995).

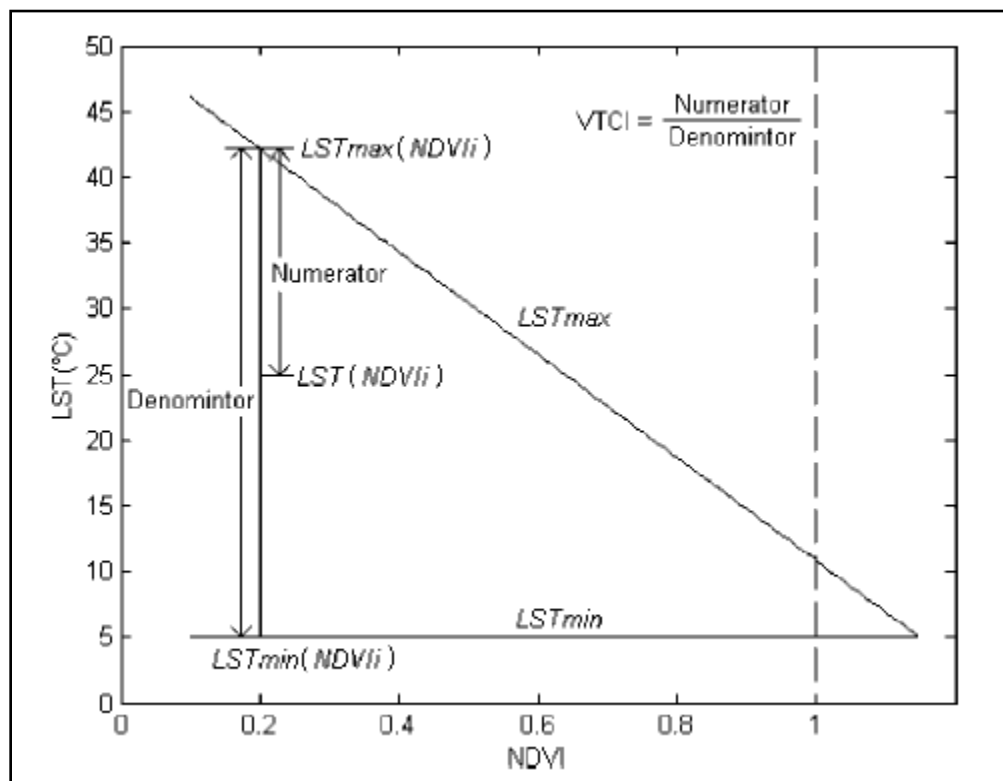


**Figure 5.1:** Schematic of the LST-NDVI scatterplot depicting the physical interpretation of the VTCI (Adapted from Wan et al., 2004a, Figure 1, pp 65)

The numerator of the VTCI is the difference between maximum LST of the pixels and the LST of one pixel and the denominator is the difference between maximum and minimum LSTs of the pixels (Wan et al., 2004a).  $LST_{max}$  is the “warm edge” where vegetation is subject to drying due to limited soil moisture.  $LST_{min}$  is the “cold edge” where there is no moisture restriction on plant growth (Carlson et al., 1995; Wan et al., 2004a). The coefficients  $a, b, a', b'$  are expressed as:

$a$  = Maximum LST value

$b$  = Slope of the warm edge or hypotenuse of the LST-NDVI triangle

$a'$  = Minimum NDVI value

$b'$  = Slope of the cold edge (= 0)

VTCI values range from 0 to 1 with lower values indicating drought conditions. The index is site- and time-specific (Wang et al., 2001) and more suitable for use during growing seasons (Wan et al., 2004a). The VTCI is recognized as a near-real time approach to drought monitoring as it is related to departure from normal precipitation over a selected study period (Wan et al., 2004a).

The VTCI is based on the assumption of a negative correlation between NDVI and LST (Sun and Kafatos, 2007). Such a negative correlation between NDVI and LST exists only when water and not energy (i.e. solar radiation) is the limiting factor for vegetation growth such as in the low latitudes (Karnieli et al., 2010).

During the Maha cultivation season, particularly during the October-November growing season, water is the limiting factor for vegetation growth in rice cultivation areas. Therefore, conditions are appropriate to apply the VTCI to monitor drought conditions in rice cultivation areas in near-real time during the early-Maha season in Sri Lanka.

The specific research questions addressed by this chapter are: 1) Does the VTCI capture drought progression during the early-Maha (October-November) season? 2) Can the VTCI be applied to monitor drought progression through the entire Maha (i.e. both October-November and December-February) season?

## **5.2: Methodology and datasets**

### ***5.2.1: Generating the VTCI for the two seasons***

For question 1, the VTCI was calculated at four stages of the season – i.e. early October, late-October, early-November and late-November – whenever cloud-free imagery could be obtained for such stages in the years 2000-2005. The years 2000, 2001 and 2002 were years of extreme drought; 2002 was a year of severe drought; 2004 was not a drought year; and 2005 was a year of moderate drought. In some years, one scene had to be selected – e.g. mid-October – if cloud contamination affected the early- or late-phases of a month. Table 5.1 provides a list of the VTCI scenes generated and the LST and NDVI imagery used.

For question 2, the year 2003 was selected as the case year because it was a drought year when both ON and DJF rainfall were below normal and the negative DJF rainfall anomalies were the largest in the period under study (see Table 2.5, Chapter 2). Nine VTCI were generated spanning the early- and late-phases of the months October-February based on the availability of cloud-free imagery (Table 5.1).



<i>VTCI image</i>	<i>8-day composite LST image</i>	<i>16-day composite NDVI image</i>
1: Early-Oct 2000 2: Late-Oct 2000 3: Early-Nov 2000 4: Late-Nov 2000	7-14 Oct 2000 23-30 Oct 2000 31 Oct – 7 Nov 2000 24 Nov – 1 Dec 2000	29 Sep – 14 Oct 2000 15-30 October 2000 1-15 Nov 2000 16 Nov – 1 Dec 2000
5: Early-Oct 2001 6: Late-Oct 2001 7: Early-Nov 2001 8: Late-Nov 2001	7-14 Oct 2001 23-30 Oct 2001 31 Oct – 7 Nov 2001 24 Nov – 1 Dec 2001	30 Sep – 15 Oct 2001 16-31 Oct 2001 1-16 Nov 2001 17 Nov – 2 Dec 2001
9: Early-Oct 2002 10: Late Oct 2002 11: Early-Nov 2002 12: Late-Nov 2002	8-15 Oct 2002 24-31 Oct 2002 1-8 Nov 2002 25 Nov – 2 Dec 2002	30 Sep– 15 Oct 2002 16 – 31 Oct 2002 1-16 Nov 2002 17 Nov – 2 Dec 2002
13: Early-Oct 2003 14: Late-Oct 2003 15: Mid-Nov 2003 16: Early-Dec 2003 17: Late-Dec 2003 18: Early-Jan 2004 19: Late-Jan 2004 20: Early-Feb 2004 21: Late-Feb 2004	8-15 Oct 2003 24-30 Oct 2003 17-24 Nov 2003 3-10 Dec 2003 27-31 Dec 2003 1-8 Jan 2004 25 Jan – 1 Feb 2004 2-9 Feb 2004 18-25 Feb 2004	30 Sep – 15 Oct 2003 16-31 Oct 2003 17 Nov – 2 Dec 2003 3-18 Dec 2003 18 Dec – 3 Jan 2004 1-16 Jan 2004 17 Jan – 1 Feb 2004 2-17 Feb 2004 18 Feb – 4 Mar 2004
22: Early-Oct 2004 23: Late-Nov2004	7-14 Oct 2004 24 Oct – 1 Dec 2004	29 Sep – 14 Oct 2004 16 Nov – 1 Dec 2004
24: Early-Oct 2005 25: Late-Oct 2005 26: Late-Nov 2005	8-15 Oct 2005 24-31 Oct 2005 25 Nov – 2 Dec 2005	30 Sep – 15 Oct 2005 16-31 Oct 2005 17 Nov – 2 Dec 2005

**Table 5.1:** VTCI images produced and LST and NDVI composites used for each VTCI image (Annex 3 provides a list of the original LST and NDVI image identification numbers (IDs) used)

### 5.2.2: Datasets used

Data products based on data acquired in the reflective and thermal infrared wavelengths by the Moderate Resolution Imaging Spectroradiometer (MODIS) aboard the Terra Satellite (Justice et al., 2002) were used in the study. The data were downloaded from the EOS data portal WIST (<http://wist.echo.nasa.gov>).

For LST, daytime values of the 8-day MOD11A2 product at 1km resolution were used. MOD11A2 is a level-3 product composed as the average value of clear-sky LST during an 8-day period from the daily 1km LST product (MOD11A1) (Wan et al., 2004b; Wang, 2008; Wan, 2009). The product is originally derived using a generalized split-window algorithm (Wan and Dozier, 1996) on MODIS bands 31  $10.780\mu\text{--}11.280\mu$  and 32  $(11.770\mu\text{--}12.270\mu)$ . It is a research-ready product that has been corrected for atmospheric noise and geo-rectified. The product is tile-based and stored in a Sinusoidal Grid. Sri Lanka is covered by two tiles (Figure 5.2).

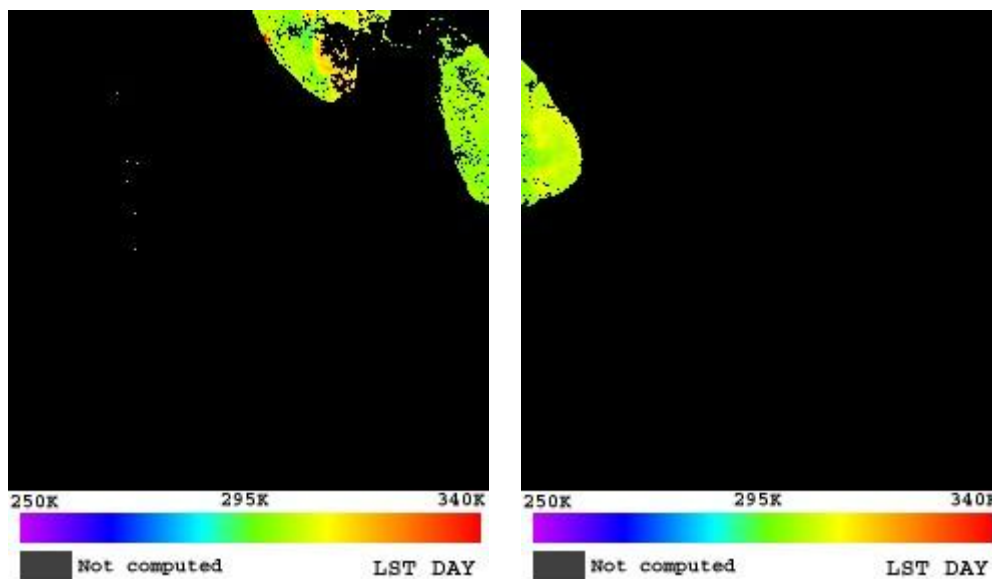


**Figure 5.2:** Two tiles of the MODIS MOD11A2 day time LST product for the period 7 September to 14 October 2000

For NDVI, daytime values of the 16-day<sup>20</sup> MOD13A2 product at 1km resolution were used. MODIS Vegetation Indices are derived from reflectance in the blue, red and near-infrared wavelengths centered at 469 nanometers (nm), 645nm and 858nm respectively<sup>21</sup>. It is a research-ready product that has been corrected for atmospheric noise and geo-rectified. MOD13A2 is a gridded level-3 product in a Sinusoidal Grid. Sri Lanka is covered by two tiles (Figure 5.3).

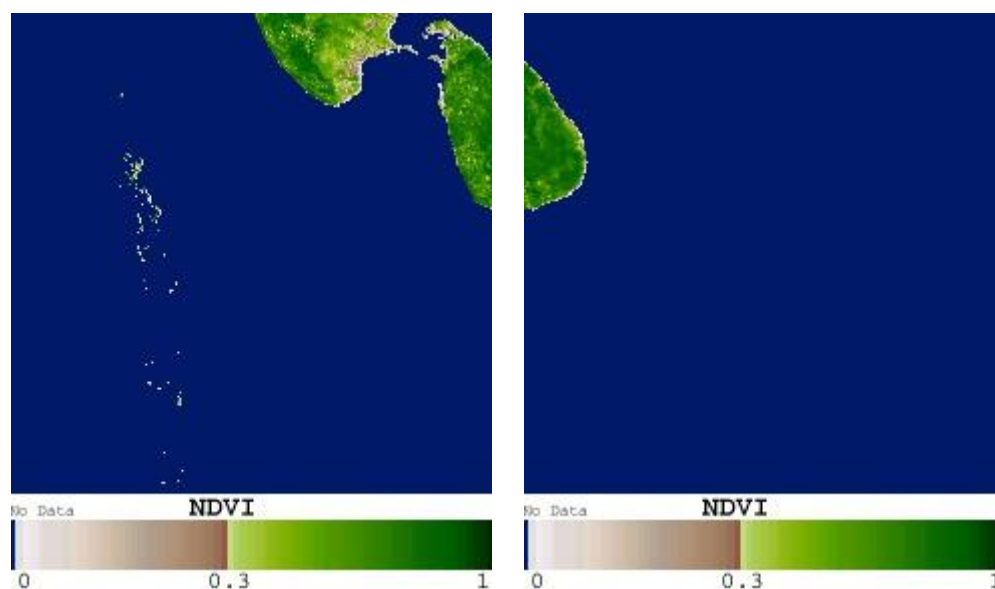


**Figure 5.3:** Two tiles of the MODIS MOD13A2 day time NDVI product for the period 29 September to 14 October 2000

<sup>20</sup>MODIS Vegetation Index products are available either as 16-day or monthly composites ([https://lpdaac.usgs.gov/lpdaac/products/modis\\_products\\_table](https://lpdaac.usgs.gov/lpdaac/products/modis_products_table)). MODIS surface reflectance data are available at 1km resolution as daily products and at 250m and 500m resolution as daily and 8-day composite products. If NDVI scenes were to be derived from scratch using surface reflectance data at the temporal and spatial resolution matching that of the LST product, it would be necessary to either create temporal composites from the daily 1km resolution data or degrade the spatial resolution of the 8-day composite products. Given the lagged response of vegetation to moisture stress, it was assumed that using a 16-day NDVI product with the 8-day LST product would not influence VTCI results much. Thus, the option of deriving NDVI based on MODIS surface reflectance data was not pursued in this study. The assumption will be tested in the future.

<sup>21</sup> [https://lpdaac.usgs.gov/lpdaac/products/modis\\_products\\_table/vegetation\\_indices/16\\_day\\_13\\_global\\_1km/v5/terra](https://lpdaac.usgs.gov/lpdaac/products/modis_products_table/vegetation_indices/16_day_13_global_1km/v5/terra)

Both products were subjected to the following pre-processing: mosaicking the tiles to obtain a single image; subsetting the image to limit the spatial coverage to just Sri Lanka; reprojection of imagery from the Sinusoidal grid to the WGS-84 Geographic Coordinate System; and rescaling data based on a conversion factor provided in image metadata. ERDAS Imagine 9.1 was used for image pre-processing and processing. Maps of results were generated using ArcGIS9.2.

Minimum and maximum LST and NDVI values and the  $a, b, a', b'$  coefficients, needed to calculate VTCI, were obtained from the NDVI-LST scatterplots. VTCI results are presented for the rice cultivation areas.

MODIS Quality Control (QC) images were extracted using the MODISQC tool in IDRISI-Taiga. Sample QC images are presented for selected VTCI images in 2003 to demonstrate the spatial distribution of pixels flagged under the three levels of quality – for LST categorized as: ‘LST not produced (clouds)’; ‘LST produced’; and ‘Good Quality’; and for NDVI categorized as: ‘Cloud Contaminated’; ‘Unreliable Quality’ and ‘Good Quality’. Results presented for the four districts affected by extreme drought in 2003, are for pixels flagged as ‘Good Quality’ in both the original LST and NDVI images.

### 5.3: Results and discussion

#### 5.3.1: *VTCI analysis for October-November*

VTCI scenes for October-November in the years, 2000, 2001, 2002, 2004 and 2005, are presented with observed and predicted October-November (ON) rainfall anomalies for those years. VTCI scenes for October-November 2003 are presented in section 3.2. Comparison of the VTCI images with observed ON rainfall anomalies, shows that the VTCI captures quite clearly the overall spatial pattern of moisture stress and wet conditions observed particularly in the drought years 2000, 2002 and 2005 (see Figures 5.4, 5.6 and 5.8).

The year 2002 had marked variations in the spatial distribution of rainfall anomalies (see Chapter 2 for discussion). The VTCI images are able to capture that marked variation (Figure 5.6). In the drought year 2001, the VTCI images (Figure 5.5) do capture the observed gradients in rainfall. However, VTCI values are not clustered near zero – giving the impression that the 2001 drought was not a drought of extreme magnitude. Districts under the category of ‘Extreme drought’ in 2001 are located primarily along the southwest of the island (see Fig. 2.5 in Chapter 2). In any given year, the southwest of the island is considerably wetter than the rest of the island (Chapter 2, section 2.1 and Fig. 2.1). Therefore, while the VTCI does capture the progression of moisture stress in a given year, its absolute values may not be ideal for comparing one drought year with the next. For such an analysis the Vegetation Condition Index (VCI) and Temperature Condition Index (TCI) (Kogan, 1997; Thenkabail et al., 2004) – developed to study the deviation of moisture at a given location from the long-term mean for that location (Wang et al., 2001) – might be a better option. VTCI images for 2004

clearly indicate large regions of wet conditions (Figure 5.7). Unfortunately, only two VTCI images could be derived for 2004 as cloud contamination severely affected other scenes for that year.

Gradients in moisture stress in the VTCI match observed ON rainfall anomalies better in most years than do predicted ON anomalies for those years. The VTCI images also indicate that it is often in November that moisture stress is most widespread as in 2001 (Fig. 5.5), 2002 (Fig. 5.6), and 2005 (Fig. 5.8). Thus, VTCI does capture the onset and spread of moisture stress. It is thus a crucial metric for drought monitoring complementing the ON seasonal rainfall forecast.

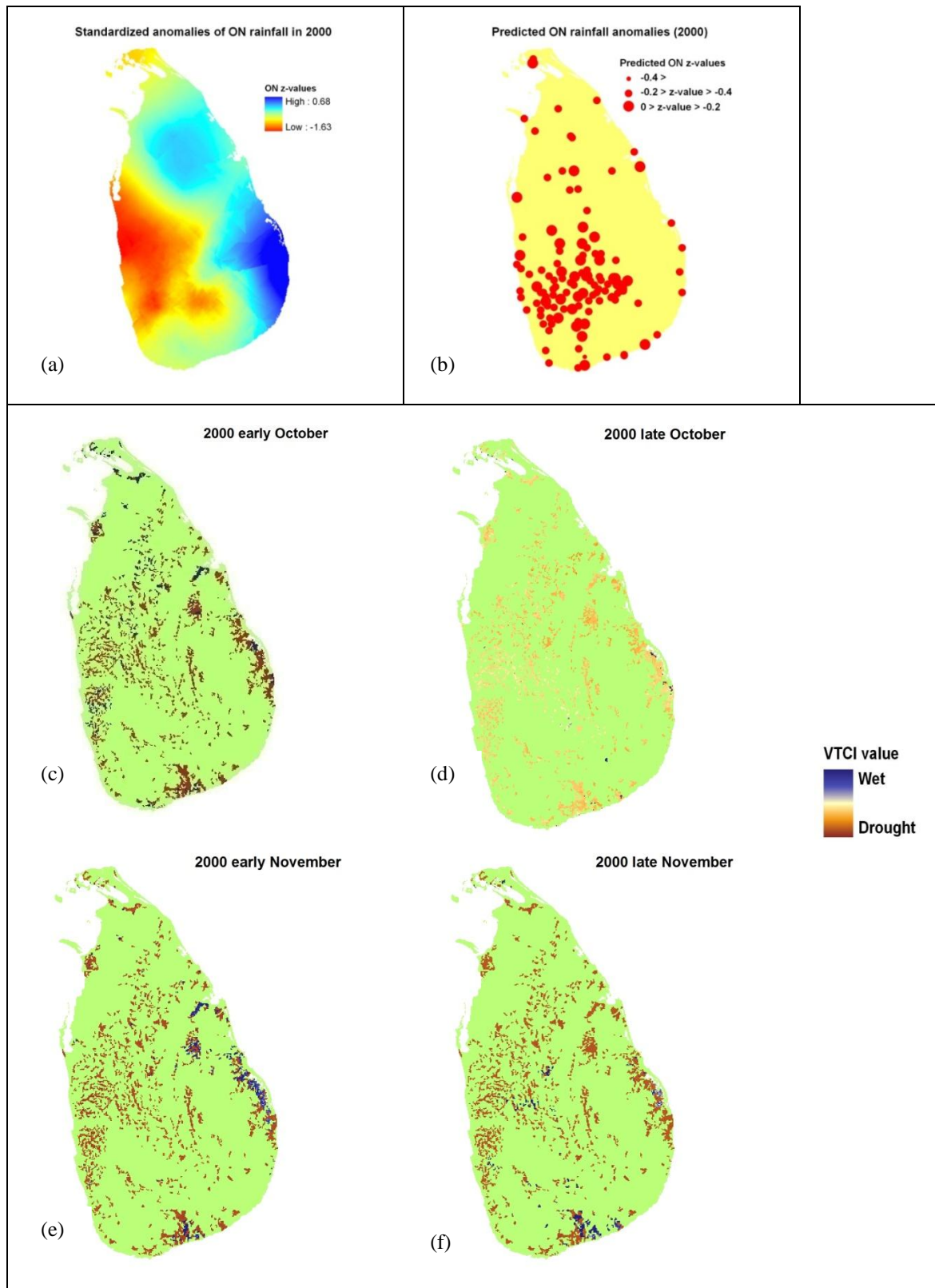


**Figure 5.4:** Observed (a) and predicted (b) standardized anomalies of October-November rainfall in 2000. VTCI images for early-October 2000 (c), late-October 2000 (d), early-November 2000 (e) and late-November 2000 (f).

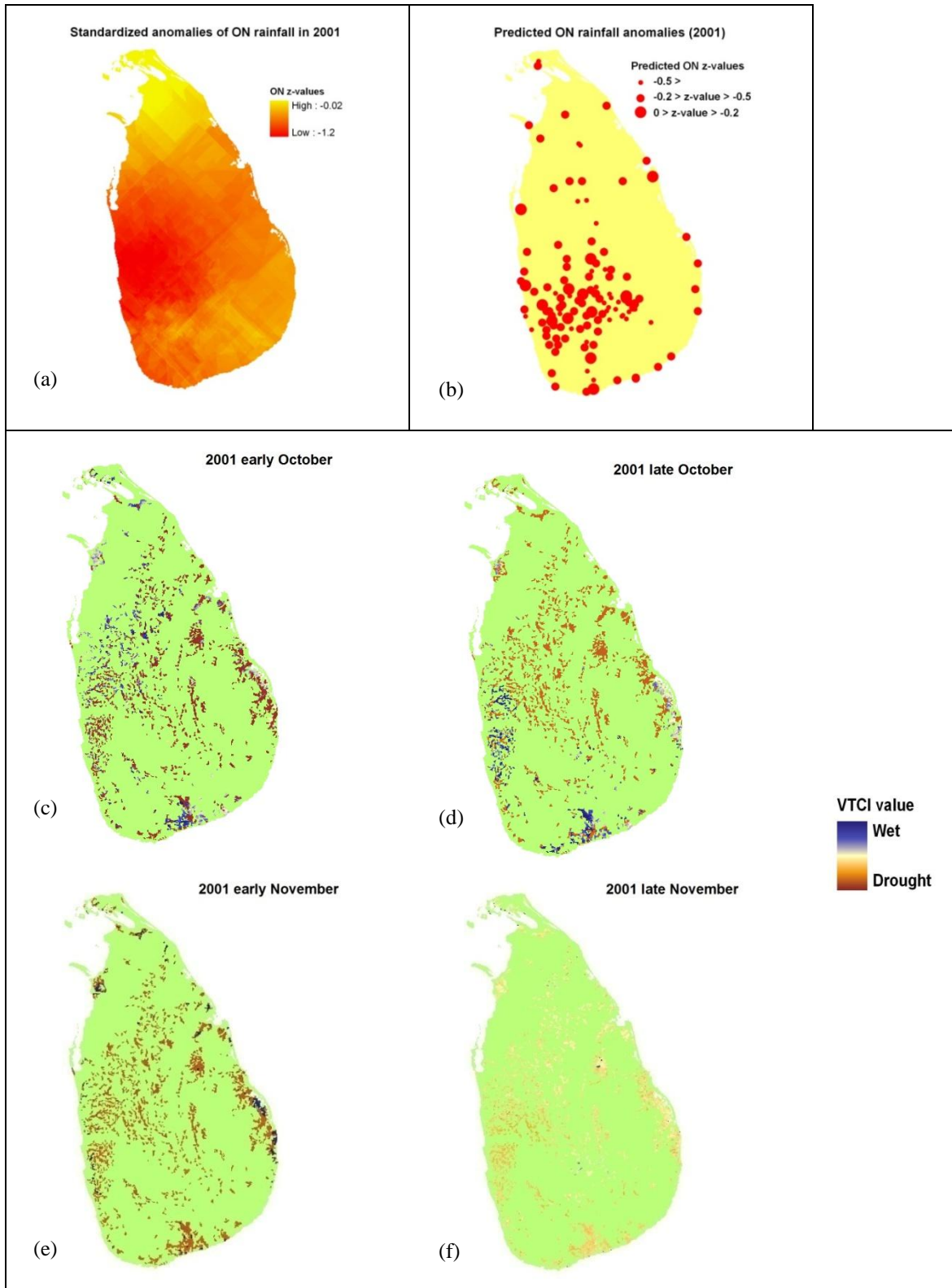


**Figure 5.5:** Observed (a) and predicted (b) standardized anomalies of October-November rainfall in 2001. VTCI images for early-October 2001 (c), late-October 2001 (d), early-November 2001 (e) and late-November 2001 (f).



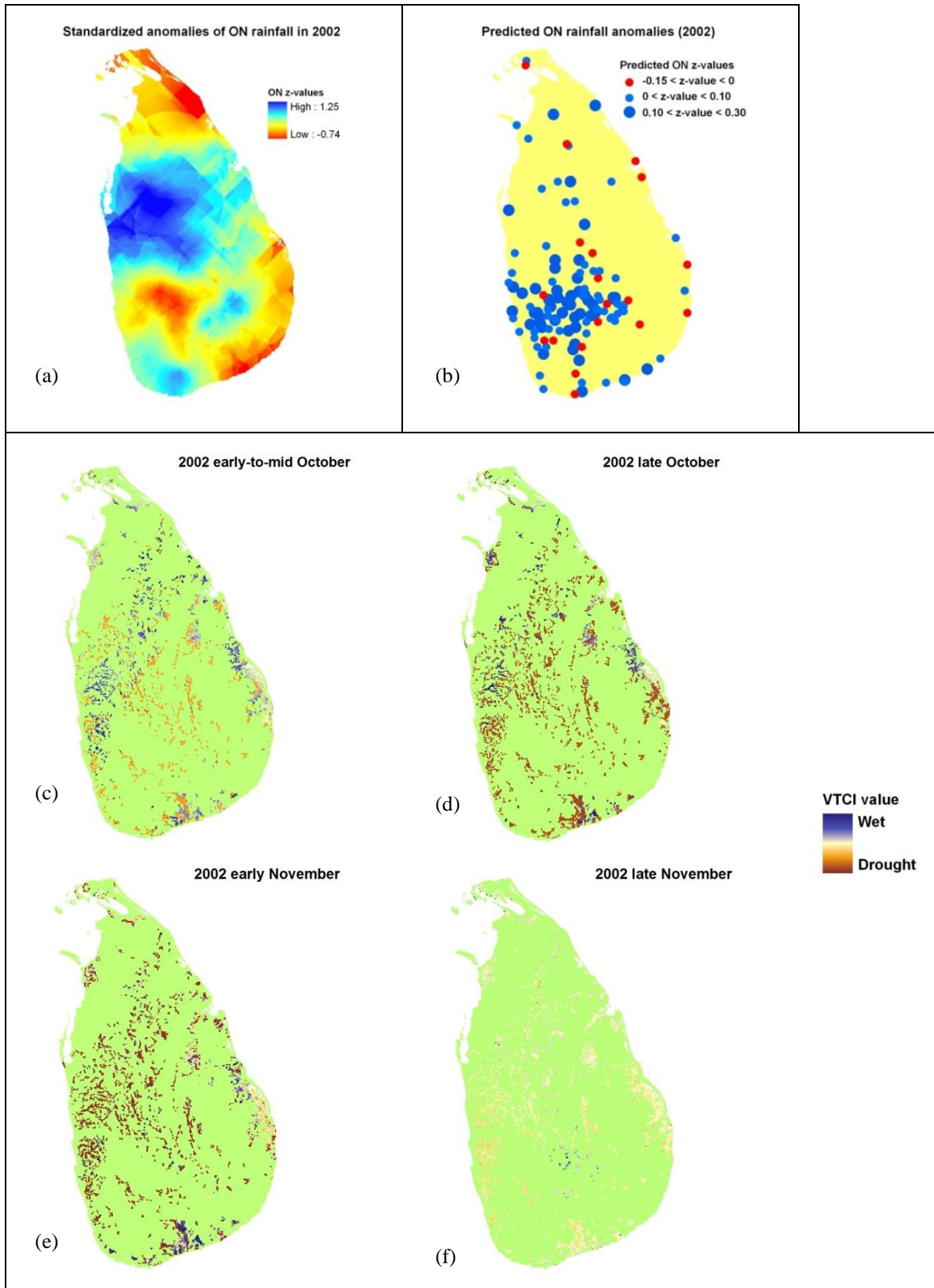


**Figure 5.6:** Observed (a) and predicted (b) standardized anomalies of October-November rainfall in 2002. VTCI images for early-October 2002 (c), late-October 2001 (d), early-November 2002 (e) and late-November 2002 (f).

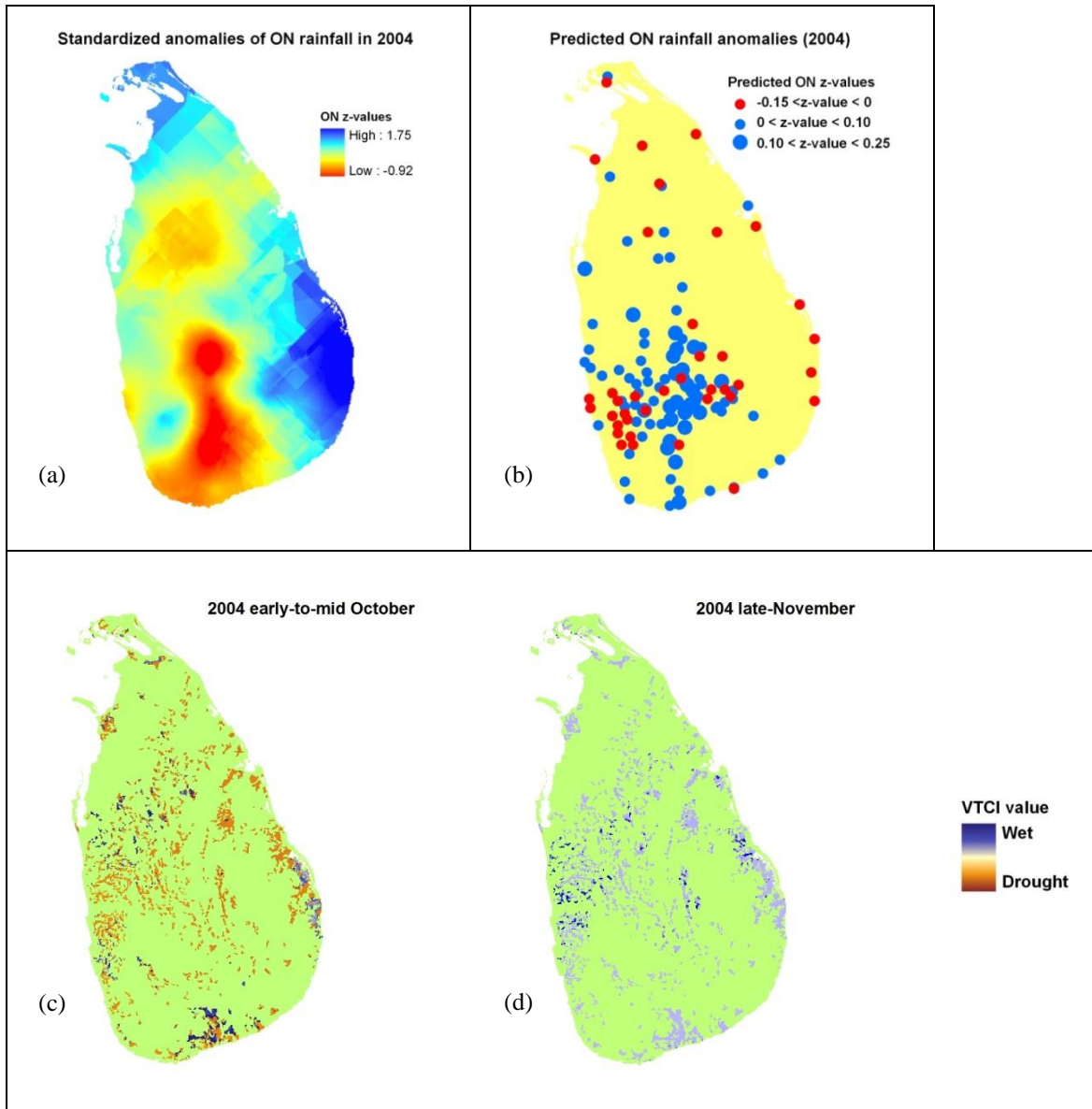


**Figure 5.7:** Observed (a) and predicted (b) standardized anomalies of October-November rainfall in 2004. VTCI images for early to mid-October 2004 (c) and late-November 2004 (d).

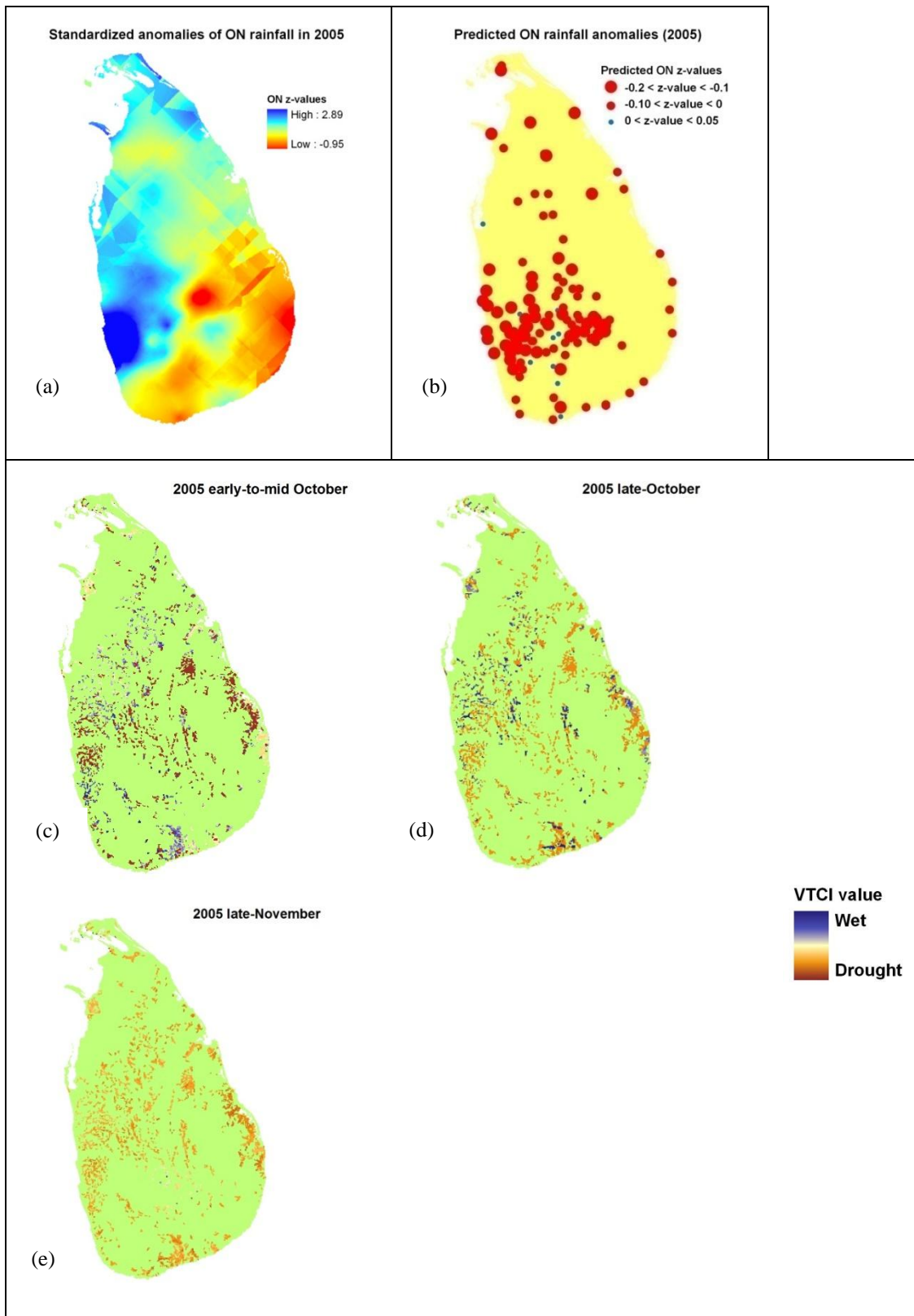


**Figure 5.8:** Observed (a) and predicted (b) standardized anomalies of October-November rainfall in 2005. VTCI images for early-October 2005 (c), late-October 2005 (d) and late-November 2005 (e).

### ***5.3.2: VTCI analysis for the entire Maha season***

VTCI scenes for October-November (Fig. 5.9) and December-February (Fig. 5.10) are presented with observed and predicted rainfall anomalies for both seasons. QC maps of the LST and NDVI products are presented for selected scenes (Fig. 5.11).

The VTCI scenes for October-November capture the observed anomalies for the season – particularly for the moisture stressed regions in the central and southern portions of the island (Fig. 5.9). Furthermore, a comparison of the VTCI image for late-October with QC maps for that scene shows that the VTCI values in the central and southeastern portions of the island are reliable (i.e. pixels flagged as ‘good quality’) (Fig. 5.11 (a) and (d)).

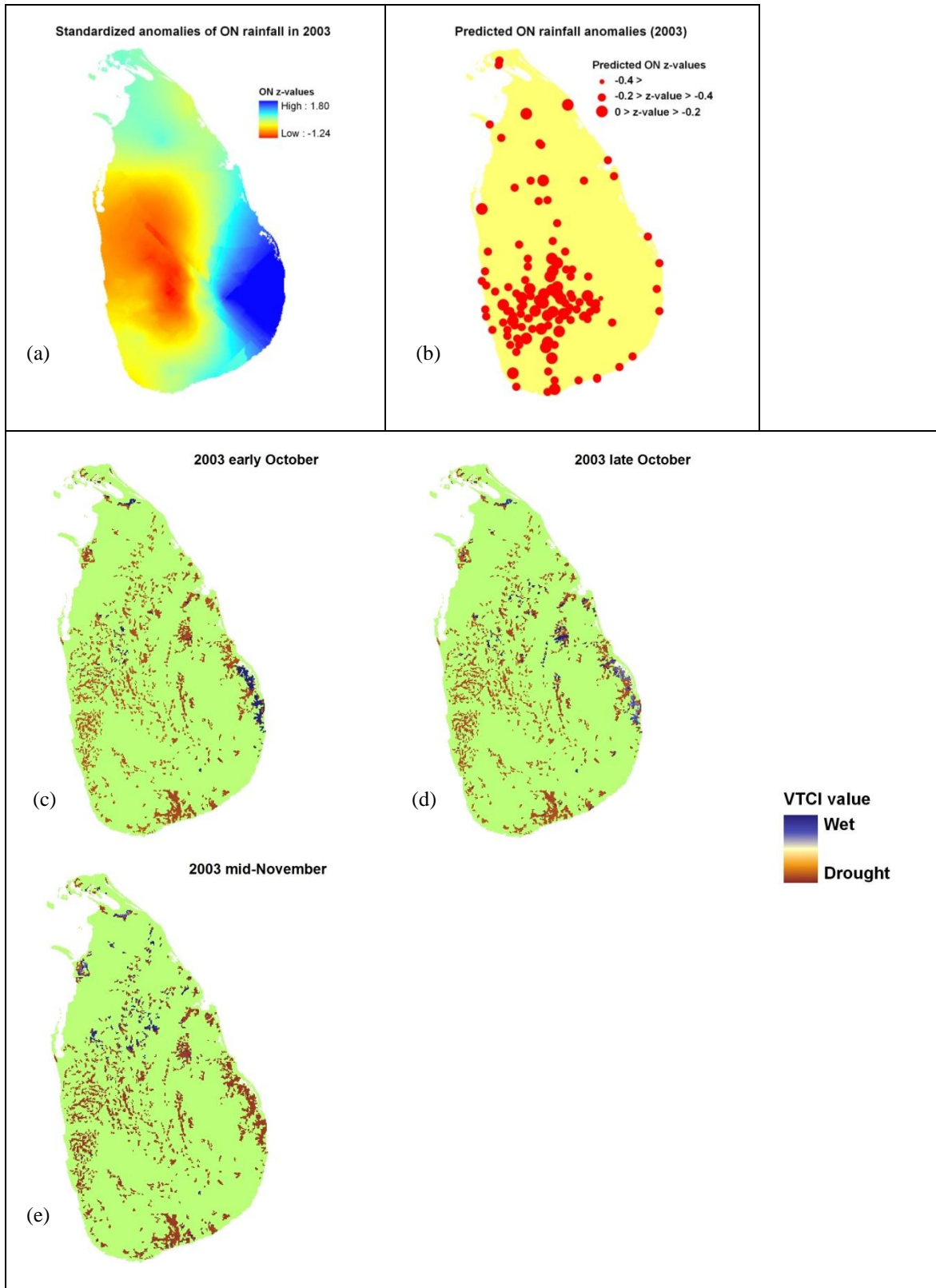


**Figure 5.9:** Observed (a) and predicted (b) standardized anomalies of October-November rainfall in 2003. VTCI images for early-October 2003 (c), late-October 2003 (d), and mid-November 2003 (e).

VTCI images for the December-February period capture the observed patterns in rainfall anomalies (Fig. 5.10). The observed concentration of negative rainfall anomalies in the southwestern and eastern parts of the country are reflected in the VTCI imagery for early-December (Fig. 5.10(a)), late-December (Fig. 5.10(b)) and early-January (Fig. 5.10(c)). Comparison of the VTCI image for early-December with the QC maps for that scene shows that reliable VTCI pixels are concentrated in the southwestern portions of the island (Fig. 5.11 (e) and (h)).



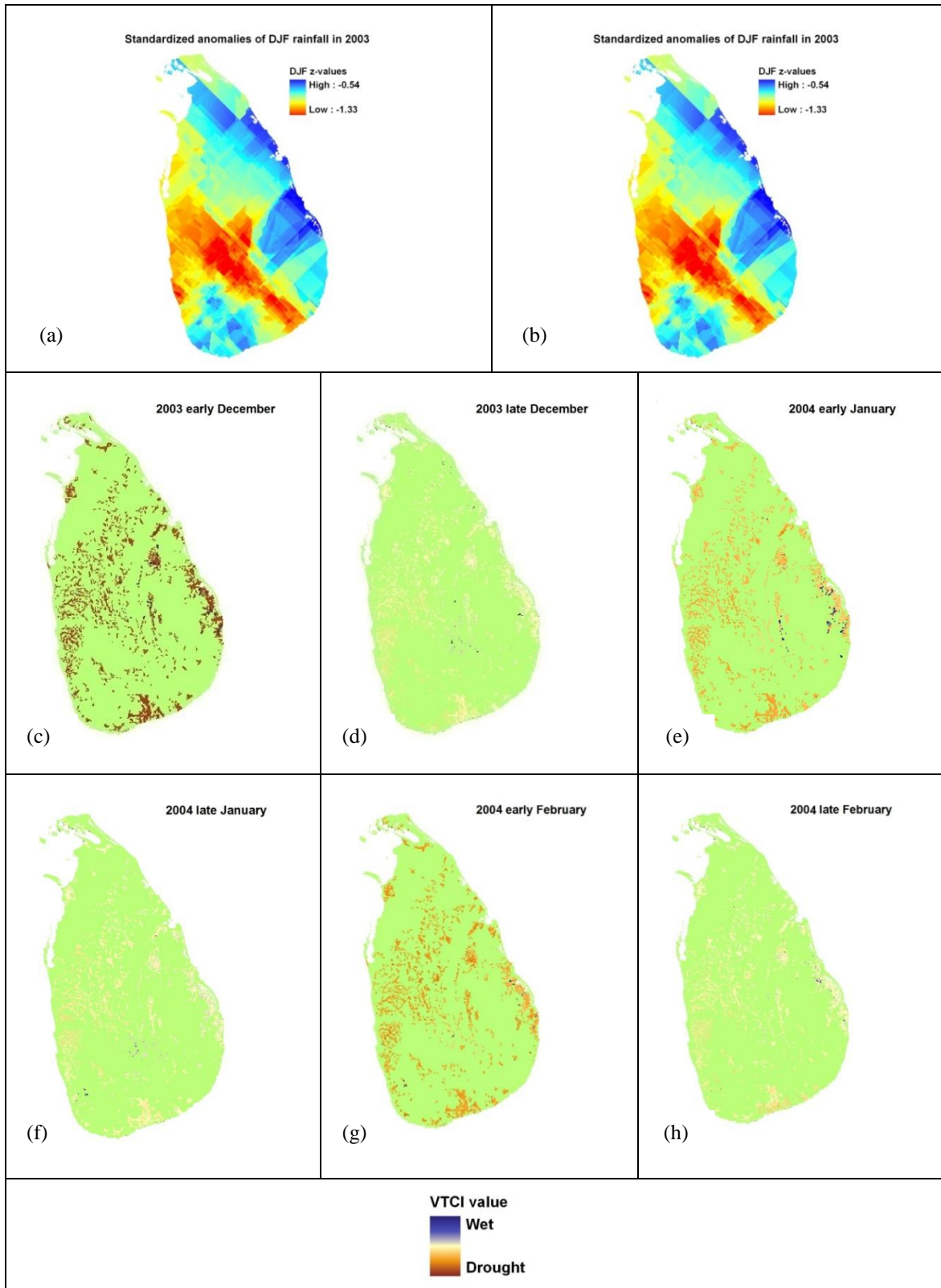


**Figure 5.10:** Observed (a) and predicted (b) standardized anomalies of December-February rainfall in 2003. VTCI images for early-December 2003 (c), late-December 2003 (d), early-January 2003 (e), late-January 2003 (f), early-February 2003 (g), and late-February 2003 (h).

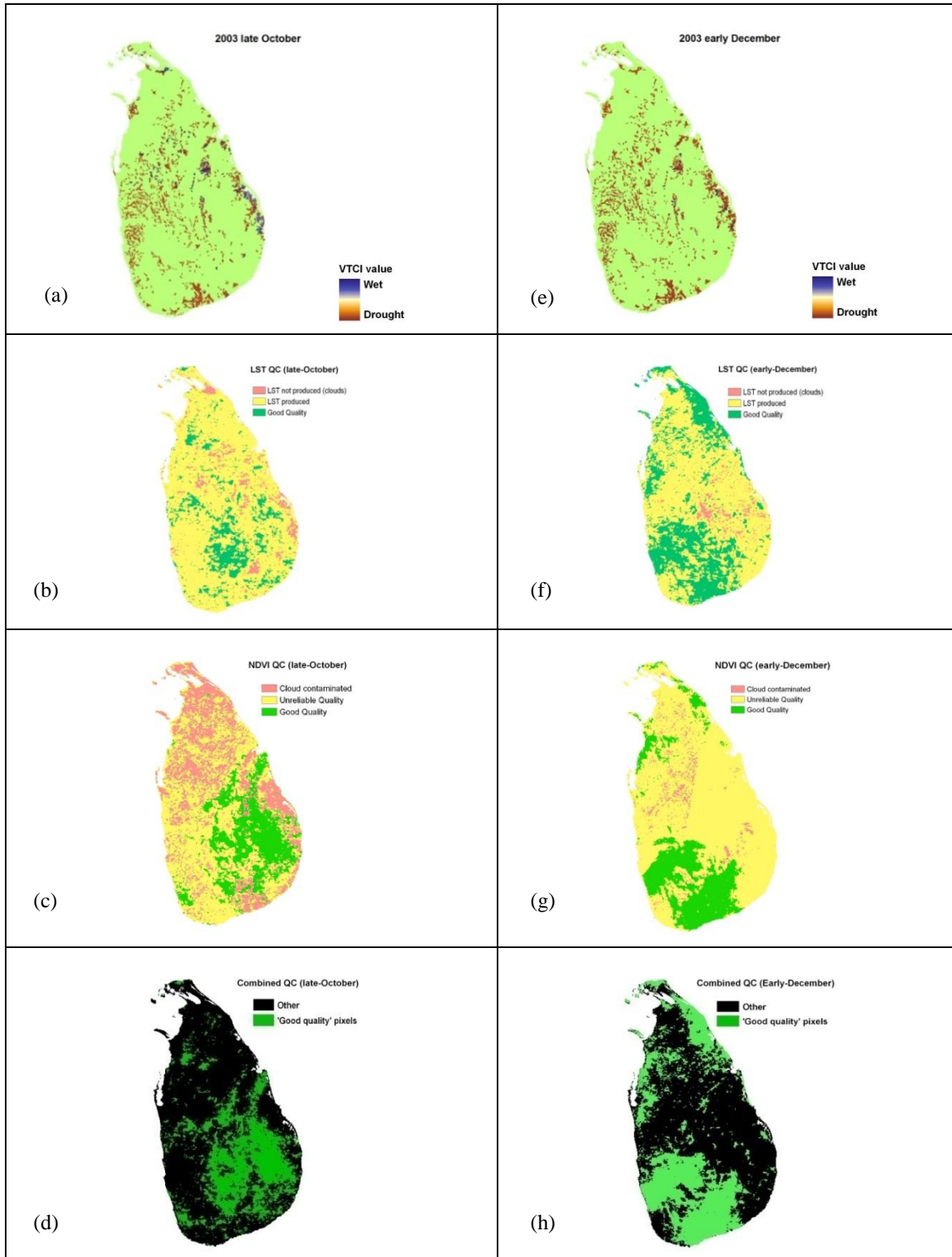


**Figure 5.11:** Examples of VTCI images and relevant MODIS Quality Control (QC) images for late-October 2003 (left panel) and early-December (right panel). Left panel: VTCI image for late-October (a); LST QC (b); NDVI QC (c) and Combined QC mask (d) prepared by intersecting raster masks of 'Good Quality' pixels extracted from the LST QC and NDVI QC images. Right panel: same as for left panel but for early-December.



Figure 5.12 presents a time series plot of VTCI variation at three sites in the four districts affected by extreme drought in 2003. The VTCI plots for the first two locations clearly indicate moisture stress (with VTCI values close to zero) throughout the season (red and blue line graphs in Fig. 5.12 (c)). VTCI for the third location shows that the moisture stress for the October-November reverses to wet conditions during the December-February season. These results indicate that moisture stress was not uniform within the districts affected by extreme drought in 2003.

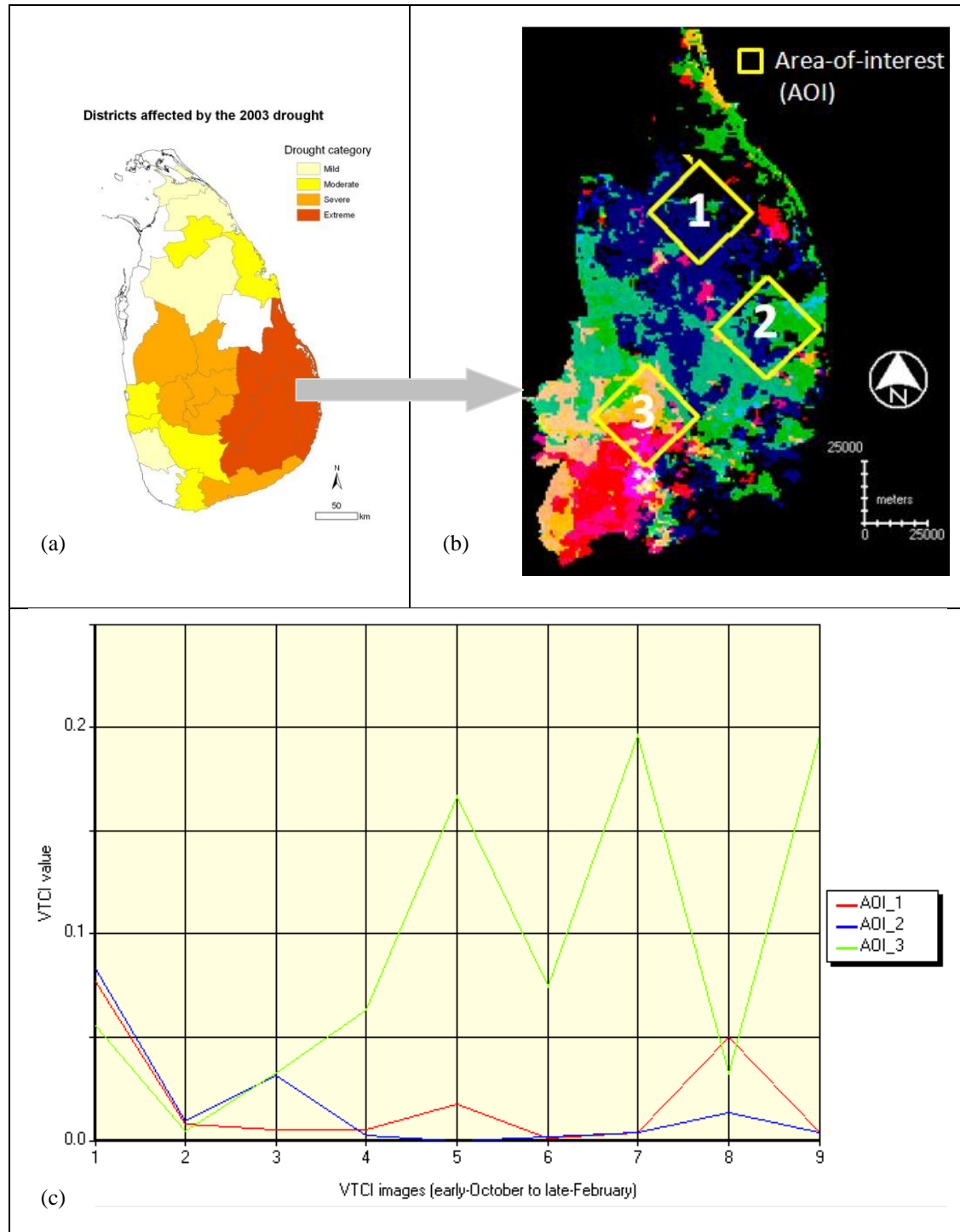


**Figure 5.12:** Time series of VTCI presented for three locations in the four districts affected by extreme drought (dark orange) in 2003 (a). Top right (b) is an image created by stacking the nine images used to study the entire Maha season in 2003 and extracting the cells falling within the districts affected by extreme drought. The display shows three of the nine images. The yellow squares are the areas-of-interest (AOIs) selected to plot VTCI values at each time step. Reds indicate higher VTCI (wetter) values and blues and greens indicate lower VTCI (drier) values in the three images used in the display. The lower plot (c) shows mean VTCI values within each AOI from early-October to late-February. The numerals 1-9 along the x-axis indicate each VTCI image stacked in chronological order from early-October (1) through late-February (9).

#### 5.4: Conclusion

Results show that the VTCI is a metric that captures the progression of moisture stress during both the October-November and December-February seasons. It is thus a valuable tool for monitoring drought conditions during the entire Maha season. It also complements the seasonal rainfall forecast by capturing the onset and progression of moisture stress.

Moisture stress is not uniform – even in locations affected by extreme conditions of drought as denoted by the Standardized Precipitation Index (SPI). Soil moisture is an integrated variable affected by a host of local factors such as soil type, vegetation cover and local topography. The VTCI, as a proxy for soil moisture, provides a continuous surface – as opposed to point based rainfall estimates at raingauges – of moisture conditions at different stages in a season. VTCI can be calculated in near real-time as MODIS LST and NDVI products are available at a lag of just around 5 days. This short time-lag is critical as there is a time-lag of almost a month before rainfall data at a majority of the rain gauges scattered across the island is reported to the main office of the Sri Lanka Department of Meteorology<sup>22</sup>.

This chapter demonstrates that the VTCI is a tool that could be used to monitor the onset and progression of anomalous wet and dry conditions during the Maha season because it provides an integrated signal of vegetation vigour and moisture stress. Whether actual values of VTCI could be input as a variable to crop models is an area requiring further investigation. How well the VTCI performs in capturing moisture stress

---

<sup>22</sup> Rainfall received at the 22 main meteorological stations is transmitted immediately to the Department of Meteorology. Rainfall at some stations is reported via telephone the next day. It takes a month before rainfall reports for a majority of the rain gauges reach the Department of Meteorology (Personal communication with Mr. K.H.M.S. Premalal, Deputy Director, Sri Lanka Department of Meteorology, 10 May 2010).

in regions under irrigation (as is the case in much of north central and northeastern Sri Lanka) is also an area that needs further investigation.

## Chapter 6: Conclusion

The dissertation finds that drought in locations in the humid tropics can be predicted on an operational basis if the failure of rainfall regimes in such regions could be predicted. It also finds that the near-real time monitoring of moisture stress, using remotely sensed data, complements drought prediction by providing critical information on the onset and progression of moisture stress. The dissertation demonstrates that an operational drought prediction and monitoring framework suitable for locations in the humid tropics should be based on a systematic study of atmospheric factors driving the suppression of seasonal rainfall over such locations, an assessment of the predictability of such atmospheric factors, and a near-real time assessment of moisture conditions over a continuous surface.

The focus of the dissertation is the humid tropics, a region highly susceptible to recurrent drought at the seasonal time scale. The specific geographical focus of the study is Sri Lanka where drought is a frequent occurrence that has been documented since ancient times. Such droughts take place when rainfall regimes associated with the main cultivation season – the *Maha* – fail. The *Maha* rainfall regimes are: the second inter-monsoon (a convective rainfall season from October-November); and the northeast monsoon (that coincides with the Asian winter monsoon from December-February).

The study objectives are: to characterize drought occurrence over Sri Lanka over the last 6 decades, to propose a methodology for predicting drought in Sri Lanka based on seasonal climate forecasts, and to propose a methodology to monitor seasonal moisture stress in near-real time during the *Maha* cultivation season. The dissertation has three major research thrusts based on these objectives.

The first research thrust characterizes *Maha* seasonal drought occurrence during the period 1951-2008. It finds that there is a marked increase in the occurrence of drought in the post-1975 period, with droughts of extreme and severe magnitude occurring only post-1975. Although drought occurrence during the *Maha* season is frequent, there is no clear periodicity to drought occurrence apart from 1975-1990 when every other year appears to have been a drought year, and from 2000-2005 when droughts in the severe to extreme category occurred simultaneously. Droughts have a significant negative impact on rice production and yield. Given the lack of clear periodicity in drought occurrence, advance knowledge of whether a forthcoming season could be affected by drought is essential for cropping decisions and irrigation scheduling. The October-November convective rainfall is significantly correlated with *Maha* seasonal drought. The December-February northeast monsoon is only weakly correlated with *Maha* seasonal drought. However, as negative anomalies in December-February rainfall are evident in most drought years, the importance of the December-February season as a factor in *Maha* drought cannot be dismissed. The October-November rains provide critical moisture to the growing season, advance knowledge of the likely strength of the October-November rains in a forthcoming season could be invaluable to decision-making in agriculture. Failure of the December-February could devastate a rice crop at the maturing stage. Advance knowledge of the strength of the forthcoming December-February rains could be critical for decisions such as (but not limited to) when, where and how much irrigation water should be released.

Past drought events have not been uniform in terms of their severity and spatial extent. However, in most drought years (except for 2001), the region most affected falls

within the “Dry Zone” (region receiving an annual rainfall of less than 2000mm) of the island. Results from Wavelet Transforms on dominant modes of variability in drought incidence indicate that the 2-8 year frequency is the dominant mode of variance at most stations. This frequency is similar to the documented dominant variance in ENSO. The 8-16 (decadal) frequency significant at certain stations is similar to the documented dominant mode of variance of the IOD. Drought occurrence and variability appears to be increasing along the eastern and southeastern regions of the island.

The second research thrust proposes a methodology for predicting drought in Sri Lanka. It first identifies large-scale atmospheric dynamics influencing the strength of the October-November and December-February rains. Next, it builds a seasonal forecast model using cross validated Canonical Correlation Analysis with the identified large-scale atmospheric field as the predictor and observed October-November and December-February rainfall at a 132 rain gauges across Sri Lanka as the predictand. It tests the operational utility of the forecast model by obtaining forecast predictor fields from three Global Climate Model (GCM) ensembles. The GCM output used in the study came from archived experimental forecasts carried out at the International Research Institute for Climate and Society (IRI) using the ECHAM4.5 AGCM forced with persisted sea surface temperature anomalies (ECHAM\_PSST) and constructed analogues of sea surface temperature anomalies (ECHAM\_CA), and from the National Centers for Environmental Prediction (NCEP) full coupled Climate Forecast System (CFS) GCM.

The study finds that the October-November rains fail when anomalously strong contemporaneous zonal winds at the 850hPa level (U850) over the central Indian Ocean suppress convection over Sri Lanka. The exact reason for the strengthening of the

westerly zonal winds is as yet unclear. It could be a consequence of strong summer monsoon winds increasing upwelling along the east African coast and thus setting up a marked SST gradient between the eastern and western Indian Ocean. Results show that in some years the anomalous strengthening of the zonal winds can be attributed to La Niña events and negative IOD events. Whether ENSO leads IOD influence on the zonal wind or vice versa, or whether both simply act in concert, is as yet unclear. The reason for there being years when the zonal winds are strong without either of these phenomena exerting a discernible influence is also unclear. It is evident that the zonal wind field is consistently above normal in years when October-November rainfall is below normal. This finding is a significant improvement on seasonal climate predictions relying purely on indices of the Southern Oscillation or the IOD given that the influences of those modes are not consistent through time. Drought years attributed only to the failure of ON rainfall (1983 and 2000) are La Niña years.

Droughts associated with the failure of October-November rainfall can be predicted on an operational basis using predicted fields of the contemporaneous zonal wind at 850hPa issued in September of a given year from Global Climate Model (GCM) ensembles. Statistically significant forecast skill was observed over the rice cultivation areas of the southern, southeastern, central and north-central portions of the island using predicted fields from the two versions of the ECHAM4.5 GCM. Estimates of expected rainfall at station-level from the two versions of the ECHAM4.5 can, therefore, be utilized to aid specific decisions on the variety and extent of rice to be planted in these areas. Tercile forecasts – indicating the likelihood of whether rainfall in an oncoming season will be below-, near- or above-normal – from the CFS and the ECHAM4.5\_PSST



can be consulted to predict whether the upcoming Maha season is likely to be susceptible to drought.

The study finds that the vertical shear of the contemporaneous (December-February) meridional wind ( $V_s$ ), in the domain  $80^{\circ}\text{E}$ - $90^{\circ}\text{E}$  and  $0^{\circ}\text{N}$ - $20^{\circ}\text{N}$ , controls December-February rainfall over Sri Lanka. December-February rainfall is suppressed when  $V_s$  is anomalously low and vice versa. Reasons for the variability in the strength of  $V_s$  are as yet unclear. There may be a connection between  $V_s$  and factors such as the Siberian High, cold surges and the Borneo Vortex that influence the strength of the East Asian winter monsoon. December-February rainfall in the two *Maha* drought years of 1983 and 2000 – La Niña years – was above normal. It could be that the influence of La Niña on  $V_s$  – and hence December-February rainfall over Sri Lanka – is manifest through the former's modulation of the strength of the Siberian High, cold surges and the Borneo Vortex.

Droughts associated with the failure of December-February rainfall can be predicted with forecast fields of contemporaneous  $V_s$  issued in November from the ECHAM4.5 forced with constructed analogues of sea surface temperature anomalies. Statistically significant prediction skill was observed over the rice cultivation regions in the eastern, central and north-central parts of the island. Forecasts of expected rainfall at stations in such locations could be consulted to determine whether drought conditions might affect rice crops at their maturing stage. Such information could guide decisions on changes to irrigation scheduling and advisories on the need to adopt mulching techniques in the advent of imminent water stress.

The third research thrust proposes a methodology to monitor moisture stress in near-real time during the *Maha* season. It finds that the Vegetation Temperature Condition Index (VTCI) – that combines vegetation indices (derived from remotely sensed data in the optical wavelengths) with land surface temperature (derived from remotely sensed data in the thermal infrared wavelengths) – to be a metric that captures the progression of moisture stress during both the October-November and December-February seasons. It is thus a valuable tool for monitoring drought conditions during the entire *Maha* season. It also complements the seasonal rainfall forecast by capturing the onset and progression of moisture stress.

The study finds that moisture stress is not uniform – even in locations affected by extreme conditions of drought as denoted by the Standardized Precipitation Index (SPI). The finding underscores the need to have a continuous field of soil moisture (or proxies for soil moisture) observations, as soil moisture is an integrated variable affected by a host of local factors such as soil type, vegetation cover and local topography that may vary drastically across space. The VTCI, as a proxy for soil moisture, provides such a continuous surface – as opposed to point based rainfall estimates at raingauges – of moisture conditions at different stages in a season. VTCI for Sri Lanka can be calculated in near real-time using the Land Surface Temperature (LST) and Normalized Difference Vegetation Index (NDVI) products, based on data acquired in the optical and thermal infrared wavelengths by the Moderate Resolution Imaging Spectroradiometer (MODIS) aboard the Terra Satellite (Terra-MODIS), available free-of-charge at time lag of ~5 days. This short time-lag is critical as there is a time-lag of almost a month before rainfall data at a majority of the rain gauges scattered across the island is reported to the

main office of the Sri Lanka Department of Meteorology. The VTCI is thus an ideal technique for operational monitoring of the onset and progression of anomalous wet and dry conditions at the ground.

The dissertation identifies a number of areas requiring further investigation. Some of the critical areas that need to be addressed in the near-future include the following:

- 1) Is the increase in drought occurrence and magnitude in the post-1975 period linked to the change in SST background state over the Indian Ocean around 1976-1977? How does the documented change in ENSO influence on the Indian Ocean region affect trends in *Maha* drought incidence? How does global warming affect ocean-atmosphere coupling in the Indian Ocean region and what are the implications for the interplay between the Madden Julian Oscillation (MJO), the IOD, the Tropical Biennial Oscillation and ENSO? How could changes in the interplay between these phenomena influence seasonal predictability skill and hence drought predictability for Sri Lanka?

Coupled ocean-atmospheric modeling is required to answer the above questions. Research hypotheses to explore through such studies could include: ‘Increased warming of the Indian Ocean decreases the strength of the winter monsoon (and hence increases *Maha* drought incidence)’; and ‘Decreased influence of ENSO on the Indian Ocean region strengthens the zonal circulation cells within the basin – leading to either increased droughts or floods during the boreal fall.’

- 2) Do factors like the Siberian High, cold surges, the Borneo Vortex and the MJO control the strength of the contemporaneous vertical shear of the mean meridional wind ( $V_s$ ) and hence December-February rainfall over Sri Lanka?

The dissertation found an apparent link between these phenomena and DJF rainfall. A definite answer requires an atmospheric modeling study. A plausible hypothesis to explore is whether snow cover anomalies over Eurasia control the Siberian High, cold surges, the Borneo Vortex and the MJO. Such a study may unravel different pathways through which all such phenomena are connected. Such understanding would definitely help improve predictability of the DJF season.

- 3) Is the observed increased trend in drought incidence and variability in the eastern and southeastern regions related to a weakening of the mean December-February wind field over eastern, north central and southeastern Sri Lanka? If yes, could such trends in the wind field be attributed to the increase in anthropogenic greenhouse gases in the atmosphere or to the increased presence of industrial aerosol loadings in the Bay of Bengal area?

These questions could be addressed by analyzing wind data from IPCC CMIP model output scenarios and remotely sensed data of aerosol loadings over the Bay of Bengal.

- 4) Can actual values of the VTCI be input as a variable to crop models? How well does the VTCI perform in capturing moisture stress irrigated areas?

The VTCI could be input as a variable to crop models after calibrating VTCI values with variables such as evapotranspiration commonly used in crop models. The performance of VTCI in capturing moisture stress in irrigated areas requires field observations and a comparison of results in irrigated versus non-irrigated areas. The incorporation of VTCI in crop models and a disaggregated analysis of VTCI in irrigated versus non-irrigated areas would improve its utility to decision makers.

In conclusion, the dissertation presents an operational methodology for predicting and monitoring drought applicable to locations in the humid tropics where rain failure is the primary causal factor for drought. Using Sri Lanka as a case study, it demonstrates a framework for drought prediction based on an assessment of seasonal rainfall predictability. It also demonstrates how a proxy for soil moisture complements the seasonal rainfall prediction by capturing moisture stress as a season unfurls. The study finds that the seasonal rainfall prediction can be issued with a lag time of one month prior to the commencement of the main cultivation season. It also finds that the proxy for soil moisture can be generated in near-real time. Such time frames are of utility for key decisions in agriculture at the study site. The wider applicability of the study stems from the proposed methodologies for drought prediction and monitoring being directly applicable to other locations in the humid tropics. The areas identified for future research could strengthen existing drought prediction capacity particularly in the humid tropics and sub-tropics and improve the overall utility of drought monitoring techniques to decision makers.

## Annex 1:

### Modifications made to original Matlab Code for Wavelet Transform Analysis

Modifications are indicated in red lettering. Yellow highlighted sections include code added to the original code. (Acronym NF=Nelun Fernando)

```
%WAVETEST Example Matlab script for WAVELET, using NINO3 SST dataset
%
% See "http://paos.colorado.edu/research/wavelets/"
% Written January 1998 by C. Torrence
%
% Modified Oct 1999, changed Global Wavelet Spectrum (GWS) to be
sideways,
%   changed all "log" to "log2", changed logarithmic axis on GWS to
%   a normal axis.

load 'battispi.mat'    % input SPI time series
SPI2 = battispi;

%----- Computation

% normalize by standard deviation (not necessary, but makes it easier
% to compare with plot on Interactive Wavelet page, at
% "http://paos.colorado.edu/research/wavelets/plot/"
variance = std(SPI2)^2;
```

```

SPI2 = (SPI2 - mean(SPI2))/sqrt(variance) ;

% [NF comment: the next three lines of code fit a lag1 autocorrelation
% (AR-1) to the data]

xvec=reshape(SPI2,length(SPI2),1); % The time series data
Xmat=[ [xvec; 0] [0; xvec] ]; Rxx=Xmat'*Xmat;
laga=-Rxx(2,1)/Rxx(2,2);

n = length(SPI2);

dt = 1 ; %(NF comment - sampling is yearly)
time = [0:length(SPI2)-1]*dt + 1870.0; % construct time array
xlim = [1870, 2005]; % plotting range
pad = 1; % pad the time series with zeroes (recommended)
dj = 0.125; % this will do 8 sub-octaves per octave (NF comment
modified)
s0 = 1*dt; % this says start at a scale of 1 year (NF comment
modified)
j1 = 7/dj; % this says do 7 powers-of-two with dj sub-octaves each
lag1 = laga; % lag-1 autocorrelation for red noise background
mother = 'MORLET';

%MOTHER = the mother wavelet function.

% The choices are 'MORLET', 'PAUL', or 'DOG'

% Wavelet transform:
[wave,period,scale,coi] = wavelet(SPI2,dt,pad,dj,s0,j1,mother);
power = (abs(wave)).^2 ; % compute wavelet power spectrum

```

```

% Significance levels: (variance=1 for the normalized SST)

[signif,fft_theor] = wave_signif(1.0,dt,scale,0,lag1,-1,-1,mother);

sig95 = (signif')*(ones(1,n)); % expand signif --> (J+1)x(N) array
sig95 = power ./ sig95; % where ratio > 1, power is significant


% Global wavelet spectrum & significance levels:

global_ws = variance*(sum(power')/n); % time-average over all times
dof = n - scale; % the -scale corrects for padding at edges
global_signif = wave_signif(variance,dt,scale,1,lag1,-1,dof,mother);


% Scale-average between drought periods of 1--16 years
avg = find((scale >= 1) & (scale < 16));

Cdelta = 0.776; % this is for the MORLET wavelet

scale_avg = (scale')*(ones(1,n)); % expand scale --> (J+1)x(N) array
scale_avg = power ./ scale_avg; % [Eqn(24)]

scale_avg = variance*dj*dt/Cdelta*sum(scale_avg(avg,:)); % [Eqn(24)]
scaleavg_signif = wave_signif(variance,dt,scale,2,lag1,-
1,[2,7.9],mother);

whos

%----- Plotting

%--- Plot time series

subplot('position',[0.1 0.75 0.65 0.2])

plot(time,SPI2)

```



```

set(gca,'XLim',xlim(:))

xlabel('Time (year)')

ylabel('SPI (unitless)')

title('a) Batticaloa station: October 6-monthly Standardized
Precipitation Index (1870-2005)')

hold off

%--- Contour plot wavelet power spectrum
subplot('position',[0.1 0.37 0.65 0.28])

levels = [0.0625,0.125,0.25,0.5,1,2,4,8,16] ;

Yticks = 2.^(fix(log2(min(period))):fix(log2(max(period)))));

contour(time,log2(period),log2(power),log2(levels)); %*** or use
'contourfill'

%imagesc(time,log2(period),log2(power)); %*** uncomment for 'image'
plot

xlabel('Time (year)')

ylabel('Period (year)')

title('b) October 6-monthly SPI Wavelet Power Spectrum')

set(gca,'XLim',xlim(:))

set(gca,'YLim',log2([min(period),max(period)]), ...
'YDir','reverse', ...
'YTick',log2(Yticks(:)), ...
'YTickLabel',Yticks)

% 95% significance contour, levels at -99 (fake) and 1 (95% signif)

hold on

[cc1 hh1]=contour(time,log2(period),sig95,[-99,1],'k');

set(hh1,'linewidth',2);

hold on

```

```

% cone-of-influence, anything "below" is dubious
plot(time,log2(coi),'k')

hold off

%--- Plot global wavelet spectrum
subplot('position',[0.77 0.37 0.2 0.28])
plot(global_ws,log2(period))

hold on

plot(global_signif,log2(period),'--')

hold off

xlabel('Power (SPI^2)')

title('c) Global Wavelet Spectrum')

set(gca,'YLim',log2([min(period),max(period)]), ...
      'YDir','reverse', ...
      'YTick',log2(Yticks(:)), ...
      'YTickLabel','')

set(gca,'XLim',[0,1.25*max(global_ws)])

%--- Plot 1--16 yr scale-average time series
subplot('position',[0.1 0.07 0.65 0.2])
plot(time,scale_avg)

set(gca,'XLim',xlim(:))

xlabel('Time (year)')

ylabel('Avg variance (SPI^2)')

title('d) 1-16 yr Scale-average Time Series')

hold on

plot(xlim,scaleavg_signif+[0,0],'--')

hold off

```

**Annex 2:****Sri Lanka rice production statistics 1952-2009**

National Annual Sown and Harvested Extent, Average Yield and Production of Paddy 1952 - 2009

Cultivation Year	Sown		Harvested		Average Yield		Production	
	000 Acres	000 Ha	000 Acres	000 Ha.	Bushels/Acre	Kg/Ha	000 Bushels	000 Mt.
1952	1,162	471	1,102	446	30.8	1,588	28,900	604
1953	1,049	425	952	385	27	1,392	21,900	458
1954	1,253	508	1,201	486	30.02	1,548	31,100	650
1955	1,347	545	1,285	520	32.45	1,673	35,700	746
1956	1,177	476	1,052	426	30.03	1,549	27,500	575
1957	1,208	489	1,139	461	32.35	1,668	31,280	654
1958	1,383	559	1,239	502	34.4	1,774	36,600	765
1959	1,330	538	1,228	497	34.91	1,800	36,400	761
1960	1,469	595	1,393	564	36.38	1,875	43,000	899
1961	1,472	596	1,407	570	36.13	1,863	43,100	901
1962	1,536	622	1,492	604	37.9	1,954	48,000	1,003
1963	1,562	633	1,526	618	37.91	1,955	49,200	1,028
1964	1,586	643	1,535	622	38.72	1,996	50,505	1,056
1965	1,456	590	1,243	503	34.32	1,770	36,252	758
1966	1,617	655	1,512	612	35.62	1,837	45,787	957
1967	1,639	664	1,567	634	41.27	2,127	54,962	1,149
1968	1,743	705	1,634	661	46.49	2,397	64,500	1,348
1969	1,709	692	1,540	624	50.33	2,595	65,864	1,377
1970	1,875	759	1,776	719	51.31	2,645	77,447	1,619
1971	1,793	726	1,714	694	45.91	2,367	66,895	1,398
1972	1,795	727	1,578	639	46.87	2,417	62,901	1,315
1973	1,789	724	1,660	672	44.58	2,299	62,900	1,315
1974	2,038	825	1,969	797	45.65	2,353	76,794	1,605
1975	1,720	697	1,475	597	44.05	2,271	55,315	1,156
1976	1,789	724	1,570	636	44.9	2,315	60,034	1,255
1977	2,046	828	1,933	783	48.88	2,520	80,387	1,680
1978	2,163	875	2,074	840	50.83	2,621	90,605	1,894
1979	2,075	839	1,936	783	53.29	2,747	91,886	1,919
1980	2,087	844	2,030	815	56.83	2,931	102,237	2,134
1981	2,166	877	2,081	837	57.84	2,982	106,845	2,229
1982	2,086	844	1,844	745	62.37	3,215	103,312	2,156
1983	2,036	824	1,922	777	70.36	3,628	119,027	2,484

1984	2,447	990	2,189	886	59.74	3,080	115,968	2,413
1985	2,176	881	2,139	864	66.77	3,443	127,552	2,661
1986	2,212	895	2,064	835	67.41	3,475	123,956	2,588
1987	1,931	781	1,677	679	69.11	3,564	101,987	2,127
1988	2,145	868	2,015	816	66.19	3,413	118,704	2,477
1989	1,797	727	1,704	690	65.45	3,375	98,916	2,063
1990	2,109	853	2,046	825	66.97	3,452	121,674	2,538
1991	2,018	817	1,954	791	65.89	3,397	114,471	2,389
1992	1,985	803	1,893	766	66.52	3,430	112,184	2,340
1993	2,061	835	2,026	820	67.97	3,504	123,213	2,570
1994	2,297	930	2,215	897	65.23	3,363	128,630	2,683
1995	2,261	915	2,198	889	68.58	3,536	134,678	2,810
1996	1,850	749	1,631	660	68.15	3,514	98,807	2,061
1997	1,804	730	1,705	690	70.19	3,619	107,333	2,239
1998	2,096	848	2,048	829	70.52	3,636	129,044	2,692
1999	2,205	892	2,154	872	71.1	3,665	136,942	2,857
2000	2,169	878	2,056	832	74.79	3,857	137,085	2,860
2001	1,973	798	1,890	765	76.68	3,953	129,134	2,695
2002	2,106	852	2,025	820	75.5	3,893	137,029	2,860
2003	2,428	983	2,250	911	72.94	3,761	146,983	3,067
2004	1,924	779	1,779	720	79.25	4,086	125,943	2,628
2005	2,316	937	2,261	915	76.86	3,963	155,577	3,246
2006	2,250	910	2,224	900	80.24	4,137	160,163	3,341
2007	2,018	816	1,966	796	85.38	4,386	150,059	3,131
2008	2,602	1,053	2,552	1,033	81.2	4,184	185,723	3,875
2009	2,415	977	2,329	941	84.11	4,337	175,009	3,652

Source:

<http://www.statistics.gov.lk/agriculture/Paddy%20Statistics/PaddyStatsPages/PaddyAnnualSHYP.html>

### **Annex 3:**

#### **List of identification numbers of original MODIS imagery analyzed in Chapter 5**

##### **October-November 2000 LST**

1. MOD11A2.A2000281.h25v08.005.2006324141248.hdf
2. MOD11A2.A2000281.h26v08.005.2006324141217.hdf
3. MOD11A2.A2000297.h25v08.005.2006329041928.hdf
4. MOD11A2.A2000297.h26v08.005.2006329041915.hdf
5. MOD11A2.A2000305.h25v08.005.2008211035808.hdf
6. MOD11A2.A2000305.h26v08.005.2008211034846.hdf
7. MOD11A2.A2000329.h25v08.005.2006340104014.hdf
8. MOD11A2.A2000329.h26v08.005.2006340103856.hdf

##### **October-November 2000 NDVI**

1. MOD13A2.A2000273.h25v08.005.2008203110759.hdf
2. MOD13A2.A2000273.h26v08.005.2008203111052.hdf
3. MOD13A2.A2000289.h25v08.005.2008205091753.hdf
4. MOD13A2.A2000289.h26v08.005.2008205091950.hdf
5. MOD13A2.A2000305.h25v08.005.2008211022803.hdf
6. MOD13A2.A2000305.h26v08.005.2008211024053.hdf
7. MOD13A2.A2000321.h25v08.005.2006341035628.hdf
8. MOD13A2.A2000321.h26v08.005.2006341040350.hdf

##### **October-November 2001 LST**

1. MOD11A2.A2001281.h25v08.005.2007065000100.hdf
2. MOD11A2.A2001281.h26v08.005.2007065002840.hdf
3. MOD11A2.A2001297.h25v08.005.2007068095843.hdf
4. MOD11A2.A2001297.h26v08.005.2007068154605.hdf

5. MOD11A2.A2001305.h25v08.005.2007070100610.hdf
6. MOD11A2.A2001305.h26v08.005.2007070100814.hdf
7. MOD11A2.A2001329.h25v08.005.2007076000607.hdf
8. MOD11A2.A2001329.h26v08.005.2007076000411.hdf

**October-November 2001 NDVI**

1. MOD13A2.A2001273.h25v08.005.2008285074944.hdf
2. MOD13A2.A2001273.h26v08.005.2008285081744.hdf
3. MOD13A2.A2001289.h25v08.005.2007076164733.hdf
4. MOD13A2.A2001289.h26v08.005.2007076170302.hdf
5. MOD13A2.A2001305.h25v08.005.2008289060815.hdf
6. MOD13A2.A2001305.h26v08.005.2008289061647.hdf
7. MOD13A2.A2001321.h25v08.005.2007082153926.hdf
8. MOD13A2.A2001321.h26v08.005.2007082154934.hdf

**October-November 2002 LST**

1. MOD11A2.A2002281.h25v08.005.2007242215944.hdf
2. MOD11A2.A2002281.h26v08.005.2007242220003.hdf
3. MOD11A2.A2002297.h25v08.005.2007243204811.hdf
4. MOD11A2.A2002297.h26v08.005.2007243204810.hdf
5. MOD11A2.A2002305.h25v08.005.2007245015554.hdf
6. MOD11A2.A2002305.h26v08.005.2007245015546.hdf
7. MOD11A2.A2002329.h25v08.005.2007257031136.hdf
8. MOD11A2.A2002329.h26v08.005.2007257031102.hdf

**October-November 2002 NDVI**

1. MOD13A2.A2002273.h25v08.005.2008253170058.hdf
2. MOD13A2.A2002273.h26v08.005.2008253135501.hdf

3. MOD13A2.A2002289.h25v08.005.2007228045703.hdf
4. MOD13A2.A2002289.h26v08.005.2007228071513.hdf
5. MOD13A2.A2002305.h25v08.005.2007235122937.hdf
6. MOD13A2.A2002305.h26v08.005.2007235124227.hdf
7. MOD13A2.A2002321.h25v08.005.2007243225153.hdf
8. MOD13A2.A2002321.h26v08.005.2007243225155.hdf

**October - February 2003/2004 LST**

1. MOD11A2.A2003281.h25v08.005.2008010145213.hdf
2. MOD11A2.A2003281.h26v08.005.2008010143725.hdf
3. MOD11A2.A2003297.h25v08.005.2008017212652.hdf
4. MOD11A2.A2003297.h26v08.005.2008017155818.hdf
5. MOD11A2.A2003321.h25v08.005.2008025120854.hdf
6. MOD11A2.A2003321.h26v08.005.2008025153025.hdf
7. MOD11A2.A2003337.h25v08.005.2008042135514.hdf
8. MOD11A2.A2003337.h26v08.005.2008042135146.hdf
9. MOD11A2.A2003361.h25v08.005.2008047160920.hdf
10. MOD11A2.A2003361.h26v08.005.2008047161255.hdf
11. MOD11A2.A2004001.h25v08.005.2008173034600.hdf
12. MOD11A2.A2004001.h26v08.005.2008173034557.hdf
13. MOD11A2.A2004025.h25v08.005.2008173063913.hdf
14. MOD11A2.A2004025.h26v08.005.2008173063926.hdf
15. MOD11A2.A2004033.h25v08.005.2007243092607.hdf
16. MOD11A2.A2004033.h26v08.005.2007243092609.hdf
17. MOD11A2.A2004049.h25v08.005.2007248182046.hdf
18. MOD11A2.A2004049.h26v08.005.2007248162910.hdf

**October – February 2003/2004 NDVI**

1. MOD13A2.A2003289.h25v08.005.2008264025847.hdf
2. MOD13A2.A2003289.h26v08.005.2008264025844.hdf
3. MOD13A2.A2003305.h25v08.005.2008022204054.hdf
4. MOD13A2.A2003305.h26v08.005.2008022204943.hdf
5. MOD13A2.A2003321.h25v08.005.2008037142318.hdf
6. MOD13A2.A2003321.h26v08.005.2008037091534.hdf
7. MOD13A2.A2003337.h25v08.005.2008266113359.hdf
8. MOD13A2.A2003337.h26v08.005.2008266113529.hdf
9. MOD13A2.A2003353.h25v08.005.2008041074831.hdf
10. MOD13A2.A2003353.h26v08.005.2008041080417.hdf
11. MOD13A2.A2004001.h25v08.005.2007236192932.hdf
12. MOD13A2.A2004001.h26v08.005.2007236193854.hdf
13. MOD13A2.A2004017.h25v08.005.2008224143324.hdf
14. MOD13A2.A2004017.h26v08.005.2008224153913.hdf
15. MOD13A2.A2004033.h25v08.005.2007246191251.hdf
16. MOD13A2.A2004033.h26v08.005.2007246190722.hdf
17. MOD13A2.A2004049.h25v08.005.2007251100843.hdf
18. MOD13A2.A2004049.h26v08.005.2007251115917.hdf

**October-November 2004 LST**

1. MOD11A2.A2004281.h25v08.005.2007324171917.hdf
2. MOD11A2.A2004281.h26v08.005.2007325024856.hdf
3. MOD11A2.A2004329.h25v08.005.2007337203800.hdf
4. MOD11A2.A2004329.h26v08.005.2007337200111.hdf



**October-November 2004 NDVI**

1. MOD13A2.A2004273.h25v08.005.2008254160357.hdf
2. MOD13A2.A2004273.h26v08.005.2008254181955.hdf
3. MOD13A2.A2004321.h25v08.005.2008227011051.hdf
4. MOD13A2.A2004321.h26v08.005.2008227012446.hdf

**October-November 2005 LST**

1. MOD11A2.A2005281.h25v08.005.2008073200814.hdf
2. MOD11A2.A2005281.h26v08.005.2008073193918.hdf
3. MOD11A2.A2005297.h25v08.005.2008077092311.hdf
4. MOD11A2.A2005297.h26v08.005.2008077074156.hdf
5. MOD11A2.A2005329.h25v08.005.2008086220038.hdf
6. MOD11A2.A2005329.h26v08.005.2008086214952.hdf

**October-November 2005 NDVI**

1. MOD13A2.A2005273.h25v08.005.2008074022517.hdf
2. MOD13A2.A2005273.h26v08.005.2008074022109.hdf
3. MOD13A2.A2005289.h25v08.005.2008077173028.hdf
4. MOD13A2.A2005289.h26v08.005.2008077123053.hdf
5. MOD13A2.A2005321.h25v08.005.2008263124621.hdf
6. MOD13A2.A2005321.h26v08.005.2008263134458.hdf

## References

- Alory, G., Wijffels, S., and Meyers, G. (2007), Observed temperature trends in the Indian Ocean over 1960-1999 and associated mechanisms, *Geophysical Research Letters*, *34*, L02606.
- Anderson, M. C., Norman, J.M., Mecikalski, J.R., Otkin, J.A., and Kustas, W.P. (2007), A climatological study of evapotranspiration and moisture stress across the continental United States based on thermal remote sensing: 2. Surface moisture climatology, *Journal of Geophysical Research*, *112*, D11112.
- Ashok, K., Chan, W.-L., Motoi, T., Yamagata, T. (2004), Decadal variability of the Indian Ocean dipole, *Geophysical Research Letters*, *31*, L24207.
- Baigorria, G. A., Hansen, J.W., Ward, N., Jones, J.W., and Brien, J.J. (2008), Assessing predictability of cotton yields in the southeastern United States based on regional atmospheric circulation and surface temperatures, *Journal of Applied Meteorology and Climatology*, *47*, 76-91.
- Bamzai, A. S., and J. Shukla (1999), Relation between Eurasian Snow Cover, Snow Depth, and the Indian Summer Monsoon: An Observational Study, *Journal of Climate*, *12*, 3117-3132.
- Barnett, T. P., Dumenil, L., Schlese, U., Roeckner, E., Latif, M. (1989), The effect of Eurasian snow cover of regional and global climate variation, *Journal of the Atmospheric Sciences*, *46*, 661-685.
- Barnett, T. P., and R. Preisendorfer (1987), Origins and Levels of Monthly and Seasonal Forecast Skill for United States Surface Air Temperatures Determined by Canonical Correlation Analysis, *Monthly Weather Review*, *115*, 1825-1850.
- Barnston, A. G., and Ropelewski, C.F. (1992), Prediction of ENSO Episodes Using Canonical Correlation Analysis, *Journal of Climate*, *5*, 1316-1345.
- Barnston, A. G., and van den Dool, H.M. (1993), A degeneracy in cross-validated skill in regression-based forecasts, *Journal of Climate*, *6*, 963-977.
- Basnayake, B. K. (1990), Droughts in the dry zone of Sri Lanka, in *Irrigation and Water Resources*, edited by E. R. N. Gunawardena, pp. 18-39, Postgraduate Institute of Agriculture, University of Peradeniya, Sri Lanka.
- Bessafi, M., and Wheeler, M.C. (2006), Modulation of South Indian Ocean tropical cyclones by the Madden-Julian Oscillation and convectively coupled equatorial waves, *Monthly Weather Review*, *134*, 638-656.
- Bretherton, C. S., et al. (1992), An Intercomparison of Methods for Finding Coupled Patterns in Climate Data, *Journal of Climate*, *5*, 541-560.

- Carlson, T. N., Gillies, R.R., and Schmugge, T.J. (1995), An interpretation of methodologies for indirect measurement of soil water content, *Agricultural and Forest Meteorology*, 77, 191-205.
- Castillo, V. (2009), Brief note on the Inter-Regional Workshop on Indices and Early Warning Systems for Drought, paper presented at Inter-Regional Workshop on Indices and Early Warning Systems for Drought, United Nations Secretariat of the Convention to Combat Desertification, Lincoln, Nebraska, U.S.A., December 11, 2009.
- Chang, C.-P. (2005a), The Asian winter-Australian summer monsoon: an introduction, in *The global monsoon system: research and forecast*, edited by C.-P. Chang, Wang, B., and Lau, N.-C.G., pp. 136-137, Secretariat of the World Meteorological Organization, Geneva, Switzerland.
- Chang, C. P., Harr, P. A., and Chen, H. J. (2005b), Synoptic Disturbances over the Equatorial South China Sea and Western Maritime Continent during Boreal Winter, *Monthly Weather Review*, 133, 489-503.
- Compo, G. P., Kiladis, G.N., and Webster, P.J. (1999), The horizontal and vertical structure of east Asian winter monsoon pressure, *Quarterly Journal of the Royal Meteorological Society*, 125, 29-54.
- de Silva, M. B. G. (1997), Climate, in *Arjuna's Atlas of Sri Lanka*, edited by T. Somasekaram, Colombo, Sri Lanka.
- Domroes, M. (1974), *The agro-climate of Ceylon: a contributions towards the ecology of tropical crops*, Franz Steiner, Wiesbaden.
- Frank, W. M., and Roundy, P.E. (2006), The Role of Tropical Waves in Tropical Cyclogenesis, *Monthly Weather Review*, 134, 2397-2417.
- Goddard, L., Mason, S. J., Zebiak, S. E., Ropelewski, C. F., Basher, R., and Cane, M. A. (2001), Current approaches to seasonal to interannual climate predictions, *International Journal of Climatology*, 21, 1111-1152.
- Goswami, B. N., Krishnamurthy, V., and Annmalai, H. (1999), A broad-scale circulation index for the interannual variability of the Indian summer monsoon, *Quarterly Journal of the Royal Meteorological Society*, 125, 611-633.
- Guttman, N. B. (1999), Accepting the Standardized Precipitation Index: a calculation algorithm, *Journal of the American Water Resources Association*, 35, 311-322.
- Hastenrath, S. (1995), Recent Advances in Tropical Climate Prediction, *Journal of Climate*, 8, 1519-1532.

- Hastenrath, S. (2000), Zonal circulations over the equatorial Indian Ocean, *Journal of Climate*, 13, 2746-2756.
- Hastenrath, S., and Polzin, D. (2003), Circulation mechanisms of climate anomalies in the equatorial Indian Ocean, *Meteorologische Zeitschrift*, 12, 81-93.
- Hastenrath, S., and Polzin, D. (2004), Dynamics of the surface wind field over the equatorial Indian Ocean, *Quarterly Journal of the Royal Meteorological Society*, 130, 503-517.
- Husak, G. H., Michaelsen, J., and Funk, C. (2007), Use of the gamma distribution to represent monthly rainfall in Africa for drought monitoring applications, *International Journal of Climatology*, 27, 935-944.
- JayaMaha, G. S. (1975), An analysis of droughts in Sri Lanka, *Proceedings of the Indian National Science Academy*, 42, 133-148.
- Justice, C. O., Townshend, J. R. G., Vermote, E. F., Masuoka, E., Wolfe, R. E., Saleous, N., Roy, D. P., and Morisette, J. T. (2002), An overview of MODIS Land data processing and product status, *Remote Sensing of Environment*, 83, 3-15.
- Karnieli, A., Agam, N., Pinker, R.T., Anderson, M., Imhoff, M.L., Gutman, G.G., Panov, N., and Goldberg, A. (2010), Use of NDVI and Land Surface Temperature for Drought Assessment: Merits and Limitations, *Journal of Climate*, 23, 618-633.
- Kistler, R., E. Kalnay, W. Collins, S. Saha, G. White, J. Woollen, M. Chelliah, W. Ebisuzaki, M. Kanamitsu, V. Kousky, H. van den Dool, R. Jenne, M. Fiorino. (2001), The NCEP-NCAR 50-Year Reanalysis: Monthly Means CD-ROM and Documentation, *Bulletin of the American Meteorological Society*, 82, 247-267.
- Kogan, F. N. (1997), Global drought watch from space, *Bulletin of the American Meteorological Society*, 78, 621-636.
- Kripalani, R. H., and Kumar, P. (2004), Northeast monsoon rainfall variability over south peninsular India vis-à-vis the Indian Ocean dipole mode, *International Journal of Climatology*, 24, 1267-1282.
- Krishnamurti, T. N., Chakraborty, A., Martin, A., Lau, W.K., Kim, K.-M., Sud, Y., and Walker, G. (2009), Impact of Arabian Sea pollution on the Bay of Bengal winter monsoon rains, *Journal of Geophysical Research*, 114.
- Kumar, K. K., Rajagopalan, B., Hoerling, M., Bates, G., and Cane, M. (2006), Unraveling the Mystery of Indian Monsoon Failure During El Nino, *Science*, 314(5796), 115-119.

- Kumar, O. S. R. U. B., Naidu, C. V., Rao, S. R. L., and Rao, B.R.S. (2004), Prediction of southern Indian winter monsoon rainfall from September local upper-air temperatures, *Meteorological Applications*, 11, 189-199.
- Kumar, P., et al. (2007), On the recent strengthening of the relationship between ENSO and northeast monsoon rainfall over South Asia, *Climate Dynamics*, 28, 649-660.
- Landman, W. A., and Mason, S.J. (2001), Forecasts of near-global sea surface temperatures using Canonical Correlation Analysis, *Journal of Climate*, 14, 3819-3833.
- Lau, K. M., and H. Weng (1995), Climate Signal Detection Using Wavelet Transform: How to Make a Time Series Sing, *Bulletin of the American Meteorological Society*, 76, 2391-2402.
- Li, S., and Goddard, L. (2005), Retrospective forecasts with the ECHAM4.5 AGCM, 16 pp, International Research Institute for Climate and Society, Palisades, New York.
- Li, T., Wang, B., Chang, C.P., and Zhang, Y. (2003), A theory for the Indian ocean dipole-zonal mode, *Journal of the Atmospheric Sciences*, 60(17), 2119-2135.
- Lyon, B., Zubair, L., Ralapanawe, V. and Yahiya, Z. (2009), Finescale evaluation of drought in a tropical setting: case study in Sri Lanka, *Journal of Applied Meteorology and Climatology*, 48, 77-88.
- Madden, R. A., and Julian, P.R. (1971), Detection of a 40-50 Day Oscillation in the Zonal Wind in the Tropical Pacific, *Journal of the Atmospheric Sciences*, 28, 702-708.
- Maddumabandara, C. M. (1983), Effect of drought on the livelihood of peasant families in the dry zone of Sri Lanka, in *Climatological Notes (33): Climate, Water and Agriculture in Sri Lanka*, edited by M. Yoshino, Kayane, I., and Maddumabandara, C.M., pp. 61-76, Institute of Geoscience, University of Tsukuba.
- Malmgren, B. A., Hullugalla, R., Lindeberg, G., Inoue, Y., Hayashi, Y., and Mikami, T. (2007), Oscillatory behavior of monsoon rainfall over Sri Lanka during the late 19th and 20th centuries and its relationships to SSTs in the Indian Ocean and ENSO, *Theoretical and Applied Climatology*, 89, 115-125.
- McKee, T. B., Doesken, N.J., and Kleist, J. (1993), The relationship of drought frequency and duration to time scales, paper presented at Eighth Conference on Applied Climatology, Anaheim, California.

- Njoku, E. G., Jackson, T. J., Lakshmi, V., Chan, T. K., and Nghiem, S. V. (2003), Soil moisture retrieval from AMSR-E, *Geoscience and Remote Sensing, IEEE Transactions on*, 41, 215-229.
- Palmer, T. N. (1993), Extended-Range Atmospheric Prediction and the Lorenz Model, *Bulletin of the American Meteorological Society*, 74, 49-65.
- Park, S., Feddema, J.J., and Egbert, S.L. (2004), Impacts of hydrologic soil properties on drought detection with MODIS thermal data, *Remote Sensing of Environment*, 89, 53-62.
- Parry, M. L., Canziani, O.F., Palutikof, J.P., and Co-authors (2007), Technical Summary. Climate Change 2007: Impacts, Adaptation and Vulnerability. Contribution of Working Group II to the Fourth Assessment Report of the Intergovernmental Panel on Climate Change, Parry, M. L., Canziani, O.F., Palutikof, J.P., van der Linden, P.J., and Hanson, C.E. (Eds.), pp. 23-78, Cambridge University Press, Cambridge, UK.
- Parthasarathy, B., Rupakumar, K., and Munot, A.A. (1991), Evidence of secular variations in Indian monsoon rainfall-circulation relationships, *Journal of Climate*, 4, 927-938.
- Peiris, T. S. G., Hansen, J.W., and Zubair, L. (2008), Use of seasonal climate information to predict coconut production in Sri Lanka, *International Journal of Climatology*, 28, 103-110.
- Prasanna, V., and Yasunari, T. (2008), Interannual variability of atmospheric water balance over South Peninsular India and Sri Lanka during northeast monsoon season, *International Journal of Climatology*, 28, 1997-2009.
- Quiring, S. M. (2009), Developing Objective Operational Definitions for Monitoring Drought, *Journal of Applied Meteorology and Climatology*, 48, 1217-1229.
- Rajeevan, M. (2001), Prediction of the Indian summer monsoon: status, problems and prospects, *Current Science*, 81, 1451-1457.
- Rajeevan, M., and Pai, D.S. (2007), On the El Niño-Indian monsoon predictive relationships, *Geophysical Research Letters*, 34, L04704, doi: 04710.01029/02006GL028916.
- Ramage, C. S. (1971), *Monsoon Meteorology*, Academic Press Inc., New York.
- Rasmusson, E. M., and Carpenter, T.H. (1982), Variations in Tropical Sea Surface Temperature and Surface Wind Fields Associated with the Southern Oscillation/El Niño, *Monthly Weather Review*, 110, 354-384.

- Rasmusson, E. M., and Carpenter, T.H. (1983), The Relationship Between Eastern Equatorial Pacific Sea Surface Temperatures and Rainfall over India and Sri Lanka, *Monthly Weather Review*, *111*(3), 517-528.
- Roeckner, E., Oberhuber, J. M., Bacher, A., Christoph, M., and Kirchner, I. (1996), ENSO variability and atmospheric response in a global coupled atmosphere-ocean GCM, *Climate Dynamics*, *12*, 737-754.
- Saha, S., Nadiga, S., Thiaw, C., Wang, J., Wang, W., Zhang, Q., Van den Dool, H. M., Pan, H. L., Moorthi, S., Behringer, D., Stokes, D., Peña, M., Lord, S., White, G., Ebisuzaki, W., Peng, P., and Xie, P. (2006), The NCEP Climate Forecast System, *Journal of Climate*, *19*, 3483-3517.
- Saji, N. H., and Yamagata, T. (2003), Structure of SST and surface wind variability during Indian Ocean dipole mode events: COADS observations, *Journal of Climate*, *16*(16), 2735-2751.
- Shabbar, A., and Barnston, A.G. (1996), Skill of seasonal climate forecasts in Canada using Canonical Correlation Analysis, *Monthly Weather Review*, *124*, 2370-2385.
- Sheffield, J., and Wood, E.F. (2007), Characteristics of global and regional drought, 1950-2000: Analysis of soil moisture data from off-line simulation of the terrestrial hydrologic cycle, *Journal of Geophysical Research*, *112*, doi: 10.1029/2006JD008288.
- Shukla, J., and Kinter III, J.L. (2006), Predictability of seasonal climate variations: a pedagogical review, in *Predictability of Weather and Climate*, edited by T. Palmer, and Hagedorn, R., pp. 306-341, Cambridge University Press.
- Stahl, K., and Hisdal, H. (2006), Hydroclimatology, in *Hydrological drought: processes and estimation methods for streamflow and groundwater*, edited by L. M. Tallaksen, and Van Lanen, H.A.J., pp. 19-51, Elsevier.
- Sun, D., and Kafatos, M. (2007), Note on the NDVI-LST relationship and the use of temperature-related drought indices over North America, *Geophysical Research Letters*, *34*, L24406.
- Suppiah, R. (1989), Relationships between the Southern Oscillation and the rainfall of Sri Lanka, *International Journal of Climatology*, *9*, 601-618.
- Suppiah, R. (1996), Spatial and temporal variations in the relationships between the Southern Oscillation phenomenon and the rainfall of Sri Lanka, *International Journal of Climatology*, *16*, 1391-1407.
- Suppiah, R. (1997), Extremes of the Southern Oscillation phenomenon and the rainfall of Sri Lanka, *International Journal of Climatology*, *17*, 87-101.

- Tallaksen, L. M., Madsen, H. and Hisdal, H. (2004), Frequency Analysis, in *Hydrological drought - processes and estimation methods for streamflow and groundwater*, edited by L. M. a. V. L. Tallaksen, H.A.J., pp. 199-271, Elsevier, B.V., Amsterdam.
- Terray, P., et al. (2005), Indian Ocean Sea Surface Temperature and El Niño-Southern Oscillation: A New Perspective, *Journal of Climate*, 18, 1351-1368.
- Teuling, A. J., Hupet, F., Uijlenhoet, R., and Troch, P.A. (2007), Climate variability effects on spatial soil moisture dynamics, *Geophysical Research Letters*, 34, L06406.
- Thenkabail, P. S., Gamage, M.S.D.N., and Smakhtin, V.U. (2004), The use of remote-sensing data for drought assessment and monitoring in Southwest Asia, pp. 34 pp, International Water Management Institute, Colombo, Sri Lanka.
- Torrence, C., and Compo, G.P. (1998), A Practical Guide to Wavelet Analysis, *Bulletin of the American Meteorological Society*, 79, 61.
- Torrence, C., and Webster, P.J. (1999), Interdecadal Changes in the ENSO-Monsoon System, *Journal of Climate*, 12, 2679.
- Trauth, M. H. (2007), *MATLAB recipes for earth sciences*, 2nd ed., 288 pp., Springer-Verlag, Berlin.
- Tucker, C. J. (1979), Red and photographic infrared linear combinations for monitoring vegetation, *Remote Sensing of Environment*, 8, 127-150.
- van den Dool, H. M. (1994), Searching for analogues, how long must we wait?, *Tellus A*, 46, 314-324.
- Vinayachandran, P. N., Iizuka, S., and Yamagata, T. (2002), Indian Ocean dipole mode events in an ocean general circulation model, *Deep Sea Research Part II: Topical Studies in Oceanography*, 49, 1573-1596.
- von Storch, H., and Zwiers, F.W. (2002), *Statistical analysis in climate research*, Cambridge University Press.
- Vose, R. S., Schmoyer, R.L., Steurer, P.M., Peterson, T.C., Heim, R., Karl, T.R., and Eischeid, J. (1992), The Global Historical Climatology Network: long-term monthly temperature, precipitation, sea level pressure, and station pressure data., 324 pp, ORNL/CDIAC-53, NDP-04, Oak Ridge National Laboratory.
- Walker, G. T., and Bliss, E.W. (1932), World weather V, *Memoirs of the Royal Meteorological Society*, 4, 53-84.



- Wan, Z. (2008), New refinements and validation of the MODIS Land-Surface Temperature/Emissivity products, *Remote Sensing of Environment*, 112, 59-74.
- Wan, Z. (2009), Collection-5 MODIS Land Surface Temperature Products Users' Guide, edited, ICES, University of California, Santa Barbara, [http://modis.datamirror.csdb.cn/resource/doc/MOD11\\_UserGuide.pdf](http://modis.datamirror.csdb.cn/resource/doc/MOD11_UserGuide.pdf).
- Wan, Z., and Dozier, J. (1996), A generalized split-window algorithm for retrieving land-surface temperature from space, *Geoscience and Remote Sensing, IEEE Transactions on*, 34, 892-905.
- Wan, Z., Wang, P., and Li, X. (2004a), Using MODIS Land Surface Temperature and Normalized Difference Vegetation Index products for monitoring drought in the southern Great Plains, USA, *International Journal of Remote Sensing*, 25, 61 - 72.
- Wan, Z., Zhang, Y., Zhang, Q., and Li, Z. L. (2004b), Quality assessment and validation of the MODIS global land surface temperature, *International Journal of Remote Sensing*, 25, 261 - 274.
- Wang, B. (Ed.) (2006), *The Asian Monsoon*, 787 pp., Praxis Publishing Ltd.
- Wang, B., and Fan, Z. (1999), Choice of South Asian summer monsoon indices, *Bulletin of the American Meteorological Society*, 80, 629.
- Wang, B., Lee, J.-Y., Kang, I. S., Shukla, J., Kug, J. S., Kumar, A., Schemm, J., Luo, J. J., Yamagata, T., and Park, C. K. (2008a), How accurately do coupled climate models predict the leading modes of Asian-Australian monsoon interannual variability?, *Climate Dynamics*, 30, 605-619.
- Wang, P., Gong, J., and Li, X. (2001), Vegetation-Temperature Condition Index and its application for drought monitoring, *Geomatics and Information Science of Wuhan University*, 26, 412-417.
- Wang, W., Liang, S., and Meyers, T. (2008b), Validating MODIS land surface temperature products using long-term nighttime ground measurements, *Remote Sensing of Environment*, 112, 623-635.
- Wickramagamage, P (2009). Seasonality and spatial pattern of rainfall of Sri Lanka: Exploratory factor analysis, *International Journal of Climatology*, 30, 1235-1245.
- Wilhite, D. A. (1996), A methodology for drought preparedness, *Natural Hazards*, 13, 229-252.
- Wilks, D. S. A. (2006), *Statistical methods in the atmospheric sciences (2nd ed.)*, 627pp., Elsevier.

- WMO (2006), *Drought monitoring and early warning: concepts, progress and future challenges*, 24 pp., World Meteorological Organization, Geneva, Switzerland.
- Xu, M. C., C.-P., Fu, C., Qi, Y., Robock, A., Robinson, D., and Zhang, H. (2006), Steady decline of east Asian monsoon winds, 1969-2000: Evidence from direct ground measurements of wind speed, *Journal of Geophysical Research*, *111*, D24111.
- Yoshino, M., and Suppiah, R. (1984), Rainfall and paddy production in Sri Lanka, *Journal of Agricultural Meteorology*, *40*, 9-20.
- Zhang, Y., Sperber, K.R., and Boyle, J.S. (1997), Climatology and Interannual Variation of the East Asian Winter Monsoon: Results from the 1979-95 NCEP/NCAR Reanalysis, *Monthly Weather Review*, *125*, 2605-2619.
- Zubair, L. (2002), El Niño-southern oscillation influences on rice production in Sri Lanka, *International Journal of Climatology*, *22*, 249-260.
- Zubair, L., and Ropelewski, C. F. (2006), The Strengthening Relationship between ENSO and Northeast Monsoon Rainfall over Sri Lanka and Southern India, *Journal of Climate*, *19*, 1567-1575.
- Zubair, L., Rao, S.A., and Yamagata, T. (2003), Modulation of Sri Lanka Maha rainfall by the Indian Ocean Dipole, *Geophys. Res. Lett.*, doi: 10.1029/2002GL015639.
- Zubair, L., Siriwardhana, M., Chandimala, J., and Yahiya, Z. (2007), Predictability of Sri Lankan rainfall based on ENSO, *International Journal of Climatology*, *28*, 91-101.

## Curriculum Vitae

### DINALI NELUN FERNANDO

#### Education

- |      |  |
|------|--|
| 2010 | Ph.D. Geography (Specialization: Climatology)<br>Department of Geography, Rutgers The State University of New Jersey<br>New Jersey, U.S.A. |
| 2006 | M.A. Climate and Society<br>Columbia University<br>New York, U.S.A.  |
| 2001 | B.A. (First Class) Geography<br>Department of Geography, University of Colombo<br>Colombo, Sri Lanka                                       |

#### Principal Occupations

- |                        |  |
|------------------------|--|
| 26/7/2010 – 15/10/2010 | <b>Ph.D. Intern</b> , Computational Modeling Center,<br>Air Products and Chemicals Inc., Allentown, PA                         |
| 6/2010 – 7/2010        | <b>Instructor – Geographic Information Systems</b> ,<br>Department of Geography, Rutgers University                            |
| 7/2008 – 6/2010        | <b>William H. Greenberg Fellow</b> , Center for Environmental<br>Prediction and Department of Geography, Rutgers<br>University |
| 5/2009 – 7/2009        | <b>Instructor – Geographic Information Systems</b> ,<br>Department of Geography, Rutgers University                            |
| 9/2008 – 1/2009        | <b>Teaching Assistant (Coadjutant) – Remote Sensing</b> ,<br>Department of Geography, Rutgers University                       |

5/2008 – 7/2008	<b>Instructor – Geographic Information Systems,</b> Department of Geography, Rutgers University
1/2007– 4/2008	<b>Research Assistant,</b> NASA Land Use Land Cover Change research on ‘Landscape resilience-vulnerability in the Southern Yucatán Peninsular Region’, Department of Geography, Rutgers University
9/2006 – 6/2008	<b>Teaching Assistant,</b> Department of Geography
9/2005 – 5/2006	<b>Graduate Research Assistant,</b> International Research Institute for Climate and Society (IRI), Earth Institute, Columbia University
12/2003 – 8/2005	<b>Lecturer,</b> Department of Geography, University of Colombo, Sri Lanka
4/2002 – 12/2003	<b>Project Officer,</b> Hydrology and Water Resources Department, World Meteorological Organization (WMO), Geneva, Switzerland
8/2001 – 3/2002	<b>Intern,</b> Hydrology and Water Resources Department, WMO, Geneva, Switzerland

## **Publications**

### **Published:**

- Schneider, L.C. and **Fernando, D.N.** (2009). *An untidy cover: invasion of bracken fern in the shifting cultivation systems of Southern Yucatán, Mexico*. Biotropica 42(1), 41-48

### **Accepted:**

*Book chapter (invited contribution):*

- **Fernando, D.N.** *Monsoons*. Encyclopaedia of Geography. Barney Warf (Ed.). SAGE Publications Inc. (In press, projected release date: Sep. 2010)

**Under revision:**

- **Fernando, D.N.**, Robinson, D.A., Ward, M.N. and Premalal, K.H.M.S. *Drought and the predictability of the October-November rains over Sri Lanka* (Submitted to Int. J.Climatol. Oct. 2009; currently under major recommended revision)

**In review:**

- Robinson, David, **Fernando, D. Nelun** and Mioduszewski, John. *Principles of meteorology and weather prediction*. Wilderness Medicine (6<sup>th</sup> edition). Paul Auerbach (Ed.). Elsevier. (Submitted: Apr. 2010)